Thesis for the Degree of Doctor of Philosophy

Photoinduced Processes in Molecular-Inorganic Materials

- Design Strategies for Control of Photophysical and Photochemical Processes

ELIN SUNDIN

Department of Chemistry and Chemical Engineering

CHALMERS UNIVERSITY OF TECHNOLOGY

Gothenburg, Sweden 2021

Photoinduced Processes in Molecular-Inorganic Materials

- Design Strategies for Control of Photophysical and Photochemical Processes

ELIN SUNDIN

ISBN: 978-91-7905-474-8

Doktorsavhandlingar vid Chalmers tekniska högskola
Ny serie nr: 4941
ISSN: 0346-718X

Department of Chemistry and Chemical Engineering
Chalmers University of Technology
SE-412 96 Gothenburg
Sweden
Telephone + 46 (0)31-772 1000

Cover:
Illustration of photoexcited molecular/inorganic materials studied within this work.

Chalmers digitaltryck

Gothenburg, Sweden 2021

Photoinduced Processes in Molecular-Inorganic Materials

- Design Strategies for Control of Photophysical and Photochemical Processes

Elin Sundin

Department of Chemistry and Chemical Engineering

Chalmers University of Technology

Abstract

Sunlight is the most abundant renewable energy resource on Earth and has the potential to provide our society with clean energy. Despite this abundancy, solar energy corresponds to only a minority of the global energy production. Two major reasons for this are the limited efficiencies of solar cells and the difficulty of storing solar energy. The work presented within this Thesis aims to investigate ways of overcoming these issues. A process called singlet fission could be utilized to increase the efficiency of solar cell. The storage issue of solar energy could be circumvented by producing fuels (*i.e.* solar fuels) instead of electricity from sunlight.

The work presented herein has been dedicated to mechanistic studies of photo-induced processes in molecular/inorganic materials. The aim has been to gather knowledge about how the materials can be designed to obtain control of the photoinduced processes; so that one process can be favored over another. Molecular/inorganic materials were used because of their favorable characteristics compared to molecules or inorganic materials alone in terms of combining the stability of inorganic materials with the tunability of molecules.

In this work, a derivative of the well-known singlet fission molecule 1,3-diphenylisobenzofuran was attached to various semiconductor films in solvents of different polarities. Studies of these materials revealed that utilizing semiconductors with a relatively low conduction band energy in a non-polar environment is favorable for achieving singlet fission followed by injection from the triplet excited state. Further, studies of molecular/semiconductor materials with both photosensitizer and catalyst molecules attached to the surfaces revealed that the charge separated lifetime between the photosensitizer and the semiconductor can be significantly extended by design of a patterned film of two different semiconductors. These studies further revealed that two-electron transfer from the conduction band to an attached molecular catalyst is possible; thus, these materials are promising for use in solar fuel generating assemblies. The results presented herein can be useful for future design of molecular/inorganic materials to achieve singlet fission as well as multi-electron transfer necessary for generating solar fuels.

Keywords: Photochemistry, solar energy conversion, dye-sensitized semiconductors, hybrid materials, mechanistic studies, singlet fission, electron transfer, charge separation.

List of Publications

This Thesis is based on the work presented in the following papers:

I. **Singlet Fission and Electron Injection from the Triplet Excited State in Diphenylisobenzofuran–Semiconductor Assemblies: Effects of Solvent Polarity and Driving Force,** Elin Sundin, Rasmus Ringström, Fredrik Johansson, Betül Küçüköz, Andreas Ekebergh, Victor Gray, Bo Albinsson, Jerker Mårtensson, Maria Abrahamsson, *The Journal of Physical Chemistry C,* ***2020,*** *124, 20794–20805*

II. **Two-Colour Photoswitching in Photoresponsive Inorganic Thin Films,** Elin Sundin, Fredrik Johansson, Valeria S. Becerril, Joachim Wallenstein, August Gasslander, Jerker Mårtensson, Maria Abrahamsson**,** *Materials Advances,* ***2021****, DOI: 10.1039/D1MA00013F*

III. **Extending Charge Separation Lifetime and Distance in Patterned Dye-Sensitized SnO_2-TiO_2 µm-Thin Films,** Valeria S. Becerril, Elin Sundin, Mohktar Mapar, Maria Abrahamsson, *Physical Chemistry Chemical Physics,* ***2017,*** *19, 22684-22690*

IV. **Evidence for Conduction Band-Mediated Two-Electron Reduction of a TiO_2-Bound Catalyst Triggered by Visible Light Excitation of Co-Adsorbed Organic Dyes,** Valeria S. Becerril[1], Elin Sundin[1], Maria Abrahamsson, *The Journal of Physical Chemistry C,* ***2018****, 122, 25822-25828*

[1] These authors contributed equally

Papers not Included in the Thesis

A. **Excited State Dynamics of Bistridentate and Trisbidentate Ru^{II} Complexes of Quinoline-Pyrazole Ligands,** Lisa A. Fredin[1], Joachim Wallenstein[1], Elin Sundin, Martin Jarenmark, Deise F. Barbosa de Mattos, Petter Persson, Maria Abrahamsson, *Inorganic Chemistry,* ***2019,*** *58, 16354-16363*

B. **Long-Lived Charge Separation in Dye–Semiconductor Assemblies: a Pathway to Multi-Electron Transfer Reactions,** Elin Sundin, Maria Abrahamsson**,** *Chemical Communications,* ***2018,*** *54, 5289-5298*

C. **DNA Threading Intercalation of Enantiopure $[Ru(phen)_2bidppz]^{2+}$ Induced by Hydrophobic Catalysis,** Bobo Feng, Elin Sundin, Per Lincoln, Anna F. K. Mårtensson, *Physical Chemistry Chemical Physics,* ***2021****, 23, 2238-2244*

D. **Binding of Thioflavin-T to Amyloid Fibrils Leads to Fluorescence Self-Quenching and Fibril Compaction,** David J. Lindberg, Anna Wenger, Elin Sundin, Emelie Wesén, Fredrik Westerlund, Elin K. Esbjörner, *Biochemistry,* ***2017****, 56, 2170-2174*

[1] These authors contributed equally

My contribution

Description of my contribution to the appended papers

I. Designed and performed the spectroscopic experiments and analyzed the data together with R.R. and B.K. Synthesis and characterization were done by F.J, A.E. and V.G. Wrote most of the manuscript.

II. Designed the study with M.A. Performed most of the spectroscopic experiments and analyzed the data. Synthesis and characterization of the complex was done by F.J. Wrote most of the manuscript.

III. Performed the spectroscopic experiments and analyzed the data together with V.S.B. Wrote part of the manuscript.

IV. Designed the study together with V.S.B and M. A. Performed the spectroscopic experiments. Calculations, electrochemistry and spectroelectrochemistry were done by V.S.B. Wrote the manuscript together with V.S.B and M.A.

Abbreviation List

A	Acceptor
AO	Atomic orbital
CB	Conduction band
CSS	Charge separated state
D	Donor
DSP	Dye-sensitized photocatalysis
DSPEC	Dye-sensitized photoelectrosynthesis cell
DSSC	Dye-sensitized solar cell
ET	Electron transfer
GS	Ground state
GVD	Group value dispersion
HOMO	Highest occupied molecular orbital
IC	Internal conversion
ISC	Intersystem crossing
KWW	Kohlrausch–Williams–Watts
LUMO	Lowest unoccupied molecular orbital
MLCT	Metal to ligand charge transfer
MO	Molecular orbital
OPA	Optical parametric amplifier
OPO	Optical parametric oscillator
PET	Photoinduced electron transfer
PMT	Photomultiplier tube
PSD	Photostationary distribution
S	Singlet
SF	Singlet fission
T	Triplet
TA	Transient absorption
TCSPC	Time correlated single photon counting
UV	Ultraviolet
VB	Valence band
VR	Vibrational relaxation

Table of Contents

1 Introduction – Light as the Starting Point

Sunlight is the start of all life on Earth. Together with carbon dioxide and water, sunlight produces oxygen and carbohydrates *via* photosynthesis which is essential for life as we know it.[1] The radiation from the sun contains a lot of energy that is not utilized to its fullest potential in today's society, just 90 minutes of sunlight at the surface of the Earth contains enough energy to power the planet for almost an entire year.[2] Despite this abundance of solar energy, only about 2 % of the global energy production originates from direct solar to energy conversion.[3] This is a number that needs to increase in order to meet the climate goals stated in the Paris agreement; limiting the temperature increase to a maximum of 1.5^{0}C compared to the pre-industrial era.[4]

As I am writing this Thesis, the temperature increase on Earth has already become apparent. In fact, last year was the warmest year since the measurements of the temperature started in the mid-19th century, with an average temperature of 1.25^{0}C above that in the pre-industrial era.[5] The vast majority of researchers and scientists agree that this temperature increase is a result of global warming caused by burning of fossil fuels such as coal and oil, resulting in emission of greenhouse gases. Moreover, the temperature is predicted to continue to increase if we don't change this behavior. Thus, to prevent a further increase of the temperature we need to replace the fossil fuels with renewable energy resources such as solar, hydro, biomass or wind that does not contribute to emission of greenhouse gases. By far the most abundant energy resource of these is solar radiation which, as previously mentioned, contains an almost endless amount of energy from a societal perspective.

Given the vast abundance of solar energy at the Earth's surface, it is almost surprising that it is not yet the dominating energy resource for our society. There are of course several reasons for this, and I will not cover them all in this Thesis but will focus on two limitations of scientific interest that I have been working with. The first is the efficiency of solar cells, which is limited by the mismatch between the solar spectrum and the band-gap of the solar cells.[6, 7] Figure 1.1 shows the spectrum of the solar radiation at the surface of Earth. As can be seen in the figure, the main part of the solar radiation consists of visible light (400-700 nm). Silicon, which is the most common material used in solar cells, however, has a band-gap of ~1000 nm.[8] Thus, a lot of the solar energy is not utilized fully in the solar cells and is lost as heat.

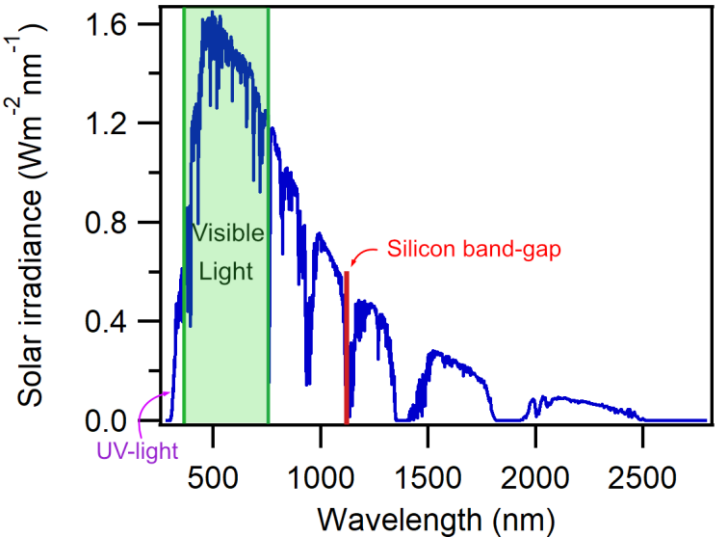

Figure 1.1. The spectrum of the solar radiation at the Earth's surface. The visible region of the spectrum is marked in green, and the UV part of the spectrum is the part to the left of the visible region. The band-gap of silicon solar cells is also indicated in the spectrum.

The mismatch between the solar spectrum and the band-gap of solar cells could possibly be circumvented by utilizing a process known as singlet fission (SF), where one high energy photon can result in two charges in the solar cell, which would reduce the thermalization losses. In short, SF is a process where a molecule in its singlet excited state interacts with and shares the excitation energy with a neighbouring ground-state molecule, resulting in both molecules ending up in their triplet excited states.[9-13] Efficient SF with quantum yields reaching the theoretical maximum have been demonstrated in several different molecules, both in concentrated solution, as dimer or trimers and in crystalline films.[14-19] However, harvesting the obtained triplets into a device with maintained high yields has proven to be difficult, which limits the use of SF.[20-25]

The second, and probably more important limitation, is the challenge of storing solar energy. Solar cells produce electricity when the sun is shining, but at night or on a cloudy day their power output is severely diminished. Finding a good way of storing solar energy is therefore of great importance. One possible way of storing solar energy could be to produce so-called solar fuels from the sunlight and store the energy in chemical bonds.[26-28] In principle, solar fuels can be generated by photoexcitation and subsequent charge

transfer into reaction centres, mimicking the key features of the photosynthesis.[29] In natural photosynthesis, light capture is followed by a series of electron transfer steps that accumulates electrons at a final acceptor, which later is used for the light-independent reduction of carbon dioxide into carbohydrates.[30-33] In order to mimic this in artificial systems, multi-electron transfer needs to be achieved since the reactions that are of interest for solar fuel production, such as reduction of carbon dioxide, require transfer of more than one electron.[29, 34] Moreover, a long-lived charge separated state following the photoexcitation is necessary to allow for the multi-electron transfer events to occur as well as to match the turn-over frequencies of the solar fuel-forming reactions.

The first example of fuel generation from irradiation with light in an artificial system is the experiment by Fujishima and Honda in 1972; using titanium dioxide (TiO_2) and platinum as electrodes, UV-light irradiation (<400 nm) produced hydrogen and oxygen from water.[35] As can be seen in Figure 1.1, the solar radiation at the Earth's surface contains a limited amount of UV-light, and it is therefore desired to instead utilize the visible part of the spectrum to drive the fuel-forming reactions. This can be achieved in some molecular and hybrid assemblies, and since the initial experiment by Fujishima and Honda, solar fuel-forming reactions have been demonstrated in several systems.[36-44] The efficiencies and stabilities of these systems are however limited, and key challenges include achieving more efficient multi-electron transfer as well as an extended charge separated lifetime.

1.1 Aim of this Work

Light, and the processes that occur in molecules and materials upon photoexcitation, is also the starting point for the work presented in this Thesis. As described above, solar energy has the potential to provide our society with clean and abundant energy, given that the limitations of solar energy conversion can be overcome. Light is also non-intrusive and an ideal trigger for other photonic devices, such as logic gates or molecular machines.[45, 46]

In this work, hybrid materials that consist of molecules immobilized onto inorganic semiconductor films have been designed and characterized. Hybrid molecular/inorganic materials are used since they come with some clear advantages compared to using pure molecular or inorganic materials alone. While pure molecular systems are tunable by chemical modifications, they often suffer from stability issues, for example, when it comes to several sequences of electron transfer events. Using pure molecular systems also typically requires working in liquid phase, which is not beneficial for practical applications. Inorganic semiconductor materials are on the other hand often stable for several sequences of excitation and electron transfer; however, they are not as easily tuned as molecular systems. Hence, assemblies that combine the selectivity of molecules with the stability of inorganic materials can be an ideal solution that takes advantage of both the selectivity of molecules and the stability of inorganic materials.[47]

Here, molecular/semiconductor materials have been designed and studied with the aim of obtaining mechanistic information about the processes that occur following

photoexcitation, and how these processes potentially can be controlled in future devices. The applications that have been in mind are materials for solar energy conversion as well as other light-responsive functional materials.

In **Paper I**, a derivative of the well-known SF molecule 1,3-diphenylisobenzofuran (DPIBF) was immobilized onto different semiconductor surfaces, and the SF and triplet injection dynamics were characterized in terms of solvent polarity and injection driving force. The aim of this work was to study if the photoinduced processes that occur on the surface, for example SF or charge separation, can be controlled by varying the substrate or surrounding environment.

In **Paper II**, the goal was to design a photoswitchable molecule that can be attached to semiconductor surfaces to generate a light-responsive photoswitchable solid film with spatial addressability. The molecule was based on a ruthenium sulfoxide complex that can undergo reversible S-to-O linkage isomerization upon photoexcitation, and the aim was to study if the photoisomerization ability is preserved when the molecule is attached to a zirconium dioxide (ZrO_2) film. In a follow-up study, the same ruthenium sulfoxide complex was used as a photosensitizer attached to TiO_2. The aim of this work was to see if the complex can inject electrons into the conduction band of TiO_2, and if the created charge separated state can be stabilized by one of the isomers.

In **Paper III**, a patterned semiconductor film was designed with the goal of extending the charge separated lifetime between an immobilized photosensitizer and the film. The patterned film was designed using two semiconductors with different conduction band energy levels; TiO_2 and tin dioxide (SnO_2). The aim with this design was to study if an electron transfer cascade could be created in the film, and if that could result in an extended charge separated lifetime. Finally, in **Paper IV**, the electron transfer events from the conduction band of TiO_2 to an immobilized catalyst molecule were studied. The aim of this work was to achieve two-electron transfer to the catalyst, both from direct UV-light excitation of TiO_2 and by visible light excitation of co-adsorbed photosensitizer molecules.

2 Theory and Experimental Methods

In this Chapter, I will briefly describe light-matter interactions and photoinduced processes that are relevant for this work. I will also describe the experimental techniques that I have been using. This Chapter aims to provide a background to the light-induced processes that occur in the following chapters, so that the results presented therein can be understood. For a more detailed description of these topics, the reader is referred to other literature on the subjects.[9, 48-55]

2.1 Light, Matter, and their Interactions

The interaction between light and matter is something that we, whether we reflect upon it or not, come across every day. The interplay between light and matter is the origin of all the colors that we see and also what initiates photosynthesis, which is the source of all life on Earth. To fully understand these interactions, it is important to first understand what we mean by light and matter.

2.1.1 Light

Light is typically described as a harmonic wave of an oscillating electric and magnetic field, where the wavelength of the light (λ) corresponds to the distance between the waves, as illustrated in Figure 2.1.

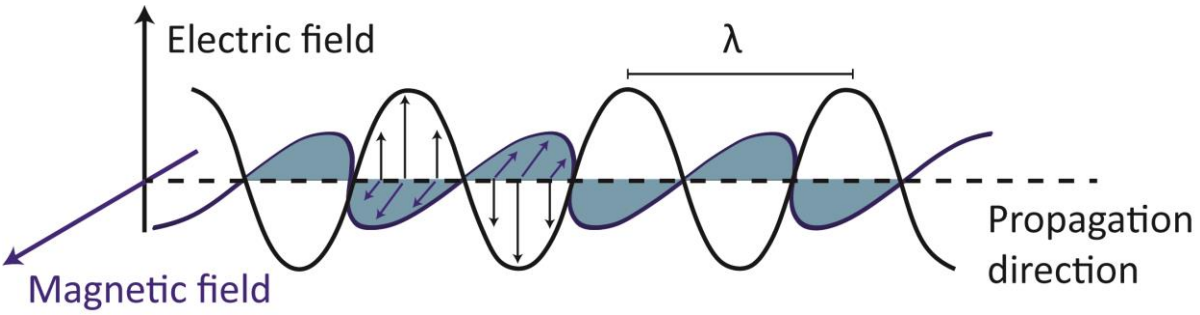

Figure 2.1. Illustration of an electromagnetic wave, with the oscillating electric and magnetic field perpendicular to each other.

Apart from being described as a wave, light can also be described as a flow of particles, called photons, with a discrete energy. The energy of the photons (E) are related to the wavelength (λ) or frequency (v) of the electromagnetic wave, the speed of light (c) and Planck's constant (h) *via* the equation[48]

$$E = hv = \frac{hc}{\lambda} \qquad (2.1)$$

As can be seen in Equation 2.1, light with a shorter wavelength has higher energy than light with a longer wavelength. A photon of UV-light is, for example, more energetic than a photon of visible light. Light can interact with matter in a few different ways, and to understand these interactions, we also first need to define what we mean by matter.

2.1.2 Matter

The smallest components of matter which we consider in chemistry are usually electrons, protons, and neutrons. These components make up the atoms, which consist of a core of neutrons and positively charged protons surrounded by negatively charged electrons. The probability of where in space the electrons can be found as they are surrounding the core of the atoms are described by the atomic orbitals (AO), which in principle are solutions to the Schrödinger equation.[56] The AO obtained from solving the Schrödinger equation have discrete energy levels, and they are occupied by electrons according to the *Aufbau principle* with the lowest energy orbitals being filled first. Each AO can only be occupied by two electrons, as is stated in the *Pauli exclusion principle*, and these electrons need to have opposite spin. In molecules, which in principle consist of several atoms bound together, the electrons are instead located in molecular orbitals (MO). The MO are linear combinations of the AO and are also occupied according to the *Aufbau* and *Pauli exclusion principles.* The highest occupied molecular orbital (HOMO) and the lowest unoccupied molecular orbital (LUMO) in molecules are especially important when it comes to photoinduced processes.[51, 55]

Instead of in orbitals, electrons in solid state materials such as semiconductors are located in discrete energy bands. The bands are in principle a combination of the individual orbitals, with orbitals of similar energy forming the continuous bands. Just as in atoms and molecules, the bands are occupied in increasing energy levels. The highest occupied band and lowest unoccupied band in the ground state of semiconductors are called the valence band (VB) and the conduction band (CB) respectively and the energy difference between these is called the band-gap.[52]

2.1.3 Light-Matter Interactions

Light, being electromagnetic radiation, can interact with matter in a few different ways, for example absorption of a photon or scattering of the light. When a photon has a suitable energy, it can be absorbed by a molecule through an interaction with the electrons in the molecule. This interaction induces an electronic transition from an orbital with a lower energy to an orbital with a higher energy. For an electronic transition between for example HOMO and LUMO to occur, the energy of the photon needs to match the energy difference between the orbitals as is stated in *Bohr's frequency condition,* Equation 2.2, where ΔE is the energy difference between the orbital with higher energy (E_{final}) and the initially occupied orbital ($E_{initial}$), h is Planck's constant and v is the frequency of the light. Electronic transitions in molecules are often induced by light in the UV to visible part of the spectrum.[48]

$$\Delta E = E_{final} - E_{initial} = hv \tag{2.2}$$

When a photon is absorbed by a molecule, the electrical component of light induces a dipole moment in the molecule known as the transition dipole moment. Hence, for light to be absorbed, the transition dipole moment also needs to be aligned with the electrical component of the light, in addition to the energy requirements. Additionally, for a transition between the electronic states to occur, the states need to be coupled, *i.e.* their wavefunctions need to overlap. The greater the overlap between the wavefunctions, the higher the probability of the transition to occur which also results in a larger absorption. The probability of an electronic transition to occur between two states is described with the *Fermi Golden rule* as[51]

$$k = \frac{2\pi}{\hbar}\rho < \Psi_1|H|\Psi_2 >^2 \tag{2.3}$$

Where k is the rate of the transition (*i.e.* the probability per time unit) between the two states Ψ_1 and Ψ_2, $\hbar$ is Planck's constant divided by 2π, ρ is the density of states that can couple the two states and H represents the perturbation that is induced on the system when the two states are mixed.

Solid state materials like semiconductors can also absorb light if the wavelength of the light matches the difference between two energy bands. Semiconductors are, as might be apparent from the name, non-conductive in the ground state but can relatively easily

become conductive if their CB gets populated with electrons by for example photoexcitation. Wide band-gap semiconductors, which are used in this work, has a relatively large band-gap and only absorb light in the UV-region. The band-gap of anatase TiO_2, SnO_2 and ZrO_2, which are all examples of wide band-gap semiconductors, are 3.2 eV[57], 3.8 eV[57] and 5.0 eV[58] respectively. Semiconductors can also become conductive by electron injection from molecules that are immobilized onto the surface *via* photoinduced electron transfer[59] as will be further described in the following section.

2.2 Photoinduced Processes in this Work

Several processes can be triggered upon photoexcitation of molecules and materials. In this section, the photophysical and photochemical processes that are relevant to the work presented in this Thesis will be described.

Figure 2.2 displays a simplified *Jablonski diagram* that summarizes the transitions that can occur in molecules upon photoexcitation. A molecule in its ground state (GS) is almost always in the lowest singlet state (*i.e.* a state where all electrons are paired with different spins), which is called S_0 and this is the starting point for the light-induced transitions.

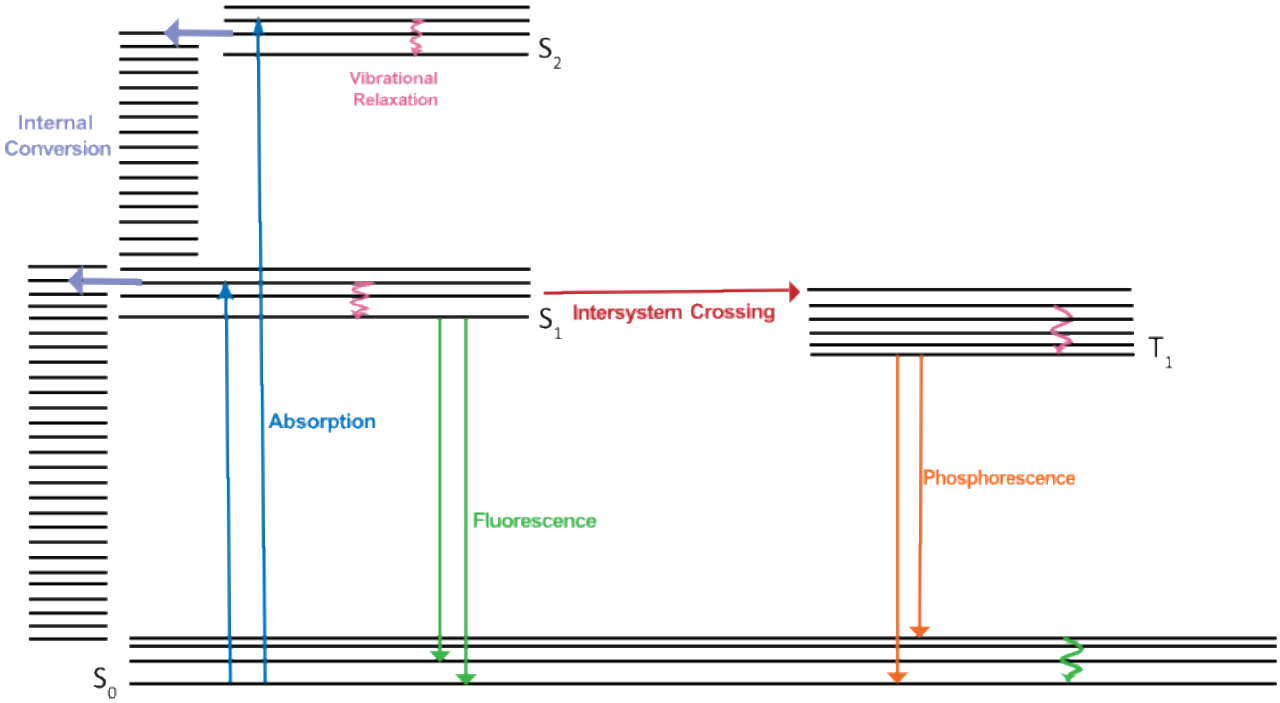

Figure 2.2. Simplified Jablonski diagram with arrows indicating absorption, fluorescence, phosphorescence, vibrational relaxation, internal conversion and intersystem crossing.

If a photon is absorbed by a molecule (blue arrows) the molecule ends up in an electronically excited singlet state, usually in the first or the second singlet excited state which are called S_1 and S_2, respectively. Each of the electronic states also has a number of vibrational energy levels that are represented by additional black lines in the figure.

According to the *Franck Condon principle,* electronic transitions are vertical in the diagram and do not involve any movement of the nuclei during the time of the transition (since the electrons are so much lighter than the nuclei). Following absorption, the molecule ends up in the so-called Franck Condon state, which typically is in a higher vibrational level in the electronically excited state. The molecule quickly relaxes from the Franck Condon state into the lowest vibrational level of the S_1 state. This relaxation occurs *via* vibrational relaxation (VR) (pink arrows, a non-radiative deactivation process that releases heat) when the Franck Condon state initially is in the S_1 state. If the Franck Condon state involves a higher electronically excited state, this relaxation occurs *via* internal conversion (IC) (purple arrows, a non-radiative process without energy loss) to a higher vibrational level of S_1 followed by VR to the lowest vibrational level of S_1.

From the S_1 state, there are a few competing non-radiative and radiative processes that can take the molecule back to the GS. One possible deactivation pathway is emission of a photon from the S_1 state, this is a radiative process and is called fluorescence (green arrow). The molecule can also return to the GS non-radiatively *via* IC into a higher vibrational level of the S_0 state followed by VR. Another possible pathway from the S_1 state is intersystem crossing (ISC) (red arrow) into a triplet excited state (T_1), which is a state with two unpaired electrons. This is a non-radiative process without energy loss, and since it involves a spin change of one electron it is typically slow. From the T_1 state, the molecule can return to the GS *via* emission of a photon, which is a radiative process called as phosphorescence (orange arrow) or ISC can take the molecule back to the S_0 state. Since phosphorescence involves the change of a spin, this process is generally slower (µs to ms) than fluorescence (ps to ns).[49]

The relative preference for a deactivation process following photoexcitation is called the quantum yield (ϕ) of the processes and is defined as the number of events per absorbed photon. For example, the quantum yield of fluorescence can be written as

$$\phi_{fluorescence} = \frac{\#emitted\ photons\ via\ fluorescence}{\#absorbed\ photons} \tag{2.4}$$

The quantum yield of fluorescence can also be expressed in terms of the rate constants as the rate constant of fluorescence (k_f) over the sum of the rate constants of all the deactivation processes, *i.e.* fluorescence and non-radiative processes (k_{nr}) as

$$\phi_{fluorescence} = \frac{k_f}{k_f + k_{nr}} \tag{2.5}$$

In addition to the processes described above, other processes such as singlet fission, photoinduced electron transfer and photoisomerization can also occur in some molecules upon photoexcitation. These processes will be described in the following sections.

2.2.1 Singlet Fission

In addition to the processes described above, some molecules can undergo singlet fission upon photoexcitation to the S_1 state. As briefly described in the introduction, SF is a process where a molecule in its singlet excited state shares the excitation energy with a neighboring ground-state molecule, which results in both molecules ending up in their T_1 state.[9] The maximum quantum yield for this process is 200%, since one absorbed photon can result in two triplet excited states. A simplified diagram illustrating the SF process is presented in Figure 2.3. The initially formed triplet states are coupled into an overall singlet configuration that is called a correlated triplet pair, $[T_1T_1]$, which makes SF a spin-allowed process.[9] After the correlated triplet pair has formed, it should ideally dissociate into two free and independent triplets but can also recombine into two ground-state molecules or undergo triplet-triplet annihilation.[9]

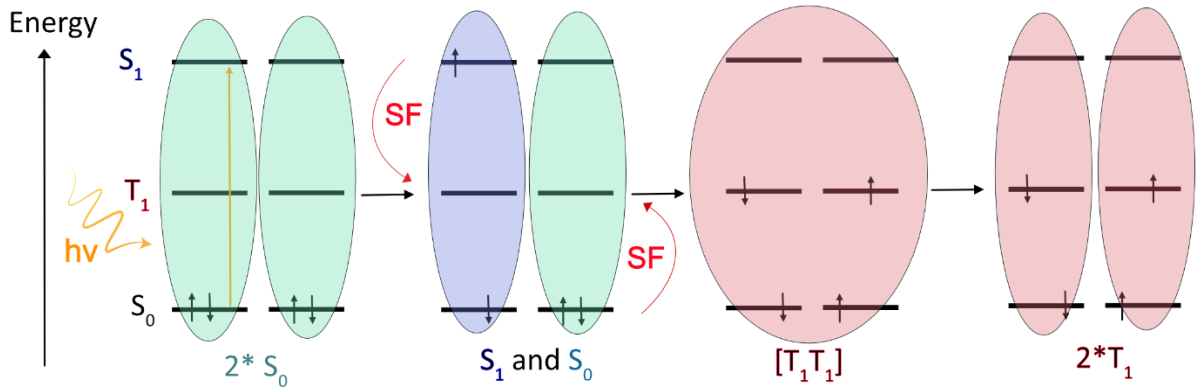

Figure 2.3. A simplified diagram of the SF process, a molecule in the S_0 state initially absorbs a photon and ends up in the S_1 state. Once in the S_1 state, the molecule shares the excitation energy with a neighboring molecule so that both molecules ends up in the T_1 state, the T_1 states are initially coupled ($[T_1T_1]$) in an overall singlet configuration and these may subsequently dissociate into two independent triplets (T_1).

There are a few requirements that need to be fulfilled for singlet fission to occur. Firstly, the energy of the S_1 state needs to be at least twice that of the T_1 state to make this process energetically possible.[9, 60] Secondly, an electronic coupling between the molecules is necessary, which requires that the molecules are in close proximity and in a favorable geometry for SF.[9] The first requirement is fulfilled in various molecules like for example pentacene[61], tetracene[62] and DPIBF[63]. The second requirement has been fulfilled by using highly concentrated solutions, crystalline films and in dimers or trimers of the compounds, and the quantum yield of SF in these systems often reaches 200%.[14-19]

The mechanism of SF has been extensively studied[14, 64-73], and Figure 2.3 represents a very simplified picture of the process. Although being extensively studied, the mechanism is not yet fully understood and appears to vary between different molecules and in different assemblies. For example, in some molecules, an initial charge transfer into a molecular charge separated state facilitates for SF whereas in others it acts as a loss channel.[14, 74, 75] Formation of a molecular charge separated state is one example of photoinduced electron transfer, which will be further described in the following section.

2.2.2 Photoinduced Electron Transfer

Reactions where electrons are transferred from a donor (D) to an acceptor (A) are known as electron transfer (ET) reactions and are essential in many biological processes as well as in solar energy conversion. For an electron transfer reaction to occur, there must be a driving force for the reaction, *i.e.* the *Gibbs free energy* needs to be lower for the resulting state than for the initial state.[76-80] Classical *Marcus Theory*[77] is often used to describe electron transfer reactions, and this will briefly be described below.

Electron transfer can happen both between molecules in the ground state and from thermally or photoexcited states.[76-80] When electron transfer occurs following photoexcitation of either the donor or acceptor, the electron transfer is referred to as photoinduced electron transfer (PET). Since photoexcitation of a molecule results in a higher energetic state of the molecule, the driving force for electron transfer increases in the excited state. Electron transfer from a photoexcited donor (*D**) to an acceptor is often written as

$$D - A \xrightarrow{h\nu} D^* - A \xrightarrow{k_{ET}} D^+ - A^- \qquad (2.6)$$

where D^+-A^- represents the charge separated state (CSS). A potential energy surface diagram illustrating PET following photoexcitation of the donor is shown in Figure 2.4.

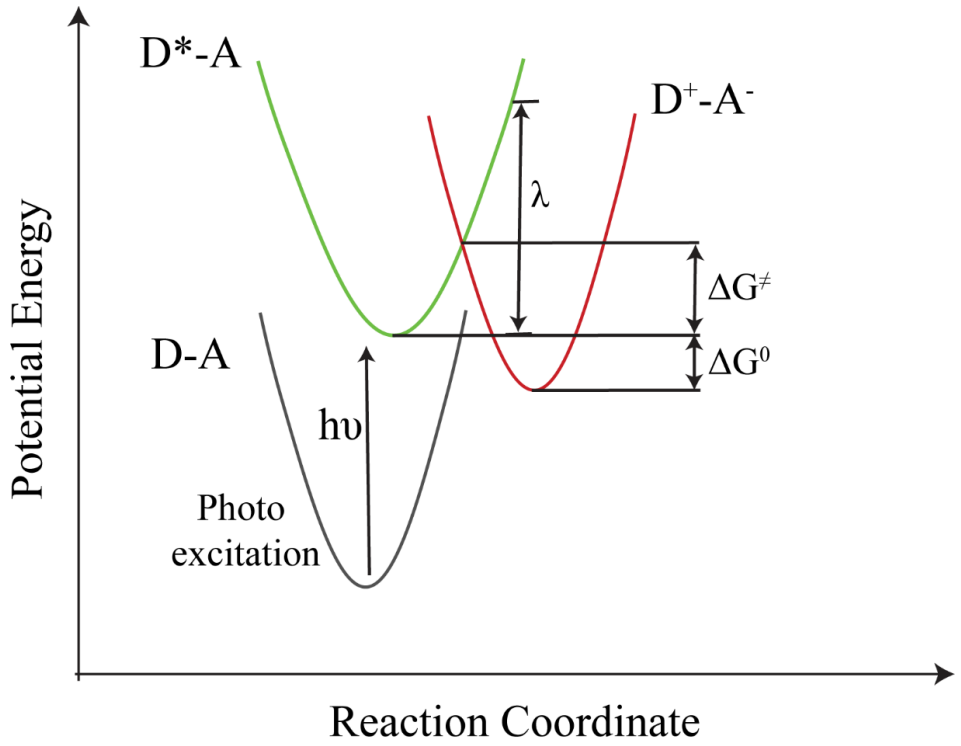

Figure 2.4. Potential energy surface diagram showing PET from photoexcitation of a donor. The diagram includes the ground state (D-A), the initially photoexcited state (D-A) and the charge separated state (D^+-A^-). The driving force (ΔG^0), activation energy ($\Delta G^{\neq}$) and reorganization energy (λ) are also indicated in the diagram.*

As can be seen in the figure, the photoexcited D*-A state is higher in energy than the CSS, thus there is a driving force for this electron transfer reaction to occur. To reach the CSS, the transition state (which is the intersection between the potential energy surfaces) needs to be crossed, and for this, an activation energy ($\Delta G^{\neq}$) is often required. The surrounding solvent molecules moreover need to rearrange following the ET, since they initially are organized with respect to the D*-A surface. This also requires energy which is called the reorganization energy (λ). The rate of electron transfer (k_{ET}) can be expressed in terms of the activation and reorganization energy together with the electronic transmission coefficient (κ_{el}), the nuclear motion (ν_{el}), Boltzmann's constant (k_B), the temperature (T) and the driving force (ΔG^0) as

$$k_{ET} = \kappa_{el}\nu_n \exp - \left(\frac{(\lambda+\Delta G^0)^2}{4\lambda k_B T}\right) \qquad (2.7)$$

By examining this equation, it is possible to identify three different regions for the electron transfer which are illustrated in Figure 2.5. The first region is called the normal region (left part of the figure), and in this region an increase in the driving force increases the rate of electron transfer. The second region (middle part of the figure) is the activationless region and represents the maximum electron transfer rate. The third region (right part of the figure) is called the inverted region, here the rate of electron transfer decreases with increasing driving force.[76, 81]

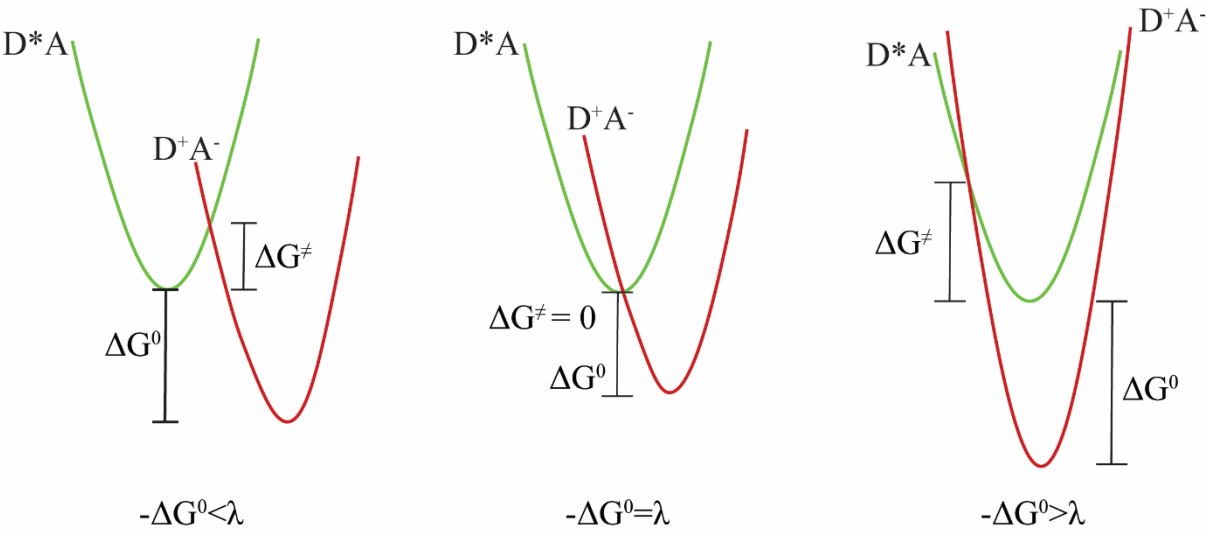

Figure 2.5. Potential energy surfaces illustrating the different regions in the Marcus theory of electron transfer. Left: normal region, center: activationless region, right: inverted region.

PET in molecular systems can occur both intra- and intermolecularly. In addition to occurring in molecular systems, PET can also occur in heterogenous assemblies between for example semiconductors and immobilized molecules.[82] If the excited state oxidation potential of an immobilized molecule is higher in energy than the CB, an electron can be transferred from the molecule into the CB[83], this process is generally referred to as electron injection.[84] Similarly, electrons can be transferred back to the now oxidized

molecule, this is called interfacial charge recombination. Further, electron transfer from the CB to an immobilized molecule resulting in a reduction of the molecule can occur if the CB energy lies above the reduction potential of the molecule.[85-87]

2.2.3 Photoinduced Isomerization

Some molecules can undergo conformational changes upon photoexcitation that results in reversible changes in the absorption spectra of the molecules, these molecules are called photochromic molecules and the process is referred to as photoisomerization.[45, 54, 88, 89] The photoisomerization process between an initial isomer (A) and a metastable isomer (B) can be written as

$$A \underset{h\nu_2/\Delta}{\overset{h\nu_1}{\leftrightarrows}} B \tag{2.8}$$

In some photochromic molecules, both the forward and reverse reaction can be triggered by irradiation with light of different wavelengths ($h\nu_1$ and $h\nu_2$, respectively), whereas in some molecules the initial state can only be regenerated thermally. Both certain organic molecules such as azobenzene[90], spiropyran[91] and diarylethene[92] display photochromism as well as a few metal complexes such as ruthenium sulfoxide complexes.[89, 93, 94] The quantum yield of photoisomerization[95] from A to B is defined as

$$\phi_{A\rightarrow B} = \frac{\#isomerized\ molecules}{\#absorbed\ photons} \tag{2.9}$$

When both the isomerization from A to B and from B to A can be triggered by light, the photostationary distribution (PSD) from irradiation with a certain wavelength depends on both the forward and reverse quantum yield of photoisomerization as well as on the molar absorptivity of the isomers at the wavelength of irradiation as

$$PSD(\lambda) = \frac{[A]}{[B]} = \frac{\varepsilon_{B\lambda}\phi_{B\rightarrow A}}{\varepsilon_{A\lambda}\phi_{A\rightarrow B}} \tag{2.10}$$

where λ is the wavelength of irradiation, ε_λ is the molar absorptivity of the isomers at that wavelength and ϕ is the quantum yield of photoisomerization.

2.3 Spectroscopic Techniques

In this work, spectroscopic methods have been used to characterize photoinduced processes in molecular/inorganic materials. Below follows a brief description of the methods used herein.

2.3.1 Steady-State Absorption Spectroscopy

The absorption spectra of molecules and materials reveal which wavelength of light that is absorbed, and thus which wavelengths that upon irradiation can result in photoinduced processes. To characterize the absorption properties of molecules and materials, steady-state absorption spectroscopy is used and the experimental setup for this is illustrated in Figure 2.6. Light from a white-light source is passed through the sample at different wavelengths, which are selected by a monochromator. The intensity of the light before (I_0) and after (I) the sample at each wavelength is measured and used to create the absorption spectrum.

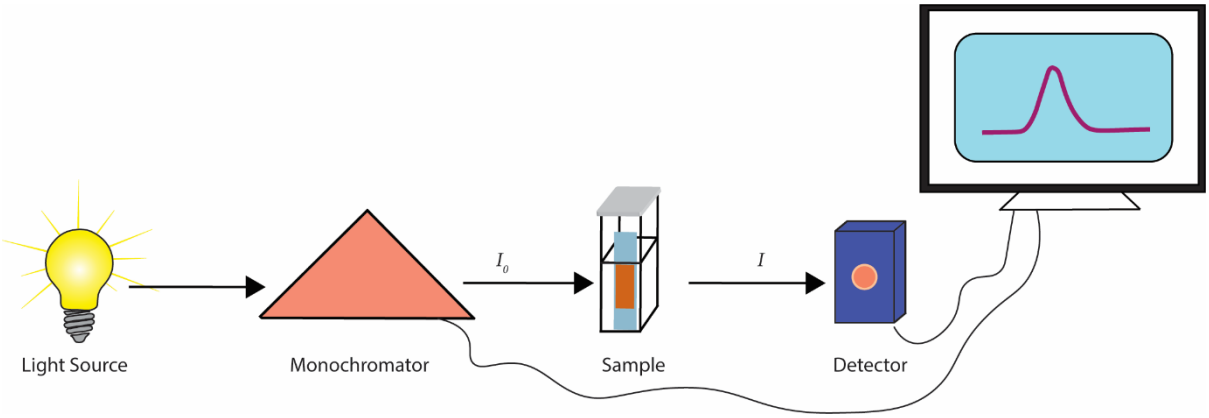

Figure 2.6. Schematic illustration of the experimental setup used for recording an absorption spectrum.

According to *Lambert-Beers law*, the absorbance (A_λ) of a molecule at a certain wavelength is directly proportional to the pathlength (l), concentration (c) and molar absorptivity of the molecule at that wavelength (ε_λ) as

$$A_\lambda = \log\frac{I_0}{I} = \varepsilon_\lambda c l \qquad (2.11)$$

The molar absorptivity, usually presented in $M^{-1}cm^{-1}$, is related to the probability for a transition between two electronic states to occur. Thus, a higher ε means a higher probability of absorbing photons, and in principle this value is used to characterize the light-harvesting ability of molecules.

2.3.1.1 Steady-State Absorption-Coupled Photolysis

By coupling an external excitation source to steady-state absorption measurements, spectral changes following continuous irradiation can be monitored. During these measurements, the absorption spectra is recorded as a function of time during the irradiation time, and processes such as photoisomerization can be characterized.

2.3.2 Transient Absorption Spectroscopy

To study photoinduced processes and their kinetics, transient absorption (TA) spectroscopy is often used. Here, a laser pulse is used to promote a sample into an excited state, and the differential absorption (ΔA) between the absorption with (A_{p+}) and without (A_{p-}) the excitation pulse is measured as a function of wavelength and time.

$$\Delta A = A_{p+} - A_{p-} \tag{2.12}$$

In principle, ΔA represents the difference in absorption between the excited state and the ground state. Positive features in the spectra (excited state absorption) occur when the absorption of the excited state is larger than the absorption of the ground state, and negative features can originate from either emission or when the excited state has a smaller absorption than the ground state (ground state bleach). Typically, the measurements are done in several time-steps following the excitation pulse and this can be used to construct a ΔA spectra as a function of time.

Depending on the process of interest, either femtosecond (fs) or nanosecond (ns) TA have been used in this work. The main difference between these two are the pulse width and this is also what determines the time resolution of the measurement. The experimental setups for these two techniques are somewhat different and will be described below.

2.3.2.1 Femtosecond Transient Absorption Spectroscopy

In fs-TA experiments, ultrafast processes that occur in the picosecond to nanosecond timescales after photoexcitation can be monitored. Ultrafast processes like solvent reorganization, stimulated emission and formation of a charge separated state can be characterized and at these timescales a correction for the group value dispersion (GVD) is also necessary. A schematic illustration of the experimental setup used in this work is shown in Figure 2.7. Ultrashort pulses (800 nm, 80 MHz) are initially generated by a femtosecond Ti:Sapphire laser, and these are amplified in a regenerative amplifier (where they are used as the seed beam) using another laser as the pump laser. The resulting pulses are approximately ~200 fs wide with an energy of ~0.5-0.8 mJ (1 kHz) in our system.

After the amplifier, the beam is split into a pump and a probe beam. The probe beam is passed through a moving CaF_2 plate to generate a white-light continuum and is then split into a probe and reference beam before passing through the sample. The pump beam is directed through an optical parametric amplifier (OPA) where the desired excitation wavelength can be obtained and is then passed through a chopper to block every other pulse. The pump beam is subsequently delayed in time relative to the probe beam by changing the path-length with a delay stage (0-10 ns), and finally overlapped with the probe beam at the sample. The probe and reference beams are then directed into optical fibers which are connected to a CCD camera, and from the recorded spectra with and

without the pump, a ΔA spectra can be obtained. By recording ΔA at several different pump-probe delays, the spectra as a function of time is constructed.

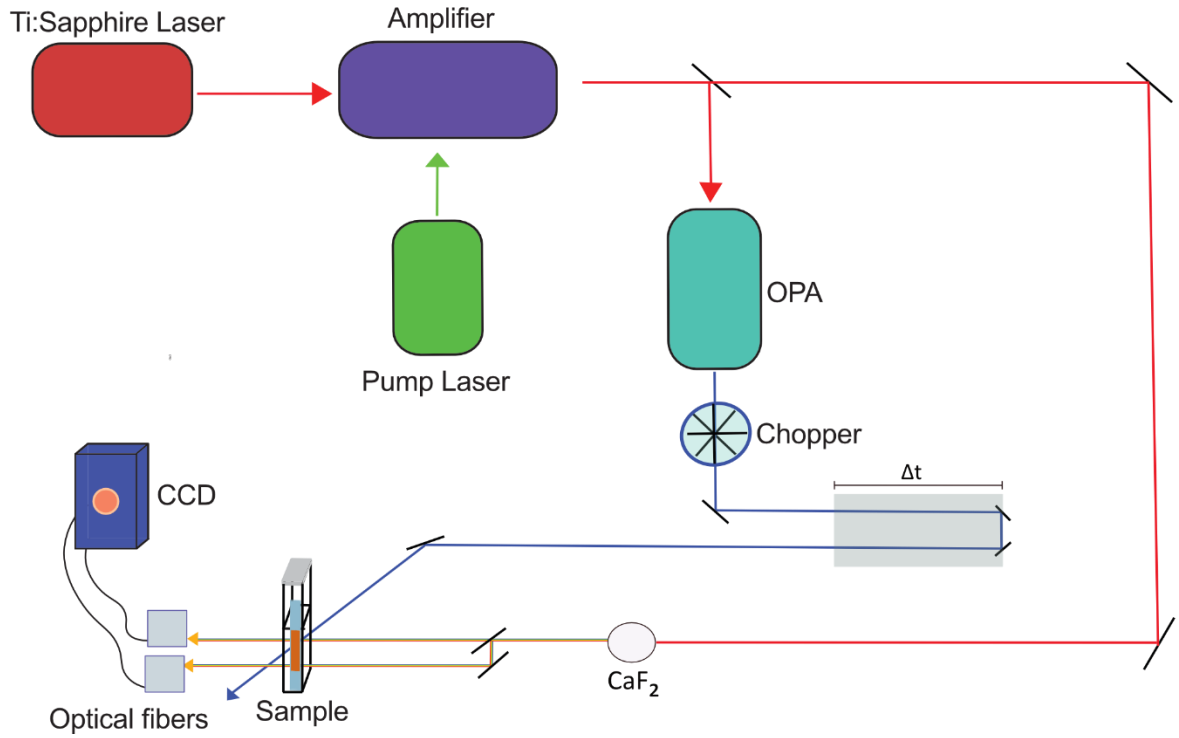

Figure 2.7. Schematic illustration of the experimental setup for fs-TA experiment used in this work.

2.3.2.2 Nanosecond Transient Absorption Spectroscopy

When the kinetics of the photoinduced processes of interest are hundreds of nanoseconds to micro- or milliseconds, for example the kinetics of interfacial charge recombination from the CB of semiconductors to immobilized photosensitizers, ns-TA experiments are used. The experimental setup for this used herein is illustrated in Figure 2.8. The excitation pulse is generated with a Nd:YAG laser (1064 nm, ~7-10 ns). By third harmonic generation of the fundamental beam, pulses of 355 nm are used in an optical parametric oscillator (OPO) to generate the desired pump wavelength.

The probe light is a continuous lamp placed perpendicular to the excitation beam, and the pump is overlapped with the probe light at the sample. The absorbance of the sample is measured using the probe light with and without the excitation pulse, and depending on the detector used, a ΔA spectra (by using a CCD camera) or a plot of ΔA vs time at a specific wavelength (by using a PMT or photodiode detector and selecting the probe wavelength with monochromators) is recorded.

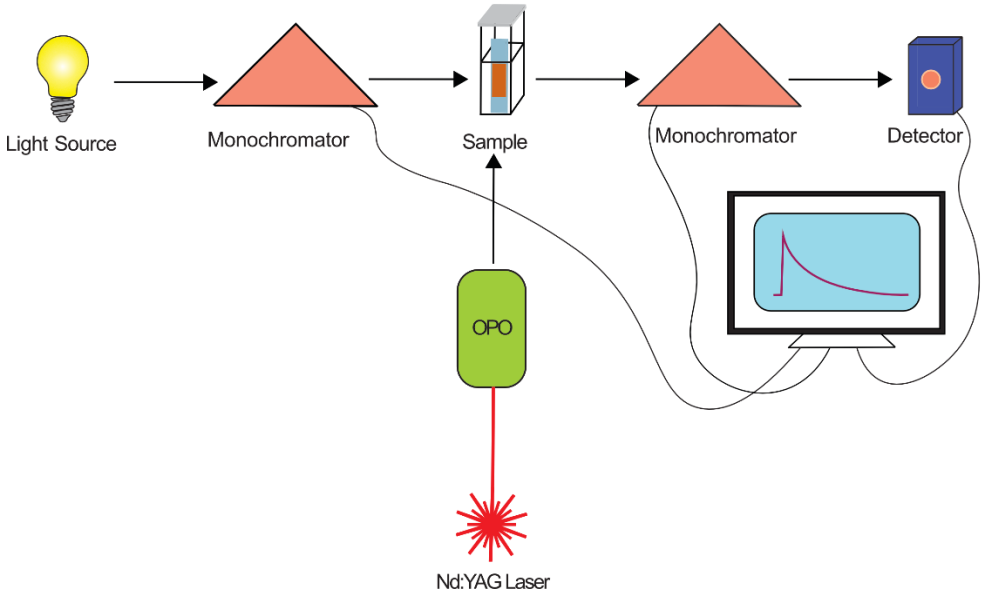

Figure 2.8. Schematic illustration of the experimental setup for ns-TA experiment using a PMT detector to record ΔA vs time at a specific wavelength.

2.3.3 Steady-State Emission Spectroscopy

To record an emission spectrum of a sample, steady-state emission spectroscopy is used, and the experimental setup for this used herein is illustrated in Figure 2.9. The excitation light is obtained from a Xe-arc lamp and the excitation wavelength is selected by a monochromator. The emission is detected with a PMT (with another monochromator to select the wavelength) which is situated perpendicular to the excitation light. The emission spectrum is obtained by scanning the detected emission at different wavelengths. An excitation spectrum can be obtained in a similar way by instead scanning the emission from different excitation wavelengths.

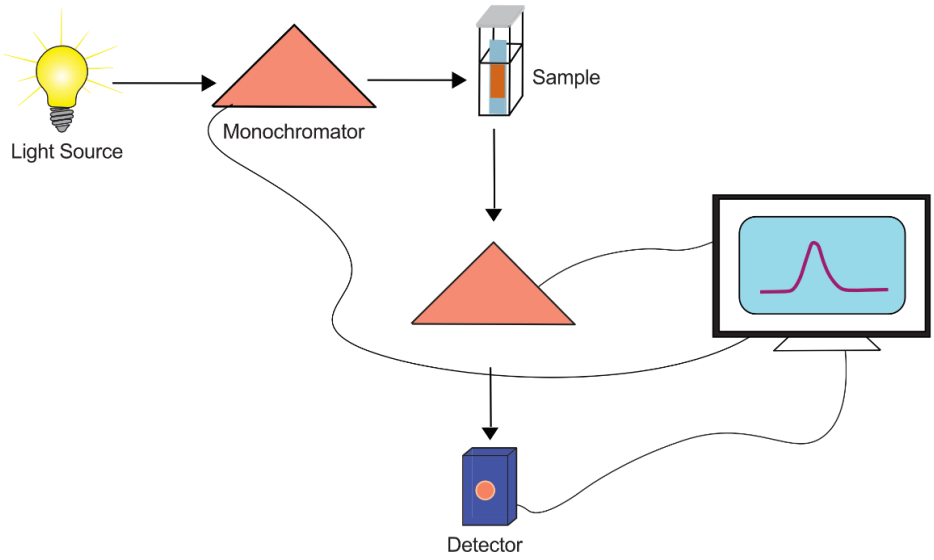

Figure 2.9. Schematic illustration of a spectrofluorometer used for recording an emission spectrum.

2.3.4 Time-Resolved Emission Spectroscopy

Time-resolved emission spectroscopy can be used to characterize the emission lifetime of a sample. In this work, time correlated single photon counting (TCSPC) was used to measure fluorescence lifetimes and the experimental setup for this is illustrated in Figure 2.10. Like in steady-state measurements, the detector (PMT) is placed perpendicular to the excitation source. A pulsed diode laser is used to excite the sample and as is apparent from the name, a single photon is detected from each excitation pulse. For each detected photon, the time between the excitation pulse and the emitted photon is measured and placed in channels with specific time intervals. The measurement is continued until enough photons are collected in the top channel (usually 5000 or 10000) for statistical reasons.

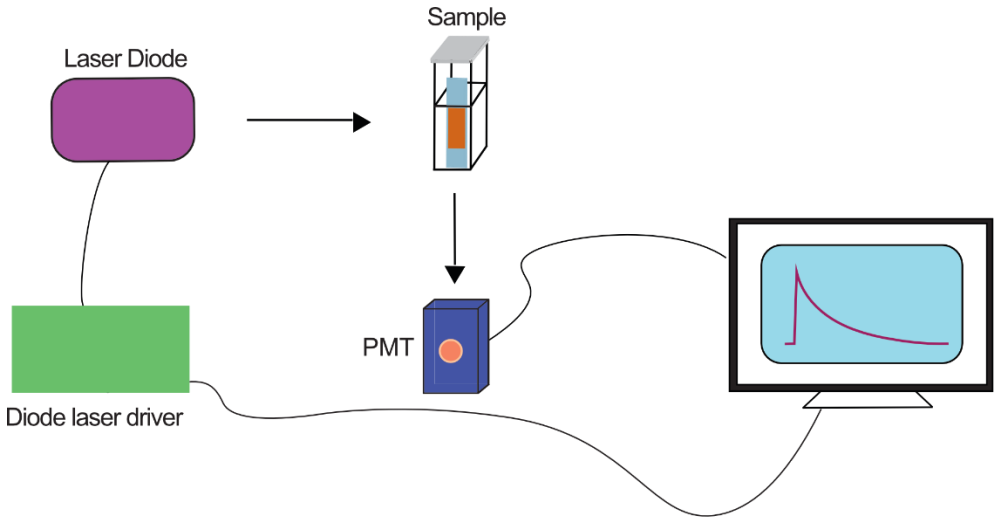

Figure 2.10. Schematic illustration of the experimental setup for TCSPC measurements.

3 Design of Molecular/Inorganic Materials - From Light to Useful Energy

In this Chapter, I will introduce some applications of molecular/inorganic materials and provide a background to the research presented herein. I will also present the specific molecular/inorganic materials that are designed and studied within this work and motivate the choice of these. All the materials used herein are based on molecules immobilized onto thin films of mesoporous wide band-gap semiconductors, and therefore I will start by briefly introducing these in general followed by a more specific description of some potential applications and the individual materials.

Mesoporous wide band-gap semiconductor films consist of a porous network of semiconductor nanoparticles with individual diameters of ~5-25 nm which are sintered together. The mesoporous films are typically coated on a glass substrate with a thickness between 2-6 μm. The porous nanoparticle network results in films with a high surface area, making them ideal substrates for applications where high surface coverages are desired since several molecules can be attached close to each other in the porous network.[47, 96, 97]

Molecules can be immobilized onto mesoporous semiconductor films *via* binding groups such as carboxylic acid or ester groups. The majority of the surface binding is described as covalent with the oxygen atoms in the binding groups forming bonds to the metal atoms in the semiconductor.[98] A schematic illustration of a semiconductor film with immobilized molecules is shown in Figure 3.1.

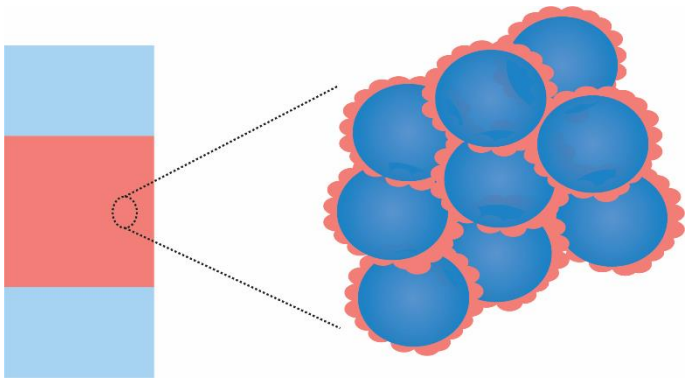

Figure 3.1. Schematic illustration of a mesoporous semiconductor film with dye molecules (illustrated as red circles) attached to the nanoparticles in the film (illustrated as blue circles).

3.1 Dye-Sensitized Solar Cells Combined with Singlet Fission

The most common application of molecular/semiconductor materials is for electricity generation in dye-sensitized solar cells (DSSC). Here, dye molecules (photosensitizers) are immobilized onto a mesoporous semiconductor thin film (usually TiO_2). The dye molecules can either be metal complexes or organic molecules that absorb light in the visible region, thus allowing for a larger part of the solar spectrum to be utilized. Ideally, the absorption spectrum of the dye should match the solar spectrum. Moreover, the excited state oxidation potential of the dye needs to be higher in energy than the CB of the semiconductor to have a driving force for the initial charge injection. The dye-sensitized semiconductor film is coated on a conductive glass and used as the photoanode in the solar cell.[59, 99-101]

The working principle of a dye-sensitized solar cell is illustrated in Figure 3.2a. When the dye absorbs light, electrons are injected from the photoexcited dye into the CB of the semiconductor *via* PET. The electron injection typically occurs fast and efficiently with a quantum yield close to unity.[99, 102-104] After the injection, electrons are transferred through the mesoporous film to the conductive glass and then to an external circuit to generate electricity. The electrons eventually reach the counter electrode, and the oxidized dye is regenerated by a redox mediator in the surrounding electrolyte solution, closing the circuit.[59, 99-101] The efficiency of DSSCs depends on both the generated photocurrent, which is determined by the overlap between the absorption spectrum of the dye and the solar spectrum, as well as on the open circuit voltage that is determined by the energy difference between the redox mediator and the CB level of the semiconductor.[59, 105]

One possible way of increasing the photocurrent in dye-sensitized solar cells and utilize a larger part of the solar spectrum is to incorporate a singlet fission molecule as the dye.[106, 107] By incorporating a SF dye on the photoanode, one incident high energy photon can result in two charges in the solar cell, if both the created triplets inject an electron[108-111], as is illustrated in Figure 3.2b. If a SF dye that absorbs the high-energy photons is

combined with an ordinary dye, the theoretical conversion efficiency of dye-sensitized solar cells increases from 32% to 46%.[106]

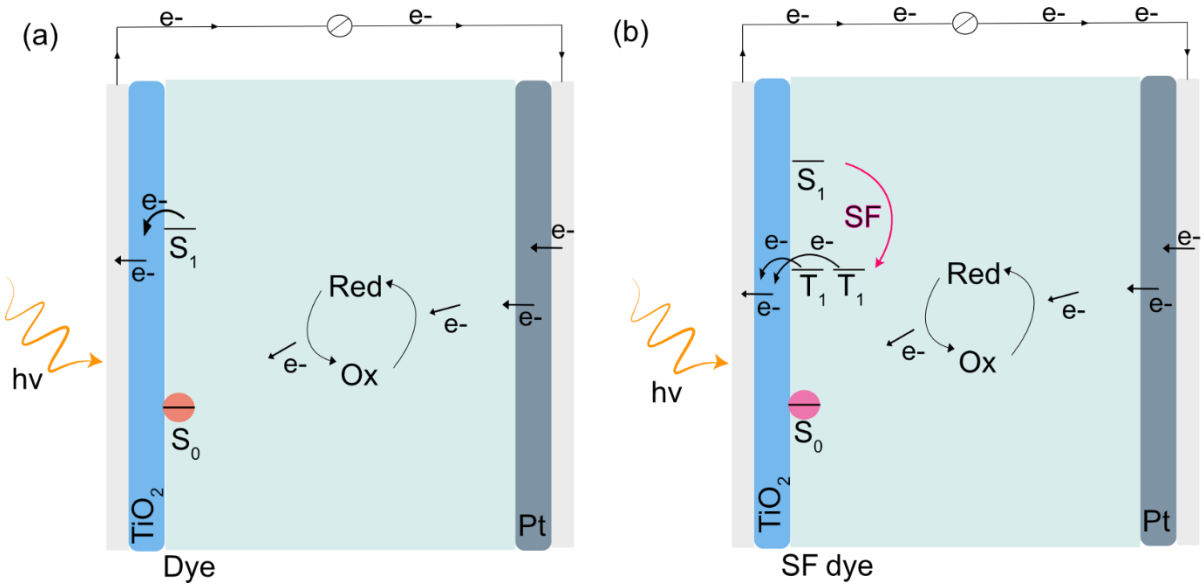

Figure 3.2. Schematic illustration of (a) a dye-sensitized solar cell and (b) a dye-sensitized solar cell with a singlet fission dye.

At a first glance, combining dye-sensitized solar cells with singlet fission molecules might appear to be straightforward. There are however several challenges that need to be overcome before an efficient solar cell based on this concept can be realized. Firstly, the singlet fission molecules need to attach to the mesoporous film in a geometry that facilitates a favourable coupling between the molecules. Secondly, competing electron injection from the singlet excited state as well as triplet-charge recombination needs to be prevented.[107] Previous studies have shown that SF can occur on mesoporous surfaces[108, 110] and lead to increased photocurrents[108, 111] and an injection yield of above 100%[109]. The efficiencies of these systems are however far from what is theoretically possible, and a mechanistic understanding is lacking. It appears as if attaching molecules that display an efficient SF in other environments onto semiconductor surfaces reduces the SF efficiency and results in limited dissociation of and injection from the created triplets.[110] These observations prompted us to study the SF and injection dynamics of singlet fission molecules attached to semiconductor surfaces in more detail.

3.1.1 DPIBF/Semiconductor Materials for Singlet Fission and Triplet Injection

In this work, we synthesized derivatives of the well-known SF molecule DPIBF[18] that can be immobilized onto mesoporous semiconductor surfaces. We chose to work with DPIBF derivatives since the parent molecule is a well-studied SF molecule[18, 63, 112-116] that displays a high quantum yield of SF[18], the effect on the SF dynamics from immobilization onto the surfaces can therefore be studied. Moreover, other DPIBF derivatives have been shown to undergo SF when attached to surfaces.[108] For example, Johnsson and co-

workers have previously studied a DPIBF derivative with a carbon chain terminated with a carboxylic acid group attached to core-shell photoanodes with a TiO_2 core and a ZrO_2 shell.[111] They observed a small increase in photocurrent with an increase in shell thickness, which is expected if triplet injection occurs following SF. Subsequent to this, Hanson and co-workers synthesized a dicarboxylated DPIBF derivative and studied both the photocurrent attached to TiO_2-Al_2O_3 core-shell photoanodes as well as the photoinduced processes of the molecule attached to ZrO_2.[108] They also observed an increase in the photocurrent with an increase in the shell thickness of the core-shell photoanodes.[108] Further, their studies revealed that the photoinduced processes of the DPIBF derivative attached to ZrO_2 were highly complex and that excimer or molecular charge separated states were formed upon photoexcitation of the assembly in acetonitrile.[108] In accordance with previous studies of DPIBF dimers, a possible charge separated state could either facilitate for SF if the molecules are strongly coupled[113, 117] or act like a loss channel if they are weakly coupled[113, 114]. These observations, together with the fact that the observed efficiencies of the core-shell assemblies were rather low, prompted us to study the photoinduced processes of DPIBF attached to semiconductor surfaces further and in different environments.

Here, the photoinduced processes that occur when a DPIBF derivative is attached to semiconductor surfaces were characterized in solvents of different polarities. This was done to study if the photoinduced processes display a polarity dependence and to elucidate the role of a possible molecular charge separated state in the SF process. The derivative synthesized herein has a flexible carbon linker (six carbons) terminated with a carboxylic acid group for the binding to the surface; this derivative is hereafter referred to as DPIBFC6.[118] The idea with the carbon linker was both to facilitate for a flexible packing on the surface so that the molecules can rotate somewhat freely, and to slow down a fast injection from the S_1 state to allow time for the SF process. A schematic illustration of DPIBFC6 attached to a nanoparticle is shown in Figure 3.3a. To study if the length of the carbon chain affects the photoinduced processes, a derivative with a five-carbon linker was also synthesized. The photoinduced processes in both derivatives were however identical, which suggests that minor differences in the carbon chain length has no effect on the photoinduced processes that occurs on the surfaces. Therefore, only the results from photoexcitation of DPIBFC6 will be presented herein.

DPIBFC6 was attached to three different semiconductors with varying CB energy levels; ZrO_2, TiO_2, and SnO_2. The molecule was studied attached to the different semiconductors to characterize the effect on the SF and injection dynamics from varying the driving force for injection. ZrO_2 has a CB energy higher than the S_1^*/S_1^+ state of DPIBFC6, thus neither singlet nor triplet injection is expected to occur, making it possible to exclusively monitor the SF process. TiO_2 has a CB energy below the energy of the S_1^*/S_1^+ state and similar in energy to the T_1^*/T_1^+ state, thus singlet injection is energetically possible and triplet injection should also be considered. Finally, the CB of SnO_2 is below both the S_1^*/S_1^+ state and the T_1^*/T_1^+, making both singlet and triplet injection energetically possible. The CB

energy levels of the semiconductors[119, 120] together with the oxidation potential of the S_1 and T_1 state of DPIBFC6[118] are summarized in Figure 3.3b.

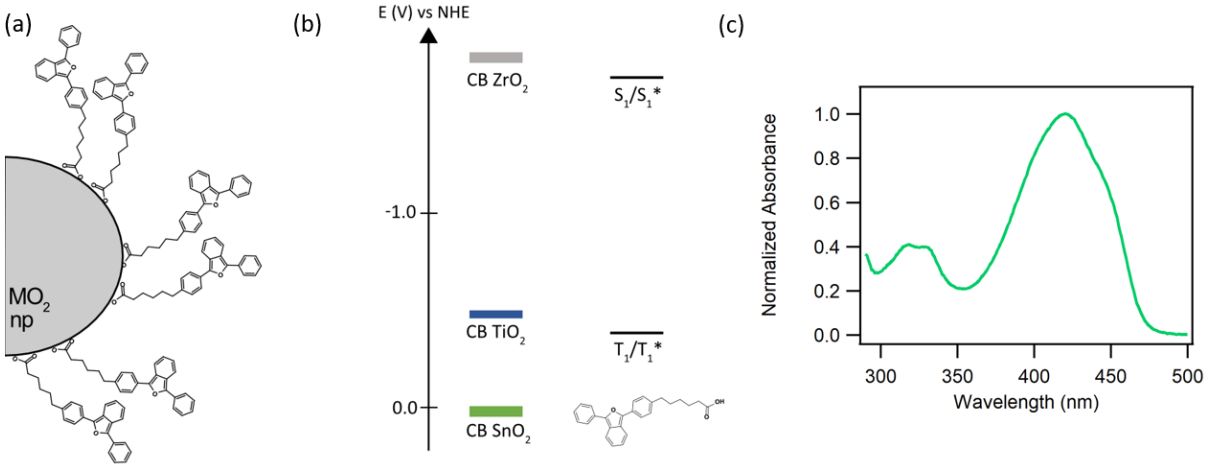

Figure 3.3. (a) Schematic illustration of DPIBFC6 attached to a semiconductor nanoparticle, (b) CB energy levels of ZrO_2, SnO_2 and TiO_2 together with the oxidation potential of DPIBFC6 in the singlet and triplet excited state and (c) absorption spectrum of DPIBFC6 attached to ZrO_2.

The absorption spectra of the molecule attached to the different semiconductors look essentially identical to each other, with a slight broadening compared to in solution. The absorption spectrum of DPIFC6 attached to ZrO_2 is shown in Figure 3.3c. The results from photoexcitation of these materials revealed some interesting differences and a polarity dependence which will be presented in Chapter 4.

3.2 Photoisomerization on Films

Another possible application of molecular/semiconductor materials, which is not as extensively studied, is as photoswitchable solid films that display spatial addressability. Achieving photoisomerization with spatial addressability is necessary for many applications, such as logic gates or memory storage.[121] Previously, organic photochromic molecules have been modified in different ways or incorporated in matrixes to make photoisomerization attached to surfaces possible.[121-128] These approaches are however often limited to monolayers of molecules on flat surfaces, which results in relatively low surface coverages and low signals.

Utilizing photochromic metal complexes attached to mesoporous semiconductor films could provide some advantages compared to using organic molecules on flat surfaces. Metal complexes are for example relatively easily synthetically tuned by varying the ligands, and the porosity of the mesoporous films allows for a significantly higher surface coverage compared to when flat surfaces are used as the substrate. Molecules that are immobilized onto semiconductor surfaces also usually keep their ground-state properties in terms of absorption, and the molecules can rotate somewhat freely after immobilization.[129] Thus, photochromic molecules are expected to keep at least some of

their solution properties following immobilization onto semiconductor films. Immobilizing photochromic molecules onto semiconductor surfaces can therefore be a straightforward way of making solid state photoswitchable materials based on molecules that previously have been studied in solution.

3.2.1 Design of a Ru-Sulfoxide/ZrO_2 Photo-Responsive Material

In this work, we used a mesoporous ZrO_2 film as the substrate when designing a molecular/semiconductor film that can display two-color photoisomerization. ZrO_2 was used since it has a high CB energy level that prevents excited state interactions (such as electron injection) between immobilized photoexcited molecules and the CB.[130-132] Further, the mesoporous ZrO_2 film is semitransparent, which makes optical detection possible.

When designing the photo-responsive film, we synthesized a photochromic ruthenium(II) sulfoxide complex, $[Ru(deeb)_2PySO\text{-}iPr]^{2+}$ (deeb is 4,4'-diethylester 2,2'-bipyridin and PySO-iPr is 2-((isopropylsulfinyl)methyl)pyridine), which can be attached to semiconductor surfaces.[133] Ruthenium sulfoxide complexes are a well-known and extensively studied type of photochromic molecules that undergo S-to-O linkage isomerization upon metal to ligand charge transfer (MLCT) excitation in liquid solutions.[89, 93, 94, 134-139] In most of these complexes, the back isomerization from the O-bonded isomer to the S-bonded form occurs only thermally and the O-to-S isomerization is typically insensitive to irradiation with light. A few years ago however, the Rack group synthesized a ruthenium sulfoxide complex, $[Ru(bpy)_2PySO\text{-}iPr]^{2+}$ (bpy is 2,2'-bipyridine), that displays reversible photoisomerization where both the S-to-O and O-to-S isomerization can be triggered by light[138, 140], something that is rare in metal complexes[93, 135, 138]. The complex synthesized herein is a modified version of this complex with the previously used sulfoxide ligand combined with deeb-ligands to allow for immobilization onto semiconductor surfaces *via* diethyl ester groups.

The ruthenium sulfoxide complex studied herein attaches successfully to ZrO_2 films, and the obtained surface coverage (~50 nmol/cm^2) is approximately 200 times higher than what is obtained for a monolayer on a flat surface.[123] The absorption spectrum of the complex attached to the film is similar to in liquid solution, which suggests that no ground-state interactions between the immobilized molecules occur. A schematic illustration of the thermodynamically stable S-bonded isomer of $[Ru(deeb)_2PySO\text{-}iPr]^{2+}$ attached to a ZrO_2 surface together with the absorption spectrum of the assembly is shown in Figure 3.4. The isomerization processes following photoexcitation of the complex in liquid solution and attached to ZrO_2 will be presented in Chapter 5.

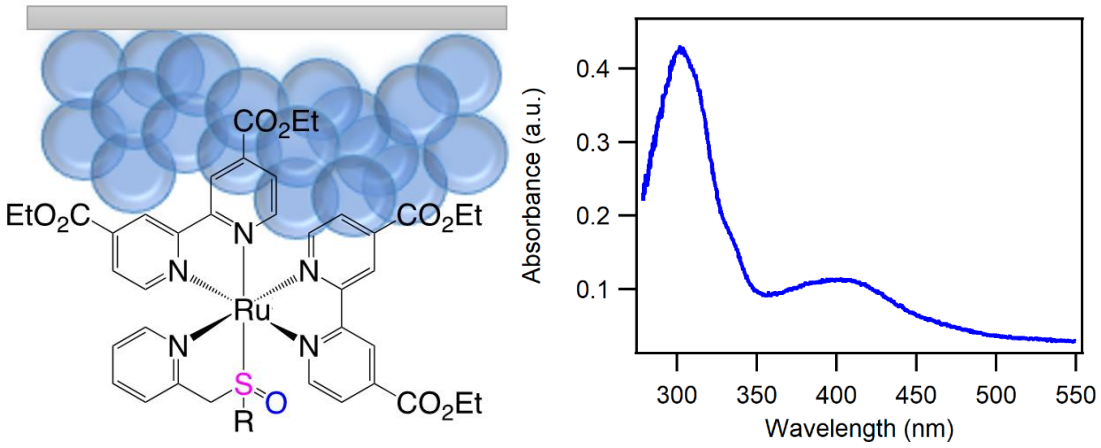

Figure 3.4. Left: Schematic illustration of $[Ru(deeb)_2PySO\text{-}iPr]^{2+}$ attached to ZrO_2 nanoparticles (R=i-Pr), right: Absorption spectrum of a $Ru(deeb)_2PySO\text{-}iPr/ZrO_2$ film. Adapted with permission from ***Paper II***[133].

3.3 Dye-Sensitized Photocatalytic Materials

A third possible application for molecular/inorganic materials is as photocatalytic assemblies that can produce solar fuels. As mentioned in the introduction, solar fuels have been generated in pure inorganic systems by irradiation with UV-light.[35] By using dye-sensitized semiconductor materials instead, the visible part of the solar spectrum can also be utilized. Moreover, in hybrid materials it is possible to use a molecular catalyst that is designed for a specific reaction, which can increase the efficiency and selectivity of the desired reaction.

There are a few different hybrid molecular/inorganic materials based on dye-sensitized semiconductors that can be used for solar fuel generation. The most common is the dye-sensitized photoelectrosynthesis cell (DSPEC), in which the solar-fuel reactions are split into two different half-cells.[141, 142] Oxidation of water occurs at the photoanode, which usually consists of a dye-sensitized TiO_2 film coupled to a catalyst active for oxidation of water. The reduction reaction, for example reduction of carbon dioxide, takes place at the photocathode, which usually consists of platinum or a dye-sensitized p-type semiconductor.[39, 141] DSPEC assemblies have been used for solar fuel generation[39, 43, 141, 143-146], however with limited efficiencies and/or stabilities.

Another possibility of generating solar fuels is *via* dye-sensitized photocatalysis (DSP) assemblies. In DSP assemblies, the dye and catalyst molecules are co-attached onto semiconductor nanoparticles, and the CB is used as a mediator for transferring electrons between the dye and the catalyst.[147-150] DSP assemblies take advantage of the ability of semiconductor nanoparticles to store electrons in their CB and transfer the electrons to co-attached molecular catalysts.[151, 152] The electron transfer processes in DSP assemblies involves electron injection from photoexcited dye molecules into the CB followed by CB mediated electron transfer to molecular catalysts, these events are illustrated in Figure 3.5.

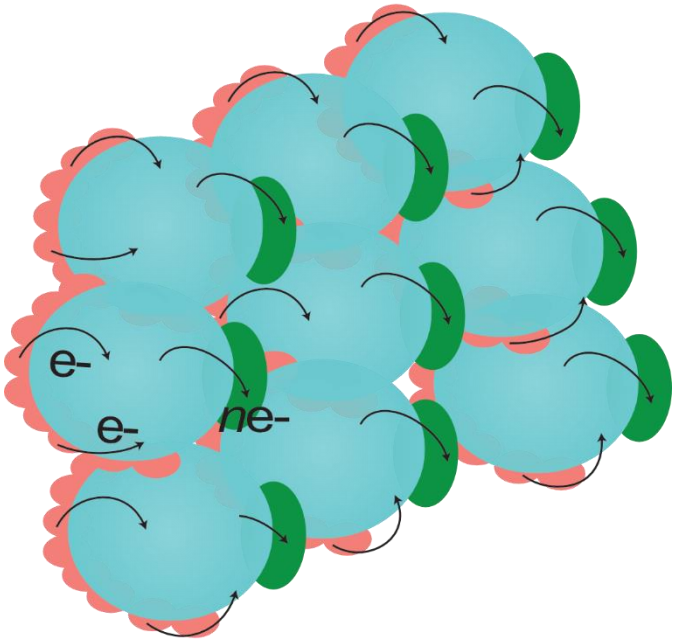

Figure 3.5. Illustration of the electron transfer events upon photoexcitation of DSP assemblies. After photoexcitation of the dye molecules (illustrated as pink circles) electrons are injected into the semiconductor nanoparticles (illustrated as blue circles) and transferred via the CB to molecular catalysts (illustrated as green circles).

After at least two electrons have been transferred to the catalyst, the reduction reaction can take place at the reduced molecular catalyst. Different types of DSP assemblies have been successfully used for both reduction of protons into hydrogen gas and carbon dioxide into carbon monoxide by using sacrificial donors to regenerate the dye, the efficiencies of these systems are however low, and a complete mechanistic picture is missing.[147, 153-157]

3.3.1 Molecular/Semiconductor Materials for a Long-Lived Charge Separation

In dye-sensitized photocatalytic assemblies, charge recombination from the CB to the oxidized dye becomes a significant loss channel[146, 158] as opposed to in DSSCs where this often is negligible[159]. The reason for this is that in solar fuel-generating assemblies, the lifetime of the charge separated state needs to be long enough to allow for multi-electron transfer events to occur as well as to match the turn-over frequencies of the fuel forming reactions.[47]

In this work, two strategies for extending the charge separated lifetime in dye-sensitized materials were explored. In the first approach, the photoisomerizable ruthenium sulfoxide complex described above was used as the photosensitizer with the hypothesis that the O-bonded isomer could stabilize and increase the lifetime of the charge separated state. In the second approach, a patterned SnO_2-TiO_2 film was designed with the aim of extending the charge separated lifetime by an electron transfer cascade through the film.

3.3.1.1 A Photoswitchable Photosensitizer

Ruthenium(II) sulfoxide complexes can, as mentioned earlier, undergo S-to-O linkage isomerization upon MLCT excitation. In addition to the photoinduced isomerization, S-to-O isomerization can also be triggered electrochemically in many of these complexes by oxidation of the ruthenium center.[94] Thus, O-bonded ruthenium sulfoxide complexes can be described as more stable in the Ru^{III} oxidation state. Given this, we questioned whether charge injection from the photoexcited ruthenium sulfoxide complex into the CB of for example TiO_2 can occur, and if this can result in an extended charge separated lifetime from the O-bonded isomer that is stable in the Ru^{III} state. To study this, the same ruthenium sulfoxide complex that was described in section 3.2.1. was immobilized onto TiO_2 surfaces since that should result in a driving force for electron injection into the CB of TiO_2. The ruthenium sulfoxide complex however displayed a limited ability to inject electrons into the CB of TiO_2, this together with the photoisomerization on TiO_2 will be further discussed and presented in Chapter 6.

3.3.1.2 Design of a Patterned SnO_2-TiO_2 Photoanode

To explore the possibility of extending the charge separated lifetime by designing a semiconductor film, we prepared a patterned SnO_2-TiO_2 film. The patterned film was inspired by previously studied core-shell structures consisting of a core of SnO_2 and a thin shell of TiO_2 to slow down charge recombination and increase the efficiencies of DSPEC assemblies.[143, 160-163] These core-shell structures utilizes the CB energy level alignment between the two semiconductors (with the CB energy level of SnO_2 being ~0.4 V below that of TiO_2)[120] to create a barrier for the back-electron transfer. Depending on the thickness of the shell, the core-shell structures have resulted in an increase of the charge separated lifetime by up to three orders of magnitude.[163]

Taking inspiration from the core-shell assemblies, we designed a patterned SnO_2-TiO_2 film with μm thick stripes of TiO_2 deposited on a SnO_2 film. The stripes were selectively sensitized with dye molecules, leaving dye-free SnO_2 parts where electrons can be accumulated and molecular catalysts can be attached.[164] The cross section of a patterned film together with the possible electron transfer events is illustrated in Figure 3.6.[164] The idea behind this design was both to take advantage of the CB energy alignment between the semiconductors to prevent back-electron transfer and create an electron transfer cascade[165, 166] as well as to allow for co-attaching molecular catalysts on the film. Moreover, by utilizing μm thick stripes of TiO_2, the high injection yield and fast electron injection on TiO_2 compared to SnO_2[167-169] can be preserved in the patterned film. Further, the high electron mobility in SnO_2 compared to TiO_2[170] could facilitate electrons being accumulated in the dye-free SnO_2 parts.

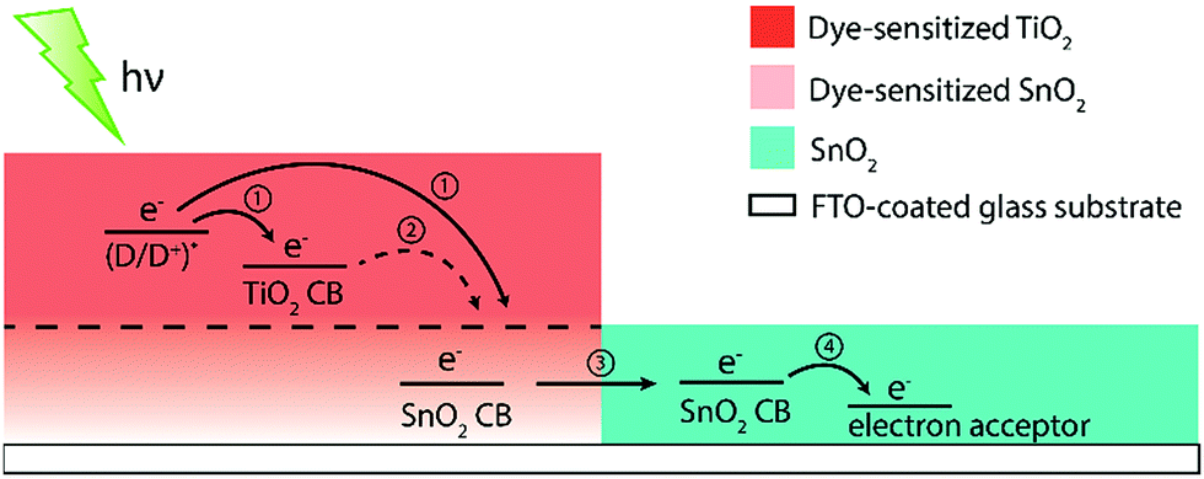

Figure 3.6. Cross section and emphasized electron transfer events in a patterned SnO_2-TiO_2 where the TiO_2 stripe have been selectively dye-sensitized. Reproduced from ***Paper III***[164] *with permission from the PCCP Owner Societies.*

An organic dye, D35, was used as the photosensitizer in the patterned films. This is a dye with a broad absorption in the visible region that displays an efficient and fast injection into the CB of TiO_2.[102, 171] The patterned design resulted in a significantly extended charge separated lifetime between the dye and the CB, this will be presented in Chapter 6.

3.3.2 Molecular/Semiconductor Materials for CB Mediated Electron Transfer

To generate solar fuels in DSP assemblies it is, as previously mentioned, important to achieve multi-electron transfer to the molecular catalyst in the assemblies. Achieving this is generally difficult, and in addition to a long-lived charge separated state between the dye and the semiconductor, control of and fundamental insights into the electron transfer processes from the CB to the catalyst is necessary. The low efficiencies in DSP assemblies have been attributed to a slow second reduction of the catalyst[172] and a lack of control over the electron transfer events[155]. Durrant and co-workers have investigated electron transfer processes from the CB to a molecular catalyst by measuring the lifetime of the electrons in the CB after band-gap excitation of catalyst/TiO_2 assemblies.[172] They concluded that the second reduction of the catalyst is orders of magnitudes slower than the first, and that most catalysts need to be singly reduced before the second reduction can take place. After this, they investigated how the multi-electron transfer events from the CB to the catalyst is affected by an applied bias or the light intensity used.[156] They found that multi-electron transfer to the catalyst is slow and that an applied potential or using high light intensities favors the multi-electron transfer events. Moreover, their study revealed that recombination to TiO_2 is a substantial loss pathway that needs to be prevented.

In the work presented herein, we were interested in studying the electron transfer events in molecular/semiconductor materials where both dye and catalyst molecules are co-attached to the surface. The focus in this work was limited to characterizing the electron

transfer processes, and for this purpose, a model catalyst was used together with the dye D35. The model catalyst used herein is a cobalt porphyrin, protoporphyrin IX cobalt chloride (CoPPIX), which is a suitable electron acceptor since it has two available redox states ($Co^{III/II}$ and $Co^{II/I}$) below the CB energy of TiO_2, Figure 3.7a, and one available redox state below the CB of SnO_2. Moreover, the spectra of the different redox states of CoPPIX have distinctly different features in the visible region, Figure 3.7b, making it possible to characterize the one- and two-electron reduction by optical spectroscopy.[173]

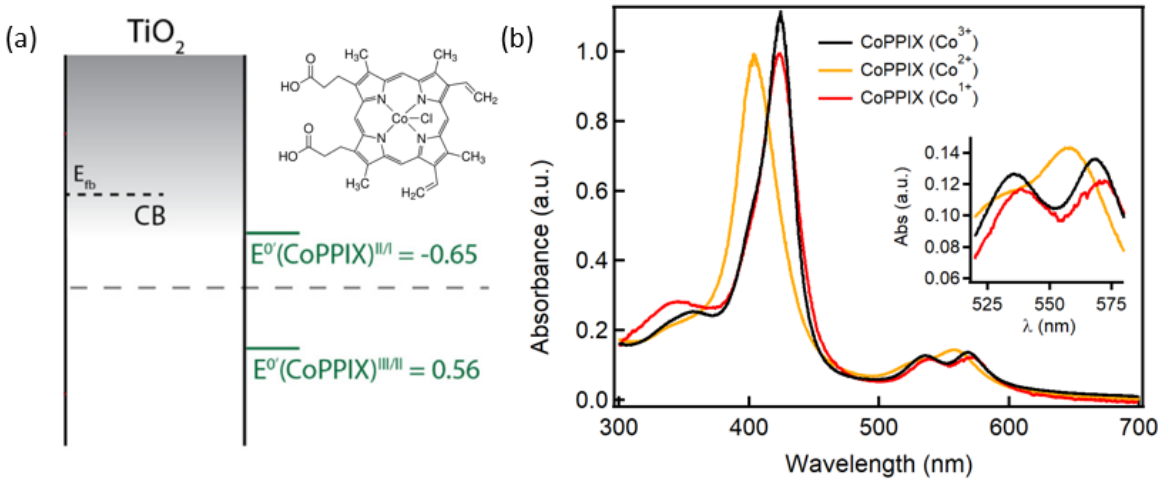

Figure 3.7. (a) Molecular structure and redox potentials for one- and two-electron reduction of CoPPIX (vs NHE) in relation to the CB energy level of TiO_2, where the dotted line represents the zero-line vs NHE (b) Absorption spectra of the different redox states of CoPPIX. Adapted with permission from ***Paper IV***[173]*. Copyright 2018 American Chemical Society.*

Two different types of samples were prepared and studied for this purpose. To study the potential of utilizing the patterned films in DSP assemblies, CoPPIX molecules were first selectively immobilized onto the dye-free SnO_2 parts in the patterned films. The electron transfer from SnO_2 to CoPPIX was then characterized, both from direct band-gap excitation of SnO_2 with UV-light and from visible light excitation of the dye molecules attached to the TiO_2 stripes in the patterned films. Since multi-electron transfer is crucial for generating solar fuels, we chose to work with TiO_2 films in addition to the patterned films, since the CB of TiO_2 allows for two-electron transfer to the catalyst. To study the electron transfer events from the CB of TiO_2 to CoPPIX, we prepared both TiO_2 films with only CoPPIX attached to the surface as well as co-sensitized TiO_2 films with dye and catalyst molecules co-attached to the surface. The electron transfer events from TiO_2 to CoPPIX was then studied, both from UV-light excitation of TiO_2 and from visible light excitation of the co-attached dye molecules. One additional benefit of the co-sensitized TiO_2 films over the patterned films is that they are similar in design to the DSP assemblies that have been used to generate fuels. Thus, the information about the electron transfer processes obtained from studying co-sensitized TiO_2 films should be possible to translate into DSP assemblies and how the electron transfer processes can be optimized in these. To study whether the relative concentrations of dye and catalyst molecules on the surface influence the electron transfer events in the co-sensitized TiO_2 films, samples with

varying dye:catalyst ratios were prepared (30:1, 15:1 and 8:1). The absorption spectra of D35/TiO_2 and CoPPIX/TiO_2 together with the absorption spectra of the co-sensitized TiO_2 films are presented in Figure 3.8. Our studies of these samples revealed one-electron transfer from SnO_2 to CoPPIX and two-electron transfer from TiO_2 to CoPPIX, these results will be presented in Chapter 6.

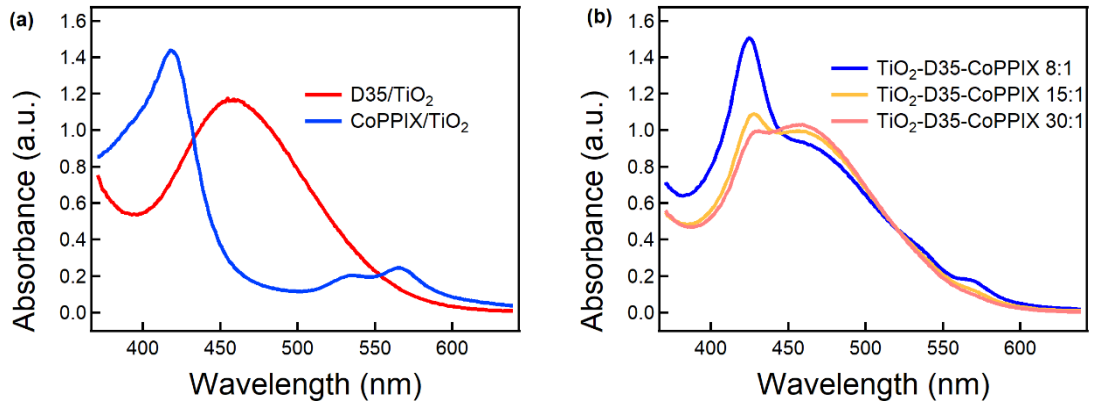

Figure 3.8. Absorption spectrum of (a) D35/TiO_2 and CoPPIX/TiO_2, and (b) co-sensitized TiO_2 films with concentration ratios (D35:CoPPIX) of 30:1, 15:1 and 8:1 on the surface. Adapted with permission from ***Paper IV***[173]*. Copyright 2018 American Chemical Society.*

4 Singlet Fission and Electron Injection in DPIBFC6/Semiconductor Materials

In this Chapter, I will present the photoinduced processes that occur in the different DPIBFC6/semiconductor materials. The processes that I will focus on involves SF, formation of a molecular charge separated state, electron injection and fluorescence. As discussed in Chapter 3, different photoinduced processes are expected to occur depending on the semiconductor substrate and the surrounding solvent. When DPIBFC6 is attached to ZrO_2, SF and formation of an excimer or molecular charge separated state are possible photoinduced processes, whereas on TiO_2 and SnO_2 electron injection can occur in addition to these processes.

In solution, DPIBFC6 displays an intense fluorescence (λ_{max} ~460 nm) with a lifetime of ~5 ns and a quantum yield close to unity, well in agreement with unmodified DPIBF. If immobilization onto the semiconductor surfaces results in additional photoinduced processes, the fluorescence is expected to be quenched by these processes. Therefore, we initially characterized the fluorescence of the DPIBFC6/semiconductor materials. The fluorescence studies of DPIBFC6 attached to the different semiconductor films revealed that the emission is quenched on all semiconductors compared to in solution, which indicates that additional photoinduced processes occur when the molecule is attached to the surfaces. As mentioned in Chapter 2, the molecules need to be in close proximity for SF or to occur. Thus, if SF or other intermolecular processes occur on the surfaces, we

expect the quenching of the fluorescence to exhibit a surface coverage dependence. Indeed, the fluorescence of DPIBFC6/ZrO_2 displays a surface coverage dependence, with a higher surface coverage resulting in a more quenched emission, indicating that SF or other intermolecular processes occur when the molecule is attached ZrO_2. The fluorescence of DPIBFC6/TiO_2 is on the other hand substantially quenched already at low surface coverages and does not follow any surface coverage dependence, indicating an efficient injection from the S_1 state. The fluorescence of DPIBFC6/SnO_2 is also substantially quenched at low surface coverage, however the fluorescence gets additionally quenched at higher surface coverages which might suggest that SF occurs in addition to injection from the S_1 state at higher surface coverages.[118]

Given the high quantum yield of fluorescence in solution, we can conclude that no ISC or intermolecular interactions occur. Thus, the solution fs-TA spectra can be used to determine the singlet excited state absorption, which displays peaks at 475 nm and 675 nm that decays uniformly to the GS, Figure 4.1a, similarly to what previously have been reported.[108, 174] To determine the triplet excited state absorption, triplet sensitization experiments of DPIBFC6 were performed, both in solution and when attached to ZrO_2. These experiments revealed a triplet excited state absorption at ~460 nm, Figure 4.1b, in agreement with literature reports.[63] Thus, if SF occurs on the surface an excited state absorption at this wavelength is expected to appear. Finally, the radical cation and anion of DPIBF has been reported to have excited state absorptions at ~550 nm and ~650 nm respectively[63], hence electron injection would give rise to a peak at ~550 nm whereas formation a molecular charge separated state between the DPIBFC6 molecules would give rise to peaks at both 550 nm and 650 nm. With this information in hand, the TA spectra of the different DPIBFC6/semiconductor materials can be analyzed to obtain information about which processes that occur on the different surfaces upon photoexcitation.

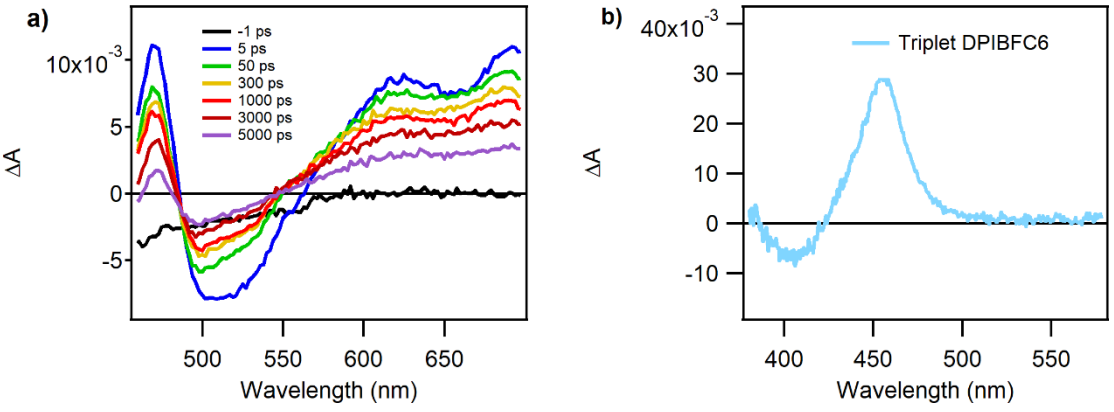

Figure 4.1. (a) fs-TA spectra of DPIBFC6 in toluene solution and (b) ns-TA spectra of the triplet excited state of DPIBFC6 in toluene solution obtained from triplet sensitization experiments with platinum octaethylporphyrin. Adapted with permission from ***Paper I***[118].

4.1 Singlet Fission and Formation of a Molecular Charge Separated State in DPIBFC6/ZrO_2 Materials

The photoinduced processes that occur on ZrO_2 were characterized using fs- and ns-TA measurements (Figure 4.2). To study if a molecular charge separated state is formed and its potential role in the SF process, the measurements were performed both in acetonitrile and toluene. The energy of the molecular charge separated state ($DPIBFC6^+/DPIBFC6^-$) was estimated using the Rehm-Weller equation,[175, 176] and in acetonitrile the energy of the $DPIBFC6^+/DPIBFC6^-$ state is below the energy of the S_1 state whereas in toluene it is slightly above the S_1 state.[118] Thus, a molecular charge separated state could be formed upon photoexcitation in acetonitrile but is not expected to form to any large extent in toluene.

As can be seen when comparing Figure 4.2a and 4.2c, the fs-spectra evolves differently in the two solvents after an initial rapid formation of the singlet excited state (with peaks at 475 and 675 nm) that decays faster than in solution in both solvents. In acetonitrile (Figure 4.2a), two new features at 550 nm and 650 nm appears as the singlet excited state decays, demonstrating that a $DPIBFC6^+/DPIBFC6^-$ state is formed. After a few nanoseconds, a shift in the excited state absorption is observed and a weak feature at 460 nm can be distinguished, matching the triplet excited state absorption. The triplet excited state appears to form in parallel to the formation of the molecular charge separated state, but to a much lower degree, and is the most long-lived species on the surface and the only feature that can be distinguished in the ns-TA spectra (Figure 4.2b). The measurements in acetonitrile suggest that charge separation and SF happens in parallel on the surface and that the molecular charge separated state acts as a loss channel for SF rather than an intermediate given the weak triplet excited state absorption and the fact that the processes happen in parallel. This role of the molecular charge separated state is also supported by the TA measurement in toluene that reveals less of a formation of a $DPIBFC6^+/DPIBFC6^-$ state and a more distinct feature at 460 nm after ~1 ns in the fs-TA spectra (Figure 4.2c) that also is more apparent in the ns-TA spectra (Figure 4.2d). The triplets on ZrO_2 decay to the ground state uniformly with biexponential kinetics with the longer component having a lifetime of >200 μs[118], in good agreement with previously reported lifetimes of the triplet excited state of DPIBF and its derivatives.[63, 108]

These results taken together suggest that SF is hindered by the formation of a molecular charge separated state on ZrO_2 surfaces and that SF occurs to a larger extent in a non-polar environment. Moreover, similar features matching a molecular charge separated state has been reported in the TA spectra of dicarboxylated DPIBF attached to ZrO_2 in acetonitrile,[108] suggesting that this is a general trend for DPIBF attached to semiconductor surfaces and that a non-polar environment is more beneficial for the SF process. However, as the triplet excited state absorption is weak also in the non-polar environment, the efficiency of SF on ZrO_2 surfaces appears to be low in general.

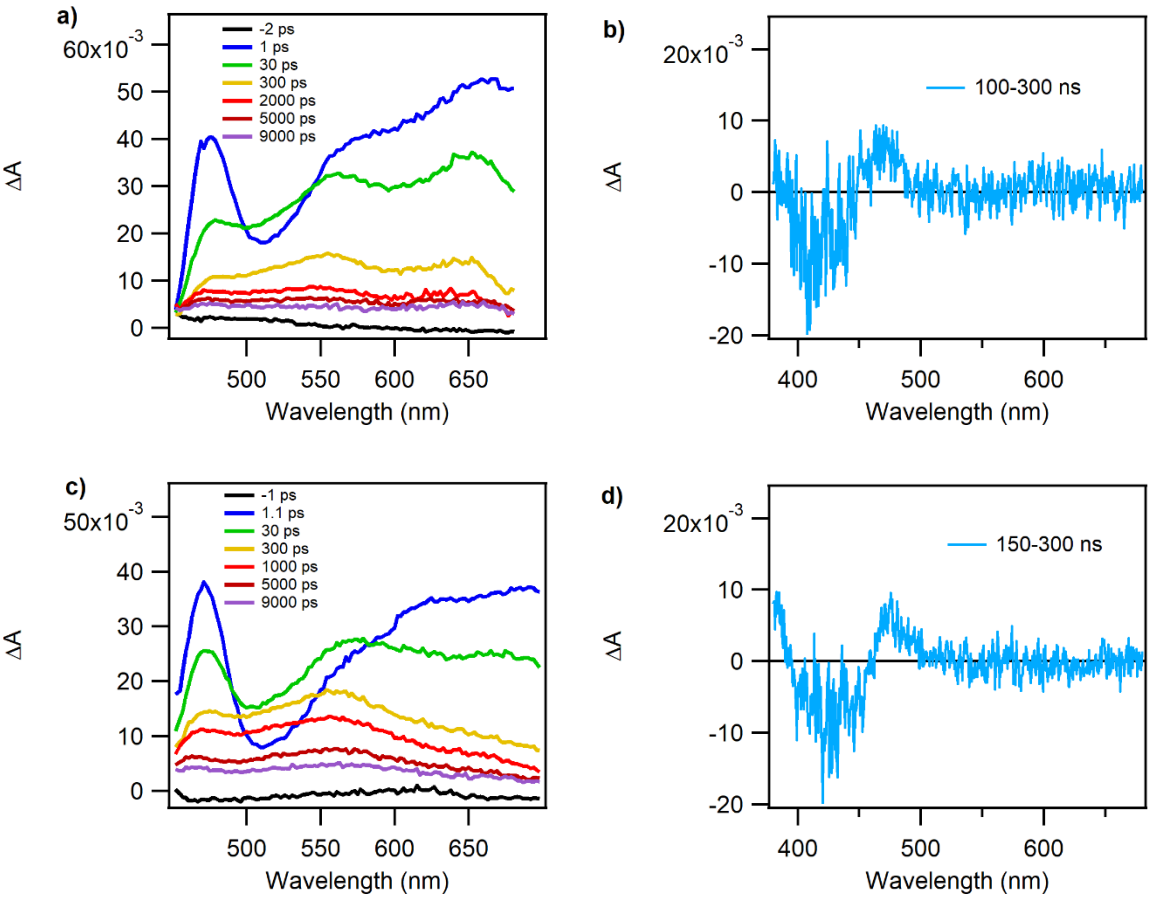

Figure 4.2. fs- and ns-TA spectra of DPIBFC6/ZrO_2 (a) fs-TA spectra in acetonitrile (b) ns-TA spectra in acetonitrile, (c) fs-TA spectra in toluene and (d) ns-TA spectra in toluene. Reproduced with permission from ***Paper I***[118].

4.2 Injection from the Singlet Excited State and Charge Recombination in DPIBFC6/TiO_2 Materials

The highly quenched fluorescence for all surface coverages on TiO_2 suggests an efficient injection from the singlet excited state. To confirm this and study a potential polarity dependence, fs-TA experiments were performed of DPIBFC6/TiO_2 in acetonitrile and toluene, Figure 4.3. As can be seen in the figure, the initially formed singlet excited state absorption rapidly transforms into a peak at 550 nm in both solvents. The peak at 550 nm corresponds to the absorption of the radical cation and confirms injection from the S_1 state. Thus, it appears as if the flexible carbon linker used herein is not enough to slow down the injection from the S_1 state on TiO_2, in agreement with previous studies of DPIBF with a carbon chain linker attached to TiO_2.[111] This observation suggests that the approach by Jonsson[111] and Hansson[108] to utilize core-shell structures indeed is necessary to slow down singlet injection from DPIBF into the CB of TiO_2 for SF to occur.

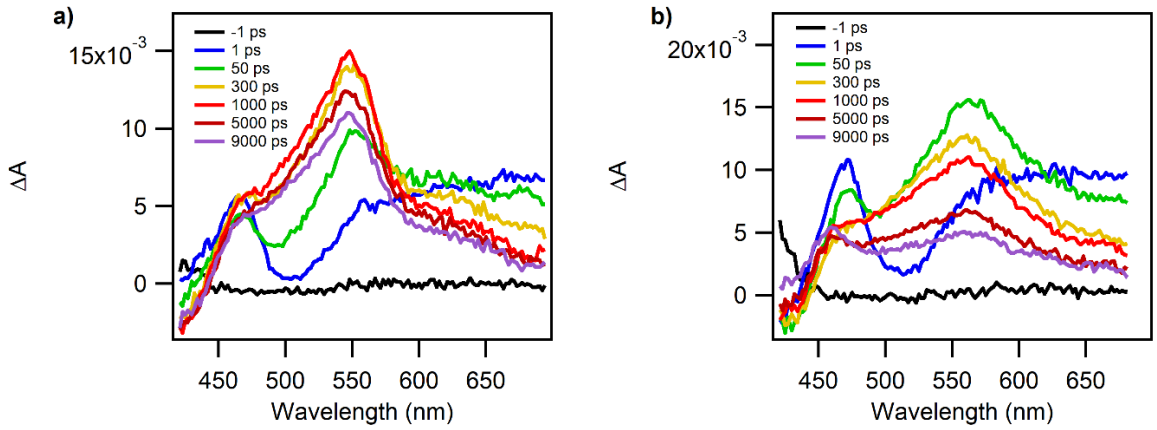

Figure 4.3. fs-TA spectra of DPIBFC6/TiO_2 in (a) acetonitrile and (b) toluene. Reproduced with permission from ***Paper I***[118].

By comparing the fs-TA spectra in the two solvents it is possible to distinguish some differences between them. Firstly, the peak at 550 nm is more intense in acetonitrile (Figure 4.3a) which suggests a higher injection yield. Secondly, the radical cation appears to decay faster in toluene (Figure 4.3b) compared to in acetonitrile, and as the radical cation decays, a feature at 460 nm that matches the triplet excited state absorption grows in. This observation suggests that in toluene, charge recombination occurs from the CB of TiO_2 to the triplet excited state of DPIBFC6. To further characterize this behavior, ns-TA experiments were performed of DPIBFC6/TiO_2 samples in acetonitrile and toluene and these spectra are presented in Figure 4.4. The ns-TA spectra reveal distinct differences between the two solvents, in acetonitrile (Figure 4.4a) a broad feature that matches the radical cation dominates the spectra and decays back to the ground state. In toluene (Figure 4.4b) however, the ns-TA spectra is dominated by the triplet excited state absorption at 460 nm. After ~100 ns, both the triplet excited state absorption and the excited state absorption from the radical cation can be distinguished. However, after 1 µs the triplet excited state absorption is the only feature that can be distinguished, which further suggests a recombination from the CB to the triplet excited state of DPIBFC6 in toluene.

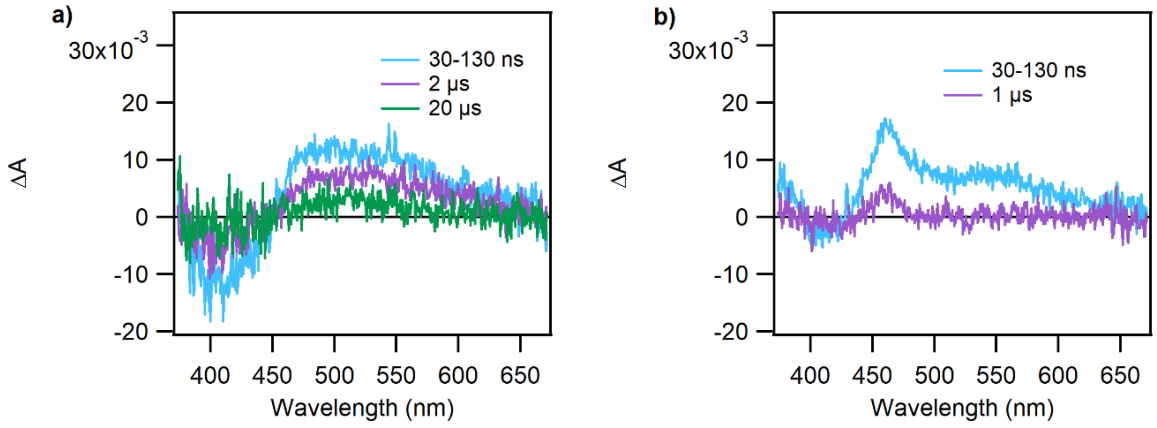

Figure 4.4. ns-TA spectra of DPIBFC6/TiO_2 in (a) acetonitrile and (b) toluene. Reproduced with permission from ***Paper I***[118].

4.3 Electron Injection and Singlet Fission in DPIBFC6/SnO_2 Materials

The highly quenched fluorescence for all surface coverages on SnO_2 suggests, as on TiO_2, injection from the S_1 state upon photoexcitation. However, since the fluorescence from high surface coverage samples is somewhat more quenched than from low surface coverage samples, there is a possibility that SF contributes to the additional quenching observed for samples with a higher surface coverage. As on TiO_2, the fs-spectra reveals formation of a peak at 550 nm as the singlet excited state decays, this peak corresponds to the radical cation and forms both in acetonitrile and toluene, Figure 4.5. In acetonitrile (Figure 4.5a), singlet injection is the dominating process. However, in toluene (Figure 4.5b) a feature at ~460 nm that matches the triplet excited state absorption forms in parallel to the radical cation, suggesting that both injection from the singlet excited state and SF occurs upon photoexcitation of DPIBFC6/SnO_2 in toluene. Interestingly, the triplet feature that appears on SnO_2 is more pronounced than on ZrO_2, suggesting that SF is more efficient when DPIBFC6 is attached to SnO_2 compared to when it is attached ZrO_2. The reason behind this is not clear but could be related with small differences in the nanoparticle network between the two semiconductors that alters how the molecules attach to the surface and in turn the geometry and/or coupling for SF.

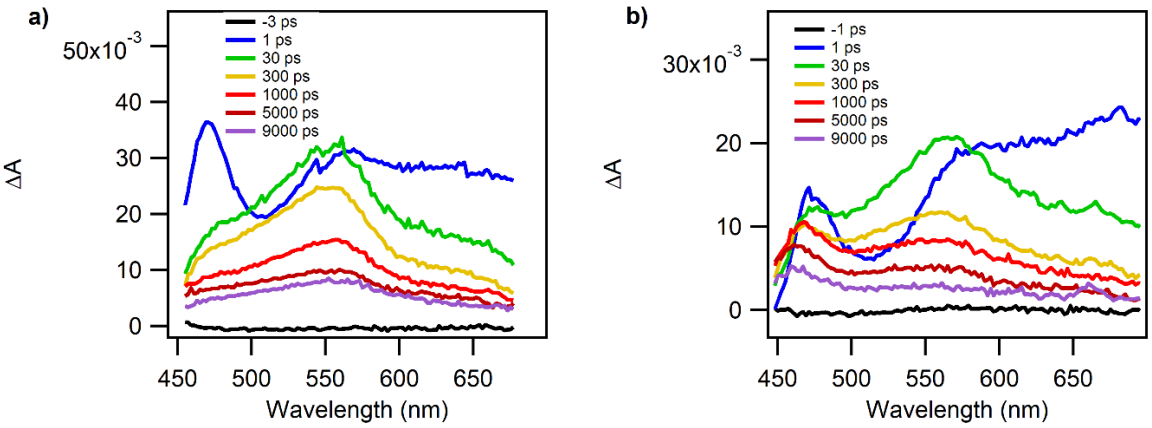

Figure 4.5. fs-TA spectra of DPIBFC6/SnO_2 in (a) acetonitrile and (b) toluene. Reproduced with permission from ***Paper I***[118].

Since the CB energy of SnO_2 lies well below the triplet excited state oxidation potential of DPIBFC6, triplet injection into the CB of SnO_2 following SF is a possibility. To elucidate whether the triplets inject electrons into the CB, ns-TA experiments were performed. The ns-TA spectra in acetonitrile and toluene are presented in Figure 4.6. Interestingly, the spectra are dominated by a broad and positive feature between 450-600 nm in both solvents, which mainly matches the absorption of the radical cation of DPIBFC6. This feature looks similar to the final spectra in the fs-TA measurements in acetonitrile (Figure 4.5a), and for DPIBFC6/SnO_2 in acetonitrile this likely corresponds to the radical cation following injection from the S_1 state. However, this feature looks markedly different from the final fs-TA spectra in toluene (Figure 4.5b) that is dominated by the triplet excited state absorption. This difference between the final spectra in the fs-TA measurement and

the initial ns-TA spectra demonstrates that triplets have injected electrons into the CB of SnO_2 in toluene and evolved into the radical cation of DPIBFC6.

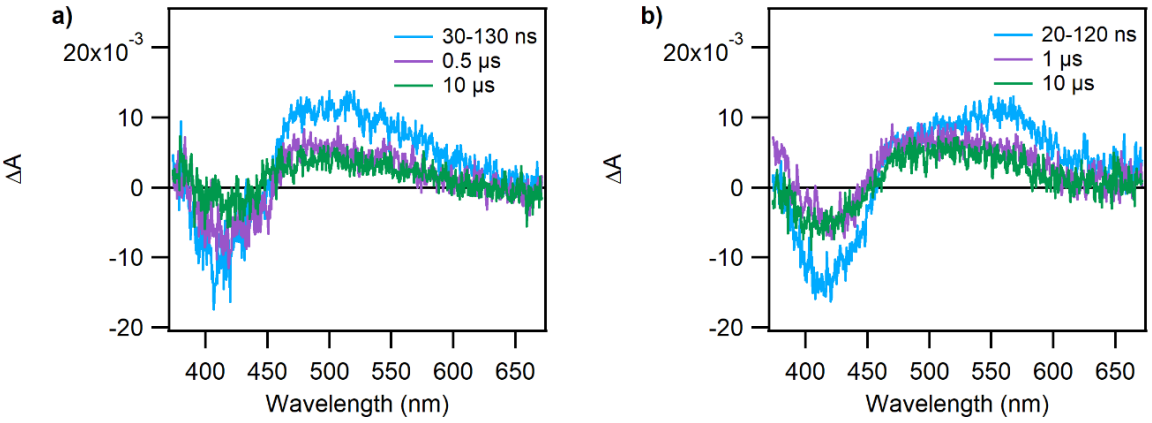

Figure 4.6. ns-TA spectra of DPIBFC6/SnO_2 in (a) acetonitrile and (b) toluene. Reproduced with permission from ***Paper I***[118].

The feature assigned to the radical cation in the ns-TA spectra is somewhat broader than the previously observed absorption of the radical cation, which could be a result of some residual triplets that did not inject electrons into the CB. This is also confirmed by the single wavelength kinetic traces that are different at 470 nm and 550 nm in both solvents. The lifetime obtained from the decay traces at 470 nm matches the lifetime of the triplet excited state. However, the lifetime obtained from the traces at 550 nm is more short-lived and likely corresponds to charge recombination from the CB into the ground state.[118] This observation suggests that SF occurs to some extent in both solvents, but with a higher efficiency in toluene.

4.4 Short Summary

In summary, these studies of DPIBFC6 attached to different semiconductor surfaces reveal that SF is more efficient in a non-polar environment and that SF on ZrO_2 is hindered by the formation of a molecular charge separated state in a polar environment. When the molecule is attached to TiO_2, SF is outcompeted by electron injection from the singlet excited state. However, when the molecule is attached to SnO_2 in a non-polar environment, SF occurs in parallel to injection from the singlet excited state. These studies further demonstrate that SF is more efficient when the molecule is attached to SnO_2 compared to when it is attached to ZrO_2, and that the triplets formed *via* SF on SnO_2 can inject electrons into the CB of SnO_2.

5 Photoisomerization of the Ru-Sulfoxide/ZrO_2 Material

In this Chapter, the results from photoexcitation of $[Ru(deeb)_2PySO\text{-}iPr]^{2+}$ in solution and attached to ZrO_2 will be presented. The aim of attaching the complex to ZrO_2 was to study if the photoisomerization ability of the molecule is preserved when it is attached to a solid surface, and if this can be used when designing photoresponsive materials with spatial addressability.

5.1 S-to-O Photoisomerization

To confirm that $[Ru(deeb)_2PySO\text{-}iPr]^{2+}$ displays S-to-O photoisomerization in solution, MLCT irradiation of the complex was initially performed in liquid solution. As expected, S-to-O photoisomerization is triggered upon MLCT excitation, both in dichloromethane (Figure 5.1a) and propylene carbonate, with a quantum yield that is estimated to ~30 %. The S-to-O photoisomerization is accompanied by a decrease of the initial MLCT absorption band at ~410 nm and two new absorption peaks growing in at 375 nm and 500 nm, similarly as previously described for other ruthenium sulfoxide complexes.[93, 94, 138, 177]

Following this, MLCT excitation of the $Ru(deeb)_2PySO\text{-}iPr/ZrO_2$ material was performed, and importantly, S-to-O photoisomerization is triggered also on the solid film, Figure

5.1b. The spectral changes are slightly muted compared to in solution, which demonstrate a somewhat lower photoisomerization ability on the surface. This is also reflected in the quantum yield of photoisomerization that is lower on the surface than in solution and estimated to ~4-7%. Although the photoisomerization ability is somewhat lower on the surface, the photoisomerization still proceeds far, with maintained isosbestic points and provides spatial addressability as is evident from Figure 5.1c where a film has been irradiated through a star-shaped scaffold.

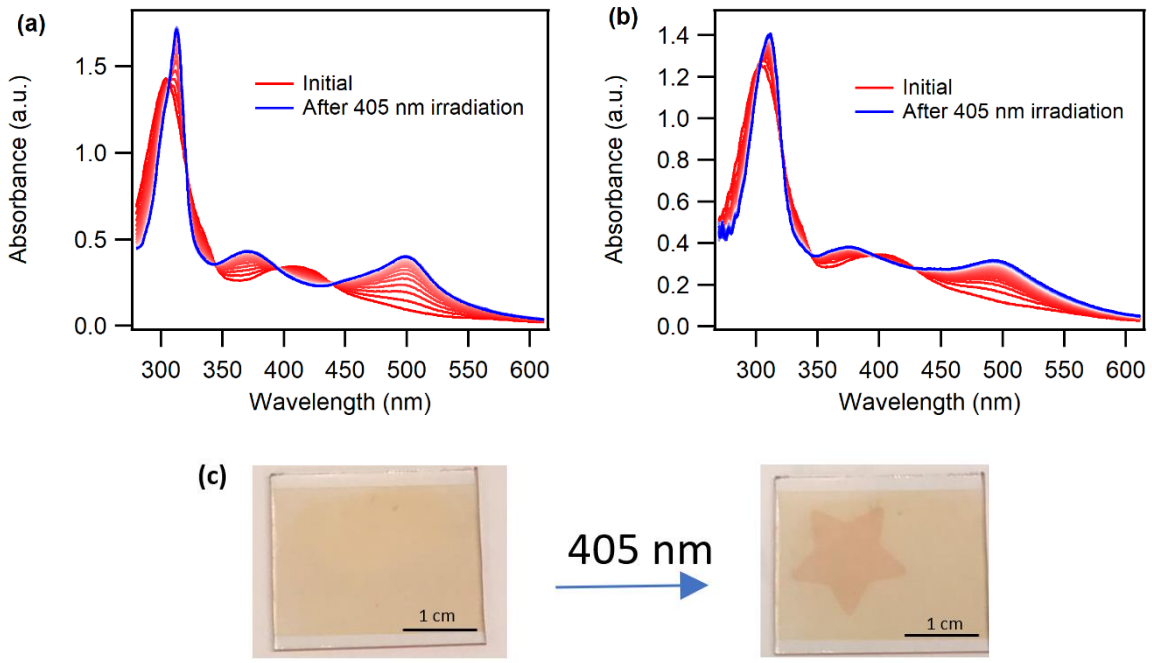

Figure 5.1. Absorption changes of $[Ru(deeb)_2PySO\text{-}iPr]^{2+}$ over time (from red to blue spectra) following continuous irradiation with 405 nm light (a) in DCM liquid solution and (b) attached to a ZrO_2 thin film (~50 nmol/cm^2) in air. (c) Photograph of S-$Ru(deeb)_2PySO\text{-}iPr/ZrO_2$ before (left) and after (right) being illuminated with 405 nm light through a star-shaped scaffold. Adapted with permission from ***Paper II***[133].

Since the origin of the lower photoisomerization ability on the surface either could be related to hindrance from neighbouring molecules or from being attached to the surface, we performed surface coverage dependent measurements of the photoisomerization. These revealed that the photoisomerization ability depends somewhat on the surface coverage, with a lower surface coverage resulting in a slightly higher photoisomerization ability. This observation suggests that the photoisomerization is hindered to some degree by neighbouring molecules. However, the photoisomerization ability is lower than in solution for all studied surface coverages, indicating that the surface is what hinders the photoisomerization the most. To further increase the photoisomerization on the surface, chemical modifications of the molecule that provides an increased flexibility on the surface is likely necessary, such as utilizing only one ligand with binding groups to the surface. Another modification that could result in an increased photoisomerization ability per area could be to utilize a ligand with two sulfoxide groups, as have previously been studied in solution.[177-180] However, since these complexes typically do not display two-

color photoswitching, this would likely result in a film that does not display reversible photoisomerization.

5.2 O-to-S Isomerization

For practical use as a photoswitchable film, it is of importance that the photo-isomerization is reversible by irradiation with light of a different wavelength and that the metastable state is long-lived. The O-bonded isomer is metastable but trapped for a significant amount of time in the dark following the photoisomerization, both in solution and when attached to ZrO_2. Thermal reversion to the S-bonded form occurs over several days, Figure 5.2. Interestingly, the thermal reversion occurs in a similar fashion on the surface as in solution, suggesting that the molecular rearrangement for thermal reversion is not affected to the same extent as for the photoinduced isomerization on the surface.

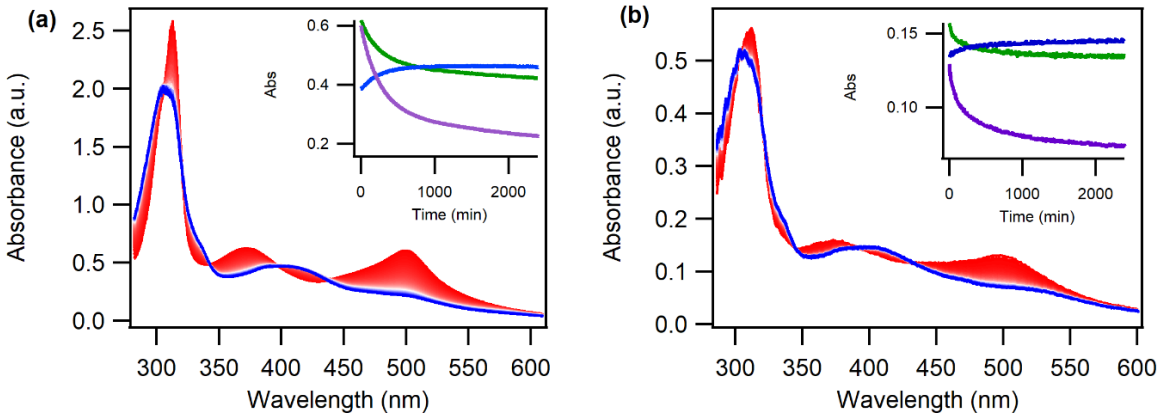

Figure 5.2. Absorption changes of O-[Ru(deeb)$_2$PySO-iPr]$^{2+}$ over time (from red to blue spectra) left in the dark for thermal reversion (a) in DCM liquid solution (inset shows single wavelength kinetics at 375 nm (green), 411 nm (blue) and 500 nm (purple)) and (b) attached to a ZrO_2 thin film (~50 nmol/cm^2) in air (inset shows single wavelength kinetics at 370 nm (green), 405 nm (blue) and 500 nm (purple)). Reproduced with permission from ***Paper II***[133].

Importantly, O-to-S isomerization of the complex can also be triggered by visible light irradiation, both in liquid solution and when attached to ZrO_2. Selective irradiation of the O-bonded isomer results in complete photoisomerization back to the S-bonded form in solution (Figure 5.3a) and an almost complete O-to-S photoisomerization when attached to ZrO_2 (Figure 5.3b). As for the S-to-O photoisomerization, the O-to-S photo-isomerization is somewhat hindered on the surface and displays muted spectral changes and a lower quantum yield, in solution the quantum yield was estimated to ~2%, whereas on the surface, it was estimated to ~0.4%. Despite the lower quantum yield, the photoisomerization can be cycled back and forth several times, both in solution and when attached to the film.[133] These results suggest that attaching photochromic molecules onto mesoporous semiconductor films is a promising approach for designing photoswitchable solid films.

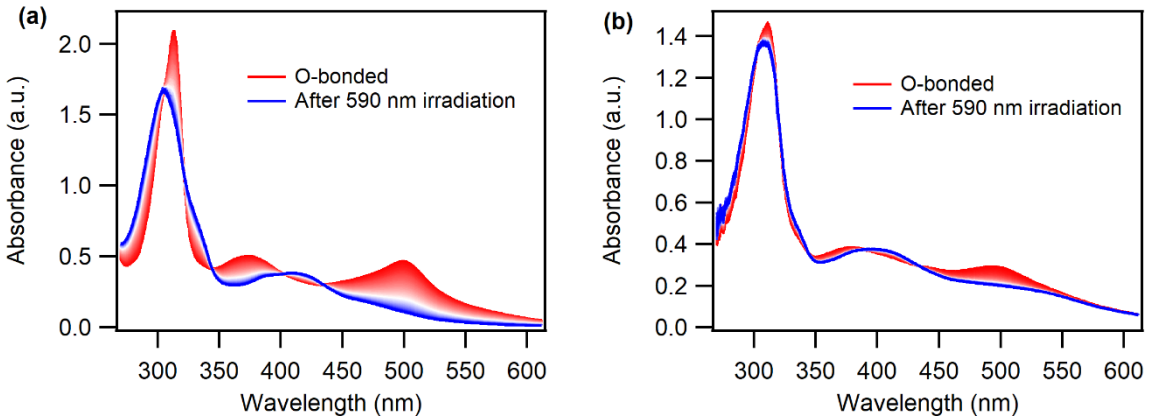

Figure 5.3. Absorption changes of O-[Ru(deeb)$_2$PySO-iPr]$^{2+}$ over time (from red to blue spectra) following continuous irradiation with 590 nm light in (a) DCM liquid solution and (b) attached to a ZrO_2 thin film (~50 nmol/cm^2) in air. Reproduced with permission from ***Paper II***[133].

5.3 Short Summary

In summary, this study demonstrates that attaching a photochromic molecule onto a mesoporous semiconductor film is a straightforward way of achieving a solid-state photoswitchable material with spatial addressability. This approach further allows for a high surface coverage compared to previously studied materials. The photoisomerization ability of the molecule is however slightly lower when it is attached to the surface compared to in solution, which is attributed to a restricted molecular movement on the surface. Further investigations into how the anchoring to the surface affects the photo-isomerization will likely be needed to improve the photoswitching efficiency on the surface.

6 Charge Separation and CB Mediated Electron Transfer in Molecular/Semiconductor Materials

As mentioned in Chapter 3, extending the charge separated lifetime between the photosensitizer and the CB is of great importance for generating solar fuels in dye-sensitized semiconductor materials. In DSP assemblies, it is further of importance to achieve CB mediated multi-electron transfer to a co-attached molecular catalyst. In this Chapter, I will present our attempts of extending the charge separated lifetime by using the photoisomerizable ruthenium sulfoxide complex as the photosensitizer and by using the patterned SnO_2-TiO_2 film. I will further present how the charge separated lifetime between the dye and the CB is affected by co-sensitizing TiO_2 films with both dye and catalyst molecules. Finally, studies of electron transfer from the CB of SnO_2 and TiO_2 to CoPPIX will be presented.

6.1 Electron Injection in Ruthenium Sulfoxide/TiO_2 Materials

Following the successful photoisomerization of $[Ru(deeb)_2PySO\text{-}iPr]^{2+}$ attached to ZrO_2, we were interested in studying if the complex could inject electrons into the CB of TiO_2 and if the O-bonded isomer could stabilize and extend the charge separated lifetime. Like when the complex is attached to ZrO_2, S-to-O photoisomerization is triggered upon MLCT excitation when the complex is attached to TiO_2, Figure 6.1.

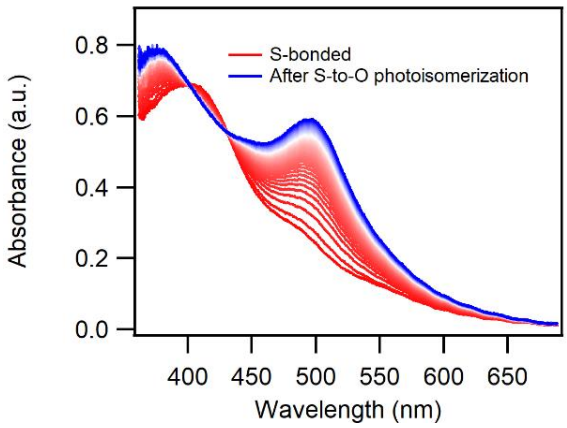

Figure 6.1. Absorption changes of Ru(deeb)$_2$PySO-iPr/TiO$_2$ over time (from red to blue spectra) following continuous irradiation with 385 nm light.

To study if the complex can inject electrons into the CB of TiO$_2$, ns-TA measurements were initially performed of the S-bonded isomer attached to TiO$_2$. If the complex injects an electron into the CB, long-lived signals in the µs to ms timescale is expected.[99] However, no signals appear in the ns-TA measurements upon photoexcitation of S-Ru(deeb)$_2$PySO-iPr/TiO$_2$, thus we can conclude that the S-bonded isomer does not inject electrons into the CB of TiO$_2$ and that S-to-O photoisomerization or other deactivation processes outcompete a possible charge injection.

Upon selective irradiation of the O-bonded isomer attached to TiO$_2$, O-to-S photoisomerization is triggered like on ZrO$_2$ and in solution. However, the back-isomerization is not completely reversible on TiO$_2$ by irradiation with light, suggesting that the O-bonded isomer is more stable when attached to TiO$_2$. Given the lower photoisomerization ability for the O-to-S isomerization on TiO$_2$, it is possible that charge injection becomes more competitive. To characterize if charge injection occurs from the O-bonded form, we performed ns-TA measurements of samples that had been photoisomerized into the O-bonded form prior to the measurements. Interestingly, long-lived signals arise in the ns-TA measurements upon photoexcitation of the O-bonded isomer attached to TiO$_2$. These signals do not appear upon photoexcitation of the O-bonded isomer attached to ZrO$_2$ or in liquid solution and can therefore be reasonably assigned to the oxidized O-bonded complex after injection of an electron into the CB of TiO$_2$. It must however be noted that the intensity of the signals is low, which suggests a low injection yield.

The charge recombination kinetics of O-Ru(deeb)$_2$PySO-iPr/TiO$_2$ is shown in Figure 6.2 and compared to the charge recombination kinetics of the commonly used ruthenium dye N3[181, 182]. As can be seen in the figure, the charge separated lifetime is substantially extended for the O-bonded isomer of our ruthenium sulfoxide complex compared to for the N3 dye. This is attributed to the O-bonded isomer being more stable in the Ru^{III} oxidation state and thus that there is a lower tendency for it to accept electrons from the CB.

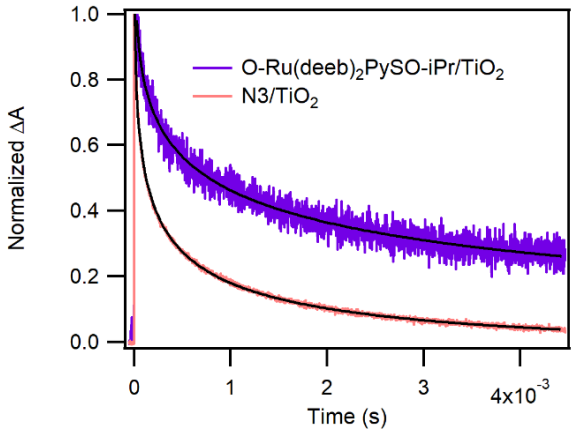

Figure 6.2. Normalized single-wavelength ns-TA traces of O-Ru(deeb)$_2$PySO-iPr/TiO$_2$ and N3/TiO$_2$ films and corresponding KWW fits. ΔA-signal were recorded at 750 nm after pulsed 500 nm laser excitation.

The decay traces of both O-Ru(deeb)$_2$PySO-iPr/TiO$_2$ and N3/TiO$_2$ were well described by a stretched exponential function, the Kohlrausch–Williams–Watts (KWW) kinetic model[183] (Equation 6.1). The β-value in this equation is related to the heterogeneity of the decay and is inversely proportional to the width of the Levy distribution of the rate constants. If the β-value reaches one the decay is homogenous, and if the β-value is close to zero the decay is heterogeneous with large variations in the rate constants.[184] Equation 6.2 represents the first moment of the KWW function where Γ is the gamma function, k_{cr} is obtained by taking $1/\langle\tau_{ww}\rangle$.

$$\Delta A(t) = \left(\Delta A_0 - \Delta A_f\right) \exp\left[-(k_{obs}t)^{\beta}\right] + \Delta A_f \qquad (6.1)$$

$$\langle\tau_{ww}\rangle = \frac{1}{k_{obs}\beta}\Gamma\left(\frac{1}{\beta}\right) \qquad (6.2)$$

The β- and k_{cr} values obtained from fitting the decay traces of O-Ru(deeb)$_2$PySO-iPr/TiO$_2$ and N3/TiO$_2$ to the KWW model are presented in Table 6.1.

Table 6.1. Charge recombination rate constants (k_{cr}) and β-values from KWW fits of the ns-TA single wavelength decay traces of O-Ru(deeb)$_2$PySO-iPr/TiO$_2$ and N3/TiO$_2$.

Sample	k_{cr} **(s^{-1})**	**β**
O-Ru(deeb)$_2$PySO-iPr/TiO$_2$	1.6x10^3	0.25
N3/TiO$_2$	1.2x10^4	0.29

As can be seen in the table, the β-values for both samples are similar, the obtained k_{cr} values can therefore be compared between the samples in a straightforward way. Comparison between the k_{cr} values reveals that the charge recombination is slowed down by one order of magnitude in the ruthenium sulfoxide samples. This result suggests that the O-bonded isomer indeed can stabilize the charge separated state and result in an

extended charge separation lifetime. Moreover, it demonstrates the possibility of designing photosensitizer molecules based on photochromic molecules where only one of the isomers can inject an electron. However, for practical use of this type of molecule as photosensitizer, it is desired to increase the injection yield.

6.2 Charge Separation in Patterned SnO_2-TiO_2 Films and Co-Sensitized TiO_2 Films

The dye used (D35) in the dye-sensitized patterned SnO_2-TiO_2 and co-sensitized TiO_2 films is a well-studied dye that displays a quantum yield of injection close to unity.[185] Therefore, the initial process that occurs upon photoexcitation of D35 in these materials is expected to be charge injection. As expected, rapid and efficient electron injection into the CB of the semiconductors is observed upon photoexcitation of the dye. To characterize the lifetime of the initially formed charge separated state, ns-TA measurements were performed where the charge recombination kinetics of the oxidized dye was probed at ~700 nm.

6.2.1 Extended Charge Separation in Patterned SnO_2-TiO_2 Films

To elucidate whether the patterned design could result in an extended charge separated lifetime by accumulation of electrons in the dye-free SnO_2 parts, patterned films that were exclusively dye-sensitized on the TiO_2 stripes (Type II) were compared to patterned films that were evenly dye-sensitized on all the film (Type I), see Figure 6.3a. These films were also compared to dye-sensitized SnO_2-TiO_2 films with a full layer of SnO_2 on top of TiO_2 and to dye-sensitized bare TiO_2 and SnO_2 films.

The charge recombination kinetics for the different samples are shown in Figure 6.3b. As can be seen by visual examination of the decay traces, the charge separated lifetime is substantially extended for patterned Type II films compared to all other studied samples. This suggests that electrons are transferred to and accumulated in the dye-free SnO_2 parts and that the barrier for back-electron transfer extends the charge separated lifetime. Moreover, the decay traces reveal that the charge recombination is faster for SnO_2 samples compared to for TiO_2 samples, in agreement with previously observed charge recombination kinetics.[186, 187]

The difference between patterned Type II samples and the other samples becomes especially apparent at higher excitation energies, suggesting that the number of electrons in the CB is important for electrons to accumulate in the dye-free parts.[164] Moreover, the difference is more apparent when a Li^+ electrolyte is used, which we attribute to an increased conductivity from the Li^+ ions[188] that can facilitate electron transport further in the film.

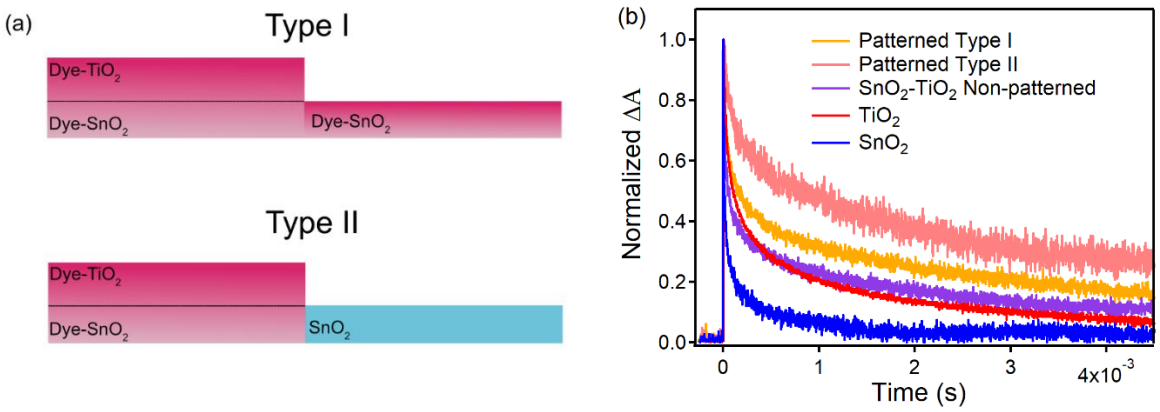

Figure 6.3. (a) Schematic illustration of the cross-section of Type I and Type II patterned SnO_2-TiO_2 films, (b) ns-TA single wavelength kinetics at 750 nm for dye-sensitized Type I and Type II patterned SnO_2-TiO_2 films as well as for dye-sensitized non-patterned SnO_2-TiO_2, TiO_2 and SnO_2. All measurements were performed in 0.1M $LiClO_4$/acetonitrile with an excitation energy of 0.4 mJcm^{-2}. Adapted from ***Paper III***[164] *with permission from the PCCP Owner Societies.*

The increase in the charge separated lifetime in patterned Type II samples is further confirmed by the charge recombination rate constants (k_{cr}) obtained by fitting the decay traces to the KWW model[183] (as described above). The k_{cr} and β-values for dye-sensitized Type I and Type II patterned films and dye-sensitized TiO_2 and SnO_2 films measured in 0.1M $LiClO_4$ in acetonitrile (0.4 mJcm^{-2}) are presented in Table 6.2. As can be seen in the table, the β-values are similar for the different samples and the k_{cr} values can therefore be directly compared between the samples. The k_{cr} values are decreased by a factor of 55, 80, and 2000 for Type II dye-sensitized patterned films compared to Type I, TiO_2 and SnO_2 films, respectively.

Table 6.2. Charge recombination rate constants (k_{cr}) and β-values from KWW global fittings of ns-TA decays of triplicate samples of dye-sensitized patterned SnO_2-TiO_2 films (Type I and Type II), TiO_2 films and SnO_2 films in 0.1 $LiClO_4$/acetonitrile with an excitation energy of 0.4 mJcm^{-2}.

Sample	**k_{cr} (s^{-1})**	**β**
Type I	4.65×10^3	0.19
Type II	8.49×10^1	0.19
TiO_2	6.67×10^3	0.20
SnO_2	1.97×10^5	0.14

Interestingly, the k_{cr} value for patterned Type II samples decreases with increasing excitation power.[164] This is opposed to the Type I samples and literature reports on how the recombination kinetics usually depends on the number of injected electrons.[164, 189] This observation further supports the conclusion that when enough electrons are injected into the CB of TiO_2, they are transferred into the dye-free SnO_2 parts.

Samples with a full layer of SnO_2 on top of TiO_2 exhibited large variations in the charge recombination kinetics and were not well described by the KWW model, thus indicating heterogeneous samples and k_{cr} values for these are therefore not included in the table. Nevertheless, these samples all exhibited faster recombination kinetics compared to the Type II samples.[164] These results demonstrate that the patterned design significantly can extend the charge separation lifetime and result in accumulation of electrons in the dye-free SnO_2 parts.

6.2.2 Charge Separation Lifetime in Co-Sensitized TiO_2 Films

The charge separated lifetime between the dye and the CB was also measured in co-sensitized TiO_2 films with varying relative concentrations of D35:CoPPIX on the surface, the charge recombination kinetics for these samples are shown in Figure 6.4. As can be seen by visual inspection of the decay traces, co-sensitizing the films with both CoPPIX and D35 extends the charge separated lifetime compared to when only D35 are attached to the surface, especially when a high relative ratio of CoPPIX is used.

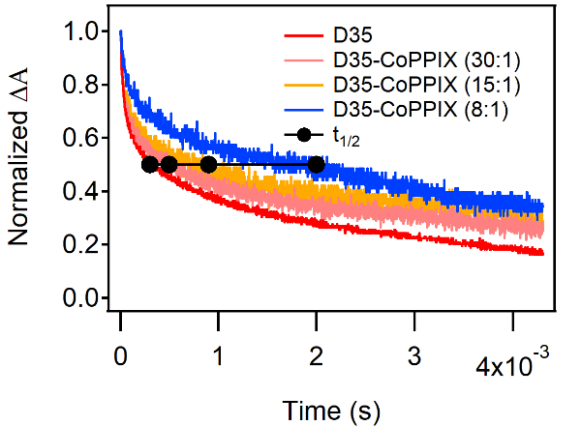

Figure 6.4. Single-wavelength ns-TA traces of D35-CoPPIX/TiO_2 films in acetonitrile and corresponding $t_{1/2}$ values as a dotted black line. ΔA-signal were recorded at 680 nm after pulsed 480 nm laser excitation to selectively excite the dye. Adapted with permission from ***Paper IV***[173]*. Copyright 2018 American Chemical Society.*

The charge recombination kinetics in co-sensitized samples were not well described by either a biexponential function or by the KWW model, it was therefore characterized using the charge separation half-life ($t_{1/2}$) which is commonly used in dye-sensitized semiconductor materials.[163, 186, 190, 191] The $t_{1/2}$ values for the different ratios of the co-sensitized samples are presented in Table 6.3 and reveal that the half-life is increased by one order of magnitude for co-sensitized samples with the highest ratio of CoPPIX compared to for D35/TiO_2 samples. These observations suggest that electrons are transferred to CoPPIX in the co-sensitized samples and that this alters the kinetics of the charge recombination to the dye. The electron transfer from TiO_2 to CoPPIX was further characterized following this and will be presented in the following section.

Table 6.3. Average half-life ($t_{1/2}$) of the charge recombination in co-sensitized TiO_2 samples with different D35:CoPPIX ratios.

Ratio D35:CoPPIX	***t*$_{1/2}$ (s)[a]**
1:0	$2.7x10^{-4} \pm 0.42x10^{-4}$
30:1	$5.5x10^{-4} \pm 0.42x10^{-4}$
15:1	$1.1x10^{-3} \pm 0.41x10^{-3}$
8:1	$2.4x10^{-3} \pm 0.12x10^{-3}$

[a]The indicated uncertainties is the standard deviation from analysis of three different samples.

6.3 Conduction Band Mediated Electron Transfer

Since CB mediated electron transfer is necessary to generate solar fuels in DSP assemblies, we were interested in studying if CoPPIX can accept electrons from the CB of SnO_2 and TiO_2. To study this, direct band-gap excitation of TiO_2 and SnO_2 films with CoPPIX immobilized to the surface was initially performed, Figure 6.5.

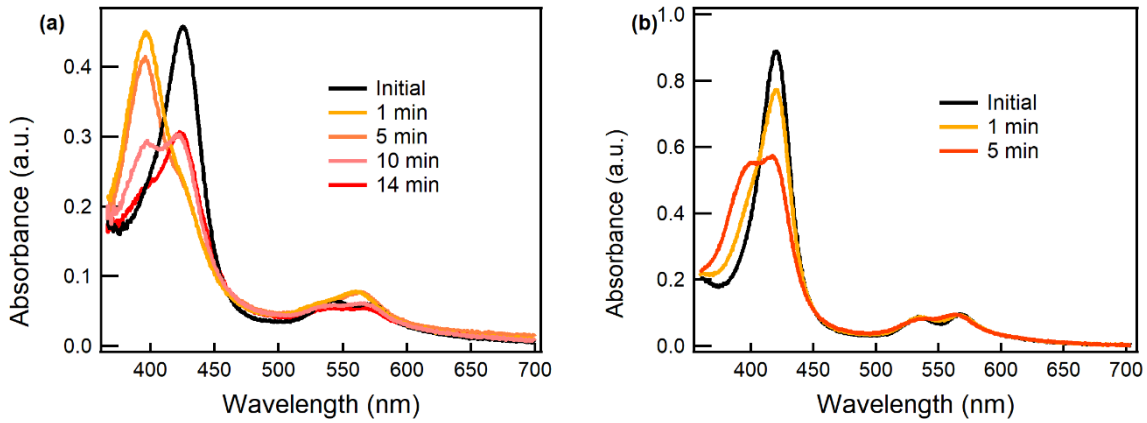

Figure 6.5. (a) Absorption changes of CoPPIX/TiO_2 following continuous irradiation with UV-light (λ=250-350 nm). Adapted with permission from ***Paper IV***[173]*. Copyright 2018 American Chemical Society. (b) Absorption changes of CoPPIX/SnO_2 following continuous irradiation with UV-light (λ=250-350 nm). Adapted from* ***Paper III***[164] *with permission from the PCCP Owner Societies*

As can be seen when comparing Figure 6.5 with the absorption spectra of the different redox states of CoPPIX (Figure 3.7b), band-gap excitation of TiO_2 results in two-electron transfer to CoPPIX whereas band-gap excitation of SnO_2 result in one-electron transfer to CoPPIX. This is evident by an initial blue-shift of the Soret band at 405 nm and an increase and merging of the Q-band around 560 nm on both semiconductors, corresponding to the first reduction. Following this, doubly reduced CoPPIX is formed on TiO_2 as is apparent by a regrowth of the initial Soret band and a decrease of the absorbance of the Q-band. These spectral changes are well in agreement with the spectral features of the redox states of CoPPIX[173] and demonstrate that two-electron transfer from the CB of TiO_2 and one-electron transfer from the CB of SnO_2 to CoPPIX indeed is possible from UV-light

excitation. To study the kinetics of these processes and if they can be initiated from visible light excitation in samples with co-attached dye molecules, ns-TA measurements were performed and the results from these will be presented in the following sections.

6.3.1 Conduction Band Mediated Electron Transfer in Patterned SnO_2-TiO_2 Films

Since electrons appear to accumulate in the dye-free SnO_2 parts of the patterned films upon photoexcitation of the dye, CoPPIX was selectively immobilized on these areas. The transient absorption of CoPPIX was then monitored to elucidate if electrons could travel through the patterned film and reach the CoPPIX molecules. For this purpose, ns-TA measurements were performed where the dye was selectively excited, and the probe light was focused to only measure on the CoPPIX/SnO_2 parts. The probe wavelength was set to ~430 nm to monitor the initial Soret band of CoPPIX. If electrons reach the CoPPIX molecules, a negative signal is expected at this wavelength. Indeed, upon photoexcitation of patterned Type II films with co-attached CoPPIX molecules, a negative signal is observed at this wavelength, Figure 6.6a, demonstrating a one-electron transfer to CoPPIX. This negative signal does not appear in patterned Type II films without CoPPIX molecules or in patterned films without dye molecules (with only CoPPIX attached to the film), Figure 6.6b. These observations confirm a CB mediated electron transfer process from the photoexcited dye across the patterned film to eventually reach CoPPIX.

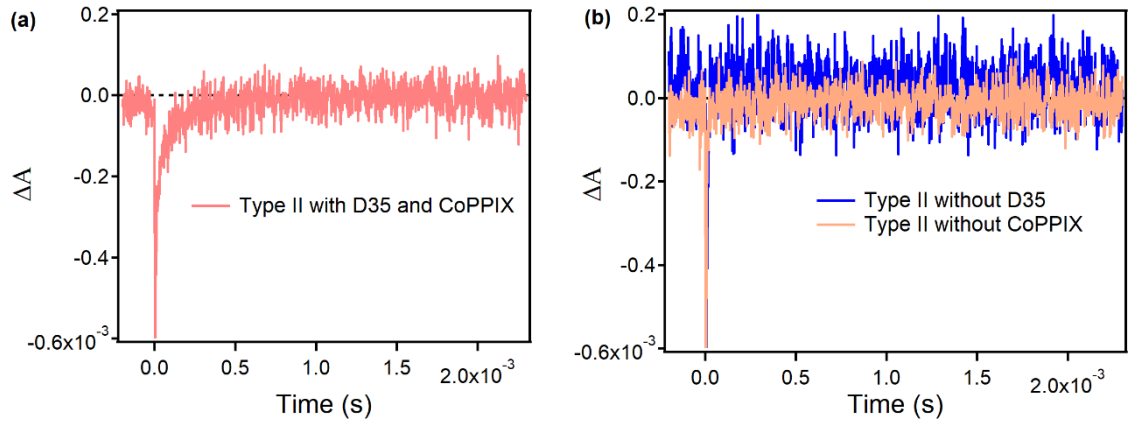

Figure 6.6. Single wavelength ns-TA decays of patterned SnO_2-TiO_2 films after pulsed 500 nm excitation. (a) Type II films with D35 sensitized on the SnO_2-TiO_2 parts and CoPPIX sensitized on the SnO_2 parts. (b) Type II films without CoPPIX and patterned films with only CoPPIX molecules on the surface. Adapted from ***Paper III***[164] *with permission from the PCCP Owner Societies.*

6.3.2 Conduction Band Mediated Electron Transfer in Co-Sensitized TiO_2 Films

Characterizing the CB mediated electron transfer in co-sensitized TiO_2 films with both D35 and CoPPIX on the surface is somewhat trickier. Since both dye and catalyst molecules are evenly attached to the film, overlapping signals from oxidized D35 and reduced CoPPIX appears in the ns-TA measurements. It was therefore of importance to carefully select the probe wavelengths to minimize the contribution from oxidized D35.

Figure 6.7a displays the ns-TA spectra of D35/TiO_2 upon photoexcitation of the dye, and as can be seen in the figure, oxidized D35 displays broad features that cover most of the wavelength range. We therefore chose to monitor the reduction of CoPPIX close to the wavelengths where the signals from the dye cross zero. Probing around the crossing point at 550-555 nm proved to be most useful given the relatively small contribution from D35 together with the fact that the different redox states of CoPPIX have different absorption properties in this region (Figure 6.7b).

To allow for a meaningful comparison between the samples, the excitation energy and concentration of dye molecules were kept constant for all co-sensitized samples (*i.e.* the number of injected electrons are the same) whereas the concentration of CoPPIX on the surface was varied.

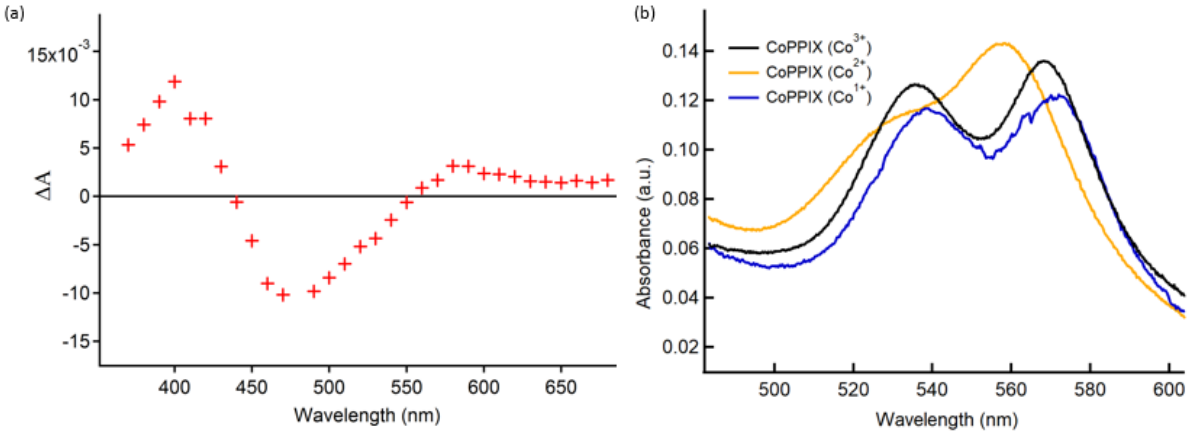

Figure 6.7. (a) ns-TA spectra of a D35/TiO_2 film upon 480 nm excitation in acetonitrile (t=10μs) (b) Absorption spectra of the Q-band for the different redox states of CoPPIX. Adapted with permission from ***Paper IV***[173]*. Copyright 2018 American Chemical Society.*

At 550 nm, oxidized D35 exhibits a negative feature whereas the first reduction of CoPPIX would result in a positive signal. This wavelength was therefore initially monitored in the co-sensitized samples to characterize the first reduction of CoPPIX. The decay traces at 550 nm for the co-sensitized samples are shown in Figure 6.8a, 6.8c and 6.8e. All co-sensitized samples display a positive feature at this wavelength as opposed to the negative feature observed for D35/TiO_2, thus suggesting a fast one-electron transfer to CoPPIX. After the initial formation of the positive feature, it decays with a markedly different kinetics compared to oxidized D35, demonstrating that this decay corresponds to a different process. Interestingly, the decay for samples with the largest excess of dye (30:1) turns negative after ~1 ms. Since doubly reduced CoPPIX would result in a negative feature at this wavelength (Figure 6.7b), this change in sign could result from a second electron transfer event. However, since oxidized D35 also displays a negative feature at this wavelength, this behavior cannot be unambiguously assigned to the formation of doubly reduced CoPPIX.

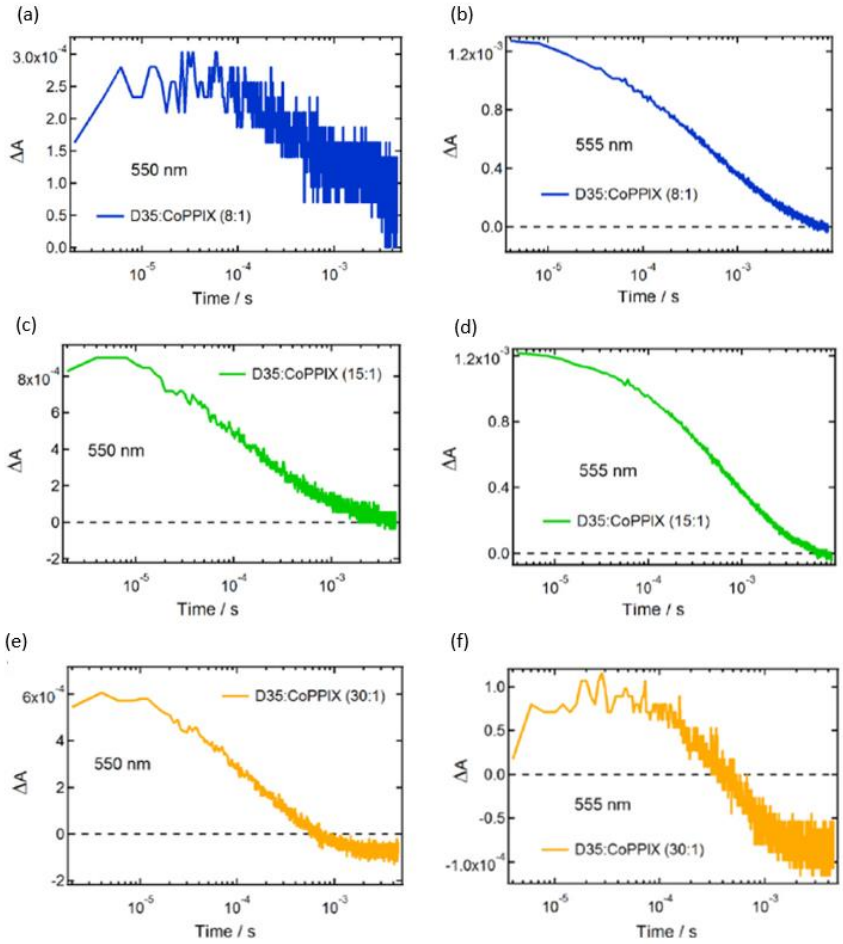

Figure 6.8. ns-TA single wavelength kinetics of co-sensitized films with varying D35:CoPPIX ratios upon 480 nm excitation, (a) D35:CoPPIX ratio of 8:1, kinetics recorded at 550 nm, (b) D35:CoPPIX ratio of 8:1, kinetics recorded at 555 nm, (c) D35:CoPPIX ratio of 15:1, kinetics recorded at 550 nm, (d) D35:CoPPIX ratio of 15:1, kinetics recorded at 555 nm, (e) D35:CoPPIX ratio of 30:1, kinetics recorded at 550 nm and (f) D35:CoPPIX ratio of 30:1, kinetics recorded at 555 nm. Reproduced with permission from ***Paper IV***[173]*. Copyright 2018 American Chemical Society.*

To elucidate whether the change in sign corresponds to formation of doubly reduced CoPPIX, decay traces at 555 nm were also measured since oxidized D35 displays a small positive feature at this wavelength. At 555 nm, the change in sign becomes more apparent for the 30:1 sample (Figure 6.8f), as is also expected if the doubly reduced species is formed when comparing with the spectra of the different redox states (Figure 6.7b). At this wavelength, also the 8:1 and 15:1 samples result in a change of sign at longer timescales (Figure 6.8b and 6.8d). This suggests that the doubly reduced species is formed at all investigated surface coverage ratios, but to a greater extent with a larger excess of dye.

These results taken together demonstrate that two-electron transfer from photoexcited dye molecules *via* the CB can take place and that a large excess of dye is beneficial for two electrons to reach the same catalyst molecule. However, these results also reveal that the first reduction occurs much faster than the second and that it appears to be necessary for most CoPPIX molecules to undergo the first reduction for the second reduction to occur.

These observations are in good agreement with previous studies where the CB mediated electron transfer to a catalyst was measured by the lifetime of the electrons in the CB[172] and with observed higher efficiencies in DSP assemblies with a high dye loading[155].

6.4 Short Summary

The results presented in this Chapter reveal that a long-lived charge separated state between a photosensitizer and the CB can be obtained by utilizing a ruthenium sulfoxide complex in the O-bonded isomer as the photosensitizer. However, the injection efficiency from this complex is low and needs to be improved for it to be competitive as a photosensitizer. Moreover, these studies demonstrate that the charge separated lifetime in dye-sensitized materials can be significantly extended by the design of a patterned SnO_2-TiO_2 film.

Studies of the CB mediated electron transfer to a model catalyst revealed that two-electron transfer from the CB of TiO_2 and one-electron transfer from the CB of SnO_2 to the catalyst indeed is possible. The second reduction step is however much slower than the first and it is necessary to utilize a large excess of dye molecules on the surface. These studies also suggest that the simple approach of co-sensitizing TiO_2 films with dye and catalyst molecules holds greater promise than the patterned films in terms of achieving CB mediated multi-electron to co-attached molecular catalysts.

7 Concluding Remarks and Outlook

The work presented in this Thesis has been dedicated to studies of light-induced processes in molecular/inorganic materials. The main aim has been to study photoinduced processes in different molecular/inorganic materials and how these potentially can be controlled by varying the structure of the molecules, the semiconductor substrate, or by changing the surrounding environment. The photo-induced processes that have been of interest are singlet fission, photoisomerization, and different electron transfer processes.

Studies of the photoinduced processes in DPIBFC6/semiconductor materials revealed that SF on ZrO_2 surfaces is inhibited by the formation of a molecular charge separated state, and that SF occurs to a larger extent in non-polar environments. This study further revealed that fast and efficient electron injection from the singlet excited state outcompetes SF on TiO_2 surfaces, despite the flexible carbon linker used in the DPIBF derivative. The fast singlet injection on TiO_2 speaks in favor of previously used core-shell structures to slow down injection from the singlet excited state on TiO_2.[108, 111] When the molecule is attached to SnO_2 surfaces in a non-polar environment, SF can however occur in parallel to injection from the singlet excited state. Moreover, the created triplets on SnO_2 can inject electrons into the CB of SnO_2. Thus, it seems like utilizing semiconductors with a low CB energy level in a non-polar environment is beneficial for SF followed by injection from the triplet excited state and that this strategy indeed has a promise in future devices. Another surprising finding from this study was that the efficiency of SF

appears to be higher when the molecule is attached to SnO_2 compared to ZrO_2. The reason behind this is not clear at this point but could be related to differences in how the molecules are oriented on the different surfaces. It is possible that slight differences in the nanoparticle network between the semiconductors affect how the molecules attach to the surface, which alters the orientation and/or coupling necessary for SF. These results further demonstrate that it is not straightforward to utilize molecules that display efficient SF in one type of environment and expect similar behavior in another environment or a device. Thus, the photoinduced processes must be carefully evaluated in each new assembly, even when seemingly similar surfaces like SnO_2 and ZrO_2 are used. Given the relatively low SF efficiencies in the materials studied herein, it appears as if the molecules do not orient in a favorable way for SF when attached to a mesoporous surface. Therefore, it would be interesting to study if the SF efficiency could be improved by attaching for example dimers of SF molecules on semiconductor surfaces, as this would allow for a better control of the orientation between the individual molecules on the surface.

The difference between the photoinduced processes of molecules in different environments was further apparent in the study of a photoswitchable ruthenium sulfoxide complex in solution and attached to ZrO_2. Despite displaying both S-to-O and O-to-S photoisomerization to completion in liquid solution, the photoisomerization is slightly hindered on the ZrO_2 film and does not proceed until completion. These observations suggest that not all molecules can be photoisomerized on the surface, possibly due to a restricted molecular rearrangement. Despite this, reversible photoisomerization with the added benefit of spatial addressability is achievable when the molecule is attached to the film. This design further allows for a high surface coverage compared to previously studied surfaces, which can make up for a slightly lower photoisomerization ability while still achieving a high density of photoisomerized molecules per area. Studies of utilizing the ruthenium sulfoxide complex as a photosensitizer revealed that the complex did not inject electrons into the CB of TiO_2 in the S-bonded form. However, after being photoisomerized into the O-bonded form, the complex could inject electrons into the CB of TiO_2 and the resulting charge separated state was remarkably long-lived compared to for other commonly used ruthenium dyes. These preliminary results demonstrate that designing photosensitizers based on photoswitchable molecules can extend the charge separated lifetime. It is however of great importance to increase the injection efficiency from the molecule for it to be competitive as a photosensitizer.

Designing a patterned semiconductor film to extend the charge separated lifetime between a photosensitizer and the CB was successful. By selectively dye-sensitizing TiO_2 stripes on a SnO_2 film, electrons were accumulated in the dye-free SnO_2 parts upon photoexcitation of the dye and this significantly extended the charge separated lifetime. Since the ultimate goal of these assemblies is for solar fuel generation, it was also of importance to study whether electrons could reach a molecular catalyst on the dye-free

SnO_2 parts. Importantly, electrons were shown to transfer from the dye-sensitized TiO_2-SnO_2 stripes to a molecular catalyst on the dye-free SnO_2 parts upon photoexcitation of the dye. The patterned design however comes with one disadvantage in terms of achieving multi-electron transfer to the catalyst, which is the lower CB energy of SnO_2. The lower CB energy results in a lower driving force for electron transfer to immobilized catalyst molecules. This was also apparent when studying the CB mediated electron transfer from SnO_2 to a model catalyst, where only one-electron reduction was observed. We therefore chose to study the electron transfer processes in TiO_2 films co-sensitized with dye and catalyst molecules as well. Although the initial charge separated state between the dye and the CB in these assemblies was more short-lived than in the patterned films, we observed two-electron transfer to the co-attached molecular catalyst in these assemblies. The second reduction step was however much slower than the first, and it was necessary to utilize an excess of dye molecules on the surface to observe the doubly reduced species. Given the slower second reduction of the catalyst, it would be desired to extend the charge separated lifetime between the dye and the CB more than what was achieved in the co-sensitized samples. This could possibly be realized by designing a photosensitizer molecule that extends the charge separated lifetime further. Another design that would be interesting to study in terms of this is to sensitize TiO_2 films with dye and catalyst molecules in a pattern, this would also allow for a more straightforward way of studying the kinetics of the electron transfer and also provide an opportunity of separating the products in future solar-fuel generating assemblies.

The work presented in this Thesis demonstrates the potential of utilizing molecular-semiconductor materials in a variety of light-responsive applications. This work further highlights the importance of a careful design of both the molecular/inorganic material and of the surrounding environment to obtain control of the processes that are triggered from photoexcitation. The results presented herein will help design future molecular/inorganic materials to achieve singlet fission as well as an extended charge separated lifetime and multi-electron transfer necessary for solar fuel generation.

8 Acknowledgements

I want to thank many people for all their support and help during my PhD studies and for making this time so enjoyable. I especially would like to thank these people:

My supervisor **Maria Abrahamsson**, for allowing me to work on these projects and to explore new ideas. Thanks for all your guidance and help during these years. I have learnt so much from you, thank you for always having your door open and for all your support, both in science and other situations.

My co-supervisor **Joakim Andréasson** and my examiner **Bo Albinsson**. Thank you for the scientific discussions and for help with the instruments in the lab.

Jerker Mårtensson, **Per Lincoln**, **Nina Kann**, **Björn Åkerman** and **Marcus Wilhelmsson** for scientific discussions and support.

Betül Küçüköz, for all your endless friendship and help during these years, both with science related problems and in every other part of my life. Thank you for always taking your time to help me and discuss both big and small problems with me. I am so thankful for our friendship and time together at Chalmers, I know that we will be friends forever!

Vandana Singh, for your countless support and friendship. Thanks for always being there for me and for all the fun times and laughter, both in the office and at after-works! Thanks also for all your help when I was writing this thesis, both with proof-reading,

providing fika and accompanying me at Chalmers on weekends. I am so grateful to have you in my life, now and forever.

Gaowa Naren, for your support and for being a great friend. Thank you for our time together at Chalmers and for all the fun, laughter, and nice times at conferences!

Fredrik Edhborg, for always taking your time to discuss scientific problems with me, your input has been truly appreciated and I am happy to have had you as a fellow PhD student almost the entire time. Thanks also for the fun times at conferences!

Deise Fernanda Barbosa de Mattos, for your kindness, always helping me out and for being an awesome friend. I am so happy that I met with you, thanks for all the nice discussions, both about science and life in general!

Rasmus Ringström, for being so kind and for always helping me with all sorts of things. Thanks also for your hard work and for keeping a good mood, it has been really fun to work with you!

Pegah Nabavi, for your support and friendship and for being a great "fadder" making me feel so welcomed when I started as a PhD student.

Damir, **Jens**, **Joachim**, **Valeria,** and **Victor** for introducing me to the labs and for all the help in the laser labs. A special thanks to **Valeria** for our common projects and for all the help during my first years.

All co-authors and collaborators for your work on the projects. A special thanks to **Fredrik**, **Andreas,** and **Victor** for your hard work in synthesizing the compounds studied herein.

Andrew, **Axel, Cassandra**, **Gerard, Liam, Lili, Long, Rita** and **Wera** for nice times in the group meetings! A special thanks to **Andrew** and **Liam** for helping me with proof-reading and improving this thesis.

All the people at floor 5 and in the chemistry division for the great working atmosphere!

My family and **friends**, for your love and encouragement. Thanks for being my reminder that there are more important things in life than science. I love you all!

And finally, to **Tobias**, thanks for all your support and love during these years and for always believing in me. I love you so much!

9 Bibliography

1. Lambers, H.; Chapin, F. S.; Pons, T. L., Photosynthesis. In *Plant Physiological Ecology*, Lambers, H.; Chapin, F. S.; Pons, T. L., Eds. Springer New York: New York, NY, **2008**; pp 11-99.

2. International Energy Agency, In *Solar Energy Perspectives;* International Energy Agency, Ed **2011.**

3. International Energy Agency, In *Key World Energy Statistics 2020;* International Energy Agency, Ed **2020**.

4. Rogelj, J.; den Elzen, M.; Höhne, N.; Fransen, T.; Fekete, H.; Winkler, H.; Schaeffer, R.; Sha, F.; Riahi, K.; Meinshausen, M., Paris Agreement climate proposals need a boost to keep warming well below 2 °C. *Nature* **2016,** *534* (7609), 631-639.

5. Lopez, N., Copernicus: 2020 warmest year on record for Europe; globally, 2020 ties with 2016 for warmest year recorded. **2021**.

6. Semonin, O. E., Multiple Exciton Generation in Quantum Dot Solar Cells. **2012**.

7. Shockley, W.; Queisser, H. J., Detailed balance limit of efficiency of p-n junction solar cells. *J. Appl. Phys.* **1961,** *32* (3), 510-519.

8. Bludau, W.; Onton, A.; Heinke, W., Temperature dependence of the band gap of silicon. *J. Appl. Phys.* **1974,** *45* (4), 1846-1848.

9. Smith, M. B.; Michl, J., Singlet Fission. *Chem. Rev.* **2010,** *110* (11), 6891-6936.

10. Geacintov, N.; Pope, M.; Vogel, F., Effect of magnetic field on the fluorescence of tetracene crystals: exciton fission. *Phys. Rev. Lett.* **1969,** *22* (12), 593.

11. Merrifield, R. E.; Avakian, P.; Groff, R. P., Fission of singlet excitons into pairs of triplet excitons in tetracene crystals. *Chem. Phys. Lett.* **1969,** *3* (6), 386-388.

12. Singh, S.; Jones, W.; Siebrand, W.; Stoicheff, B.; Schneider, W., Laser generation of excitons and fluorescence in anthracene crystals. *J. Chem. Phys.* **1965,** *42* (1), 330-342.

13. Swenberg, C.; Stacy, W., Bimolecular radiationless transitions in crystalline tetracene. *Chem. Phys. Lett.* **1968,** *2* (5), 327-328.

14. Margulies, E. A.; Logsdon, J. L.; Miller, C. E.; Ma, L.; Simonoff, E.; Young, R. M.; Schatz, G. C.; Wasielewski, M. R., Direct observation of a charge-transfer state preceding high-yield singlet fission in terrylenediimide thin films. *J. Am. Chem. Soc.* **2017,** *139* (2), 663-671.

15. Walker, B. J.; Musser, A. J.; Beljonne, D.; Friend, R. H., Singlet exciton fission in solution. *Nat. Chem.* **2013,** *5* (12), 1019.

16. Burdett, J. J.; Müller, A. M.; Gosztola, D.; Bardeen, C. J., Excited state dynamics in solid and monomeric tetracene: The roles of superradiance and exciton fission. *J. Chem. Phys.* **2010,** *133* (14), 144506.

17. Eaton, S. W.; Miller, S. A.; Margulies, E. A.; Shoer, L. E.; Schaller, R. D.; Wasielewski, M. R., Singlet exciton fission in thin films of tert-butyl-substituted terrylenes. *J. Phys. Chem. A* **2015,** *119* (18), 4151-4161.

18. Johnson, J. C.; Nozik, A. J.; Michl, J., High triplet yield from singlet fission in a thin film of 1, 3-diphenylisobenzofuran. *J. Am. Chem. Soc.* **2010,** *132* (46), 16302-16303.

19. Sanders, S. N.; Kumarasamy, E.; Pun, A. B.; Trinh, M. T.; Choi, B.; Xia, J.; Taffet, E. J.; Low, J. Z.; Miller, J. R.; Roy, X.; Zhu, X.-Y.; Steigerwald, M. L.; Sfeir, M. Y.; Campos, L. M., Quantitative intramolecular singlet fission in bipentacenes. *J. Am. Chem. Soc.* **2015,** *137* (28), 8965-8972.

20. Congreve, D. N.; Lee, J.; Thompson, N. J.; Hontz, E.; Yost, S. R.; Reusswig, P. D.; Bahlke, M. E.; Reineke, S.; Van Voorhis, T.; Baldo, M. A., External Quantum Efficiency Above 100% in a Singlet-Exciton-Fission–Based Organic Photovoltaic Cell. *Science* **2013,** *340* (6130), 334.

21. Pace, N. A.; Korovina, N. V.; Clikeman, T. T.; Holliday, S.; Granger, D. B.; Carroll, G. M.; Nanayakkara, S. U.; Anthony, J. E.; McCulloch, I.; Strauss, S. H.; Boltalina, O. V.; Johnson, J. C.; Rumbles, G.; Reid, O. G., Slow charge transfer from pentacene triplet states at the Marcus optimum. *Nat. Chem.* **2020,** *12* (1), 63-70.

22. Pazos-Outón, L. M.; Lee, J. M.; Futscher, M. H.; Kirch, A.; Tabachnyk, M.; Friend, R. H.; Ehrler, B., A Silicon–Singlet Fission Tandem Solar Cell Exceeding 100% External Quantum Efficiency with High Spectral Stability. *ACS Energy Lett.* **2017,** *2* (2), 476-480.

23. Rao, A.; Friend, R. H., Harnessing singlet exciton fission to break the Shockley–Queisser limit. *Nat. Rev. Mater.* **2017,** *2* (11), 1-12.

24. Thompson, N. J.; Congreve, D. N.; Goldberg, D.; Menon, V. M.; Baldo, M. A., Slow light enhanced singlet exciton fission solar cells with a 126% yield of electrons per photon. *Appl. Phys. Lett.* **2013,** *103* (26), 263302.

25. Zukun, W.; Wu, R.; Chen, Z.; Ye, L.; Li, H.; Zhu, H., Ultrafast Electron Transfer Before Singlet Fission and Slow Triplet State Electron Transfer in Pentacene Single Crystal/C60 Heterostructure. *J. Phys. Chem. A* **2020**.

26. Gray, H. B., Powering the planet with solar fuel. *Nat. Chem.* **2009,** *1* (1), 7-7.

27. Tran, P. D.; Wong, L. H.; Barber, J.; Loo, J. S. C., Recent advances in hybrid photocatalysts for solar fuel production. *Energy Environ. Sci.* **2012,** *5* (3), 5902-5918.

28. Xia, Y.; Zhang, L.; Hu, B.; Yu, J.; Al-Ghamdi, A. A.; Wageh, S., Design of highly-active photocatalytic materials for solar fuel production. *Chem. Eng. J.* **2020**, 127732.

29. Hammarström, L., Accumulative charge separation for solar fuels production: coupling light-induced single electron transfer to multielectron catalysis. *Acc. Chem. Res.* **2015,** *48* (3), 840-850.

30. Barber, J., Photosynthetic energy conversion: natural and artificial. *Chem. Soc. Rev.* **2009,** *38* (1), 185-196.

31. Rappaport, F.; Guergova-Kuras, M.; Nixon, P. J.; Diner, B. A.; Lavergne, J., Kinetics and pathways of charge recombination in photosystem II. *Biochemistry* **2002,** *41* (26), 8518-8527.

32. Tachibana, Y.; Vayssieres, L.; Durrant, J. R., Artificial photosynthesis for solar water-splitting. *Nat. Photon.* **2012,** *6* (8), 511-518.

33. Hammarström, L.; Wasielewski, M. R., Biomimetic approaches to artificial photosynthesis. *Energy Environ. Sci.* **2011,** *4* (7), 2339-2339.

34. Hammarström, L., Artificial photosynthesis and solar fuels. ACS Publications: **2009**.

35. Fujishima, A.; Honda, K., Electrochemical photolysis of water at a semiconductor electrode. *nature* **1972,** *238* (5358), 37-38.

36. Lee, J. S.; Won, D. I.; Jung, W. J.; Son, H. J.; Pac, C.; Kang, S. O., Widely Controllable Syngas Production by a Dye-Sensitized TiO2 Hybrid System with Re-I and Co-III Catalysts under Visible-Light Irradiation. *Angew. Chem. Int. Ed.* **2017,** *56* (4), 976-980.

37. Roy, S. C.; Varghese, O. K.; Paulose, M.; Grimes, C. A., Toward solar fuels: photocatalytic conversion of carbon dioxide to hydrocarbons. *ACS Nano* **2010,** *4* (3), 1259-1278.

38. Sheridan, M. V.; Hill, D. J.; Sherman, B. D.; Wang, D. G.; Marquard, S. L.; Wee, K. R.; Cahoon, J. F.; Meyer, T. J., All-in-One Derivatized Tandem p(+)n-Silicon-SnO2/TiO2 Water Splitting Photoelectrochemical Cell. *Nano Lett.* **2017,** *17* (4), 2440-2446.

39. Sherman, B. D.; Sheridan, M. V.; Wee, K. R.; Marquard, S. L.; Wang, D. G.; Alibabaei, L.; Ashford, D. L.; Meyer, T. J., A Dye-Sensitized Photoelectrochemical Tandem Cell for Light Driven Hydrogen Production from Water. *J. Am. Chem. Soc.* **2016,** *138* (51), 16745-16753.

40. Shi, X. J.; Zhang, K.; Shin, K.; Ma, M.; Kwon, J.; Choi, I. T.; Kim, J. K.; Kim, H. K.; Wang, D. H.; Park, J. H., Unassisted photoelectrochemical water splitting beyond 5.7% solar-to-hydrogen conversion efficiency by a wireless monolithic photoanode/dye-sensitised solar cell tandem device. *Nano Energy* **2015,** *13*, 182-191.

41. Low, J.; Yu, J.; Ho, W., Graphene-Based Photocatalysts for CO2 Reduction to Solar Fuel. *J. Phys. Chem. Lett.* **2015,** *6* (21), 4244-4251.

42. Vyas, V. S.; Lau, V. W.-h.; Lotsch, B. V., Soft Photocatalysis: Organic Polymers for Solar Fuel Production. *Chem. Mater.* **2016,** *28* (15), 5191-5204.

43. Ashford, D. L.; Lapides, A. M.; Vannucci, A. K.; Hanson, K.; Torelli, D. A.; Harrison, D. P.; Templeton, J. L.; Meyer, T. J., Water Oxidation by an Electropolymerized Catalyst on Derivatized Mesoporous Metal Oxide Electrodes. *J. Am. Chem. Soc.* **2014,** *136* (18), 6578-6581.

44. Logan, M. W.; Ayad, S.; Adamson, J. D.; Dilbeck, T.; Hanson, K.; Uribe-Romo, F. J., Systematic variation of the optical bandgap in titanium based isoreticular metal–organic frameworks for photocatalytic reduction of CO2 under blue light. *J. Mater. Chem. A* **2017,** *5* (23), 11854-11863.

45. Balzani, V.; Credi, A.; Venturi, M., Light powered molecular machines. *Chem. Soc. Rev.* **2009,** *38* (6), 1542-1550.

46. Ceroni, P.; Credi, A.; Venturi, M.; Balzani, V., Light-powered molecular devices and machines. *Photochem. Photobiol. Sci.* **2010,** *9* (12), 1561-1573.

47. Sundin, E.; Abrahamsson, M., Long-lived charge separation in dye–semiconductor assemblies: a pathway to multi-electron transfer reactions. *ChemComm* **2018,** *54* (42), 5289-5298.

48. Hollas, J. M., *Modern spectroscopy*. John Wiley & Sons: **2004**.

49. Lakowicz, J. R., Principles of Fluorescence Spectroscopy, (1999). Kluwer Academic/Plenum Publishers, New York: **2004**.

50. Marcus, R., RA Marcus, J. Chem. Phys. 24, 966 (1956). *J. Chem. Phys.* **1956,** *24*, 966.

51. Turro, N. J., *Modern molecular photochemistry*. University science books: **1991**.

52. Smart, L. E.; Moore, E. A., *Solid state chemistry: an introduction*. CRC press: 2012.

53. Atkins, P.; De Paula, J.; Friedman, R., *Quanta, matter, and change: a molecular approach to physical chemistry*. Oxford University Press: **2009**.

54. Irie, M., Photochromism: Memories and SwitchesIntroduction. *Chem. Rev.* **2000,** *100* (5), 1683-1684.

55. Anslyn, E. V.; Dougherty, D. A., *Modern physical organic chemistry*. University science books: **2006**.

56. Schrödinger, E., An Undulatory Theory of the Mechanics of Atoms and Molecules. *Physical Review* **1926,** *28* (6), 1049-1070.

57. Grätzel, M., Photoelectrochemical cells. *nature* **2001,** *414* (6861), 338.

58. Emeline, A. V.; Rudakova, A. V.; Ryabchuk, V. K.; Serpone, N., Photostimulated Reactions at the Surface of Wide Band-Gap Metal Oxides (ZrO2 and TiO2): Interdependence of Rates of Reactions on Pressure−Concentration and on Light Intensity. *J. Phys. Chem. B* **1998,** *102* (52), 10906-10916.

59. Grätzel, M., Dye-sensitized solar cells. *J. Photochem. Photobiol. C* **2003,** *4* (2), 145-153.

60. Smith, M. B.; Michl, J., Recent Advances in Singlet Fission. *Annu. Rev. Phys. Chem.* **2013,** *64* (1), 361-386.

61. Wilson, M. W. B.; Rao, A.; Ehrler, B.; Friend, R. H., Singlet Exciton Fission in Polycrystalline Pentacene: From Photophysics toward Devices. *Acc. Chem. Res.* **2013,** *46* (6), 1330-1338.

62. Burdett, J. J.; Bardeen, C. J., The Dynamics of Singlet Fission in Crystalline Tetracene and Covalent Analogs. *Acc. Chem. Res.* **2013,** *46* (6), 1312-1320.

63. Schwerin, A. F.; Johnson, J. C.; Smith, M. B.; Sreearunothai, P.; Popovic, D.; Černý, J. i.; Havlas, Z.; Paci, I.; Akdag, A.; MacLeod, M. K.; Chen, X.; David, D. E.; Ratner, M. A.; Miller, J. R.; Nozik, A. J.; Michl, J., Toward designed singlet fission: electronic states and photophysics of 1, 3-diphenylisobenzofuran. *J. Phys. Chem. A* **2010,** *114* (3), 1457-1473.

64. Basel, B. S.; Zirzlmeier, J.; Hetzer, C.; Reddy, S. R.; Phelan, B. T.; Krzyaniak, M. D.; Volland, M. K.; Coto, P. B.; Young, R. M.; Clark, T.; Thoss, M.; Tykwinski, R. R.; Wasielewski, M. R.; Guldi, D. M., Evidence for charge-transfer mediation in the primary events of singlet fission in a weakly coupled pentacene dimer. *Chem.* **2018,** *4* (5), 1092-1111.

65. Greyson, E. C.; Vura-Weis, J.; Michl, J.; Ratner, M. A., Maximizing singlet fission in organic dimers: theoretical investigation of triplet yield in the regime of localized excitation and fast coherent electron transfer. *J. Phys. Chem. B* **2010,** *114* (45), 14168-14177.

66. Johnson, J. C.; Nozik, A. J.; Michl, J., The role of chromophore coupling in singlet fission. *Acc. Chem. Res.* **2013,** *46* (6), 1290-1299.

67. Krishnapriya, K.; Musser, A. J.; Patil, S., Molecular Design Strategies for Efficient Intramolecular Singlet Exciton Fission. *ACS Energy Lett.* **2018,** *4* (1), 192-202.

68. Monahan, N.; Zhu, X.-Y., Charge transfer–mediated singlet fission. *Annu. Rev. Phys. Chem.* **2015,** *66*, 601-618.

69. Zimmerman, P. M.; Musgrave, C. B.; Head-Gordon, M., A correlated electron view of singlet fission. *Acc. Chem. Res.* **2013,** *46* (6), 1339-1347.

70. Musser, A. J.; Clark, J., Triplet-Pair States in Organic Semiconductors. *Annu. Rev. Phys. Chem.* **2019,** *70* (1), 323-351.

71. Wilson, M. W. B.; Rao, A.; Clark, J.; Kumar, R. S. S.; Brida, D.; Cerullo, G.; Friend, R. H., Ultrafast Dynamics of Exciton Fission in Polycrystalline Pentacene. *J. Am. Chem. Soc.* **2011,** *133* (31), 11830-11833.

72. Musser, A. J.; Al-Hashimi, M.; Maiuri, M.; Brida, D.; Heeney, M.; Cerullo, G.; Friend, R. H.; Clark, J., Activated Singlet Exciton Fission in a Semiconducting Polymer. *J. Am. Chem. Soc.* **2013,** *135* (34), 12747-12754.

73. Yost, S. R.; Lee, J.; Wilson, M. W. B.; Wu, T.; McMahon, D. P.; Parkhurst, R. R.; Thompson, N. J.; Congreve, D. N.; Rao, A.; Johnson, K.; Sfeir, M. Y.; Bawendi, M. G.; Swager, T. M.; Friend, R. H.; Baldo, M. A.; Van Voorhis, T., A transferable model for singlet-fission kinetics. *Nat. Chem.* **2014,** *6* (6), 492-497.

74. Johnson, J. C.; Michl, J., 1,3-Diphenylisobenzofuran: a Model Chromophore for Singlet Fission. *Topics in Current Chemistry* **2017,** *375* (5), 80.

75. Margulies, E. A.; Miller, C. E.; Wu, Y.; Ma, L.; Schatz, G. C.; Young, R. M.; Wasielewski, M. R., Enabling singlet fission by controlling intramolecular charge transfer in π-stacked covalent terrylenediimide dimers. *Nat. Chem.* **2016,** *8* (12), 1120.

76. Bolton, J. R.; Archer, M. D., *Basic electron-transfer theory*. The American Chemical Society: Washington: 1991.

77. Marcus, R. A., Electron transfer reactions in chemistry. Theory and experiment. *Reviews of Modern Physics* **1993,** *65* (3), 599.

78. Sutin, N., Theory of electron transfer reactions: insights and hindsights. *Progress in Inorganic Chemistry: An Appreciation of Henry Taube* **1983**, 441-498.

79. Sutin, N.; Creutz, C.; Fujita, E., Photo-induced generation of dihydrogen and reduction of carbon dioxide using transition metal complexes. *Comments Mod Chem A Comments Inorg Chem* **1997,** *19* (2), 67-92.

80. Wasielewski, M. R., Photoinduced electron transfer in supramolecular systems for artificial photosynthesis. *Chem. Rev.* **1992,** *92* (3), 435-461.

81. Barbara, P. F.; Meyer, T. J.; Ratner, M. A., Contemporary issues in electron transfer research. *J. Phys. Chem.* **1996,** *100* (31), 13148-13168.

82. Gerischer, H., Heterogeneous electrochemical systems for solar energy conversion. *Pure and Applied Chemistry* **1980,** *52* (12), 2649-2667.

83. Gerischer, H.; Michel-Beyerle, M. E.; Rebentrost, F.; Tributsch, H., Sensitization of charge injection into semiconductors with large band gap. *Electrochim. Acta* **1968,** *13* (6), 1509-1515.

84. Watson, D. F.; Meyer, G. J., Electron Injection at dye-sensitized semiconductor electrodes. *Annu. Rev. Phys. Chem.* **2004,** *56* (1), 119-156.

85. Ardo, S.; Achey, D.; Morris, A. J.; Abrahamsson, M.; Meyer, G. J., Non-Nernstian two-electron transfer photocatalysis at metalloporphyrin–TiO2 interfaces. *J. Am. Chem. Soc.* **2011,** *133* (41), 16572-16580.

86. Staniszewski, A.; Morris, A. J.; Ito, T.; Meyer, G. J., Conduction band mediated electron transfer across nanocrystalline TiO2 surfaces. *J. Phys. Chem. B* **2007,** *111* (24), 6822-6828.

87. Hu, K.; Blair, A. D.; Piechota, E. J.; Schauer, P. A.; Sampaio, R. N.; Parlane, F. G. L.; Meyer, G. J.; Berlinguette, C. P., Kinetic pathway for interfacial electron transfer from a semiconductor to a molecule. *Nat. Chem.* **2016,** *8* (9), 853-859.

88. Tian, H.; Yang, S., Recent progresses on diarylethene based photochromic switches. *Chem. Soc. Rev.* **2004,** *33* (2), 85-97.

89. Rack, J. J.; Mockus, N. V., Room-Temperature Photochromism in cis- and trans-[Ru(bpy)2(dmso)2]2+. *Inorg. Chem.* **2003,** *42* (19), 5792-5794.

90. Bandara, H. M. D.; Burdette, S. C., Photoisomerization in different classes of azobenzene. *Chem. Soc. Rev.* **2012,** *41* (5), 1809-1825.

91. Klajn, R., Spiropyran-based dynamic materials. *Chem. Soc. Rev.* **2014,** *43* (1), 148-184.

92. Matsuda, K.; Irie, M., Diarylethene as a photoswitching unit. *J. Photochem. Photobiol. C* **2004,** *5* (2), 169-182.

93. McClure, B. A.; Rack, J. J., Isomerization in photochromic ruthenium sulfoxide complexes. *Eur. J. Inorg. Chem.* **2010,** *2010* (25), 3895-3904.

94. Rack, J. J., Electron transfer triggered sulfoxide isomerization in ruthenium and osmium complexes. *Coord. Chem. Rev.* **2009,** *253* (1-2), 78-85.

95. Stranius, K.; Börjesson, K., Determining the Photoisomerization Quantum Yield of Photoswitchable Molecules in Solution and in the Solid State. *Sci. Rep.* **2017,** *7* (1), 41145.

96. Gonzalez, A.; Kengmana, E. S.; Fonseca, M. V.; Han, G. G. D., Solid-state photoswitching molecules: structural design for isomerization in condensed phase. *Mater. Today Adv.* **2020,** *6*, 100058.

97. Wang, J. C.; Hill, S. P.; Dilbeck, T.; Ogunsolu, O. O.; Banerjee, T.; Hanson, K., Multimolecular assemblies on high surface area metal oxides and their role in interfacial energy and electron transfer. *Chem. Soc. Rev.* **2018,** *47* (1), 104-148.

98. Zhang, L.; Cole, J. M., Anchoring Groups for Dye-Sensitized Solar Cells. *ACS Appl. Mater. Interfaces* **2015,** *7* (6), 3427-3455.

99. Hagfeldt, A.; Boschloo, G.; Sun, L.; Kloo, L.; Pettersson, H., Dye-sensitized solar cells. *Chem. Rev.* **2010,** *110* (11), 6595-6663.

100. Kalyanasundaram, K., *Dye-sensitized solar cells*. EPFL press: **2010**.

101. Sharma, K.; Sharma, V.; Sharma, S. S., Dye-Sensitized Solar Cells: Fundamentals and Current Status. *Nanoscale Res. Lett.* **2018,** *13* (1), 381.

102. Oum, K.; Lohse, P. W.; Klein, J. R.; Flender, O.; Scholz, M.; Hagfeldt, A.; Boschloo, G.; Lenzer, T., Photoinduced ultrafast dynamics of the triphenylamine-based organic sensitizer D35 on TiO 2, ZrO 2 and in acetonitrile. *Phys. Chem. Chem. Phys.* **2013,** *15* (11), 3906-3916.

103. Johansson, P. G.; Zhang, Y.; Abrahamsson, M.; Meyer, G. J.; Galoppini, E., Slow excited state injection and charge recombination at star-shaped ruthenium polypyridyl compounds—TiO 2 interfaces. *ChemComm* **2011,** *47* (22), 6410-6412.

104. Koops, S. E.; O'Regan, B. C.; Barnes, P. R.; Durrant, J. R., Parameters influencing the efficiency of electron injection in dye-sensitized solar cells. *J. Am. Chem. Soc.* **2009,** *131* (13), 4808-4818.

105. Snaith, H. J., Estimating the Maximum Attainable Efficiency in Dye-Sensitized Solar Cells. *Adv. Funct. Mater.* **2010,** *20* (1), 13-19.

106. Paci, I.; Johnson, J. C.; Chen, X.; Rana, G.; Popović, D.; David, D. E.; Nozik, A. J.; Ratner, M. A.; Michl, J., Singlet Fission for Dye-Sensitized Solar Cells: Can a Suitable Sensitizer Be Found? *J. Am. Chem. Soc.* **2006,** *128* (51), 16546-16553.

107. Rao, A.; Friend, R. H., Harnessing singlet exciton fission to break the Shockley–Queisser limit. *Nat. Rev. Mater.* **2017,** *2* (11), 17063.

108. Banerjee, T.; Hill, S. P.; Hermosilla-Palacios, M. A.; Piercy, B. D.; Haney, J.; Casale, B.; DePrince, A. E.; Losego, M. D.; Kleiman, V. D.; Hanson, K., Diphenylisobenzofuran Bound to Nanocrystalline Metal Oxides: Excimer Formation, Singlet Fission, Electron Injection, and Low Energy Sensitization. *J. Phys. Chem. C* **2018,** *122* (50), 28478-28490.

109. Kunzmann, A.; Gruber, M.; Casillas, R.; Zirzlmeier, J.; Stanzel, M.; Peukert, W.; Tykwinski, R. R.; Guldi, D. M., Singlet Fission for Photovoltaics with 130 % Injection Efficiency. *Angew. Chem. Int. Ed.* **2018,** *57* (33), 10742-10747.

110. Pace, N. A.; Arias, D. H.; Granger, D. B.; Christensen, S.; Anthony, J. E.; Johnson, J. C., Dynamics of singlet fission and electron injection in self-assembled acene monolayers on titanium dioxide. *Chem. Sci.* **2018,** *9* (11), 3004-3013.

111. Schrauben, J. N.; Zhao, Y.; Mercado, C.; Dron, P. I.; Ryerson, J. L.; Michl, J.; Zhu, K.; Johnson, J. C., Photocurrent Enhanced by Singlet Fission in a Dye-Sensitized Solar Cell. *ACS Appl. Mater. Interfaces* **2015,** *7* (4), 2286-2293.

112. Akdag, A.; Wahab, A.; Beran, P.; Rulisek, L.; Dron, P. I.; Ludvik, J.; Michl, J., Covalent dimers of 1, 3-Diphenylisobenzofuran for singlet fission: synthesis and electrochemistry. *J. Org. Chem.* **2015,** *80* (1), 80-89.

113. Johnson, J. C.; Akdag, A.; Zamadar, M.; Chen, X.; Schwerin, A. F.; Paci, I.; Smith, M. B.; Havlas, Z.; Miller, J. R.; Ratner, M. A.; Nozik, A. J.; Michl, J., Toward designed singlet fission: solution photophysics of two indirectly coupled covalent dimers of 1, 3-diphenylisobenzofuran. *J. Phys. Chem. B* **2013,** *117* (16), 4680-4695.

114. Johnson, J. C.; Michl, J., 1, 3-Diphenylisobenzofuran: a Model Chromophore for Singlet Fission. In *Physical Organic Chemistry of Quinodimethanes*, Springer: **2017**; pp 249-277.

115. Ryerson, J. L.; Schrauben, J. N.; Ferguson, A. J.; Sahoo, S. C.; Naumov, P.; Havlas, Z.; Michl, J.; Nozik, A. J.; Johnson, J. C., Two thin film polymorphs of the singlet fission compound 1, 3-diphenylisobenzofuran. *J. Phys. Chem. C* **2014,** *118* (23), 12121-12132.

116. Schrauben, J. N.; Ryerson, J. L.; Michl, J.; Johnson, J. C., Mechanism of singlet fission in thin films of 1, 3-diphenylisobenzofuran. *J. Am. Chem. Soc.* **2014,** *136* (20), 7363-7373.

117. Schrauben, J. N.; Akdag, A.; Wen, J.; Havlas, Z.; Ryerson, J. L.; Smith, M. B.; Michl, J.; Johnson, J. C., Excitation Localization/Delocalization Isomerism in a Strongly Coupled Covalent Dimer of 1,3-Diphenylisobenzofuran. *J. Phys. Chem. A* **2016,** *120* (20), 3473-3483.

118. Sundin, E.; Ringström, R.; Johansson, F.; Küçüköz, B.; Ekebergh, A.; Gray, V.; Albinsson, B.; Mårtensson, J.; Abrahamsson, M., Singlet Fission and Electron Injection from the Triplet Excited State in Diphenylisobenzofuran–Semiconductor Assemblies: Effects of Solvent Polarity and Driving Force. *J. Phys. Chem. C* **2020,** *124* (38), 20794-20805.

119. Butler, M. A.; Ginley, D. S., Prediction of Flatband Potentials at Semiconductor-Electrolyte Interfaces from Atomic Electronegativities. *J. Electrochem. Soc.* **1978,** *125* (2), 228-230.

120. Tiwana, P.; Docampo, P.; Johnston, M. B.; Snaith, H. J.; Herz, L. M., Electron mobility and injection dynamics in mesoporous ZnO, SnO2, and TiO2 films used in dye-sensitized solar cells. *ACS Nano* **2011,** *5* (6), 5158-5166.

121. Tegeder, P., Optically and thermally induced molecular switching processes at metal surfaces. *J. Phys. Condens. Matter* **2012,** *24* (39), 394001.

122. Bronner, C.; Schulze, M.; Hagen, S.; Tegeder, P. J. N. J. o. P., The influence of the electronic structure of adsorbate–substrate complexes on photoisomerization ability. **2012,** *14* (4), 043023.

123. Chu, Z.; Klajn, R., Polysilsesquioxane Nanowire Networks as an "Artificial Solvent" for Reversible Operation of Photochromic Molecules. *Nano Lett.* **2019,** *19* (10), 7106-7111.

124. Comstock, M. J.; Levy, N.; Kirakosian, A.; Cho, J.; Lauterwasser, F.; Harvey, J. H.; Strubbe, D. A.; Fréchet, J. M. J.; Trauner, D.; Louie, S. G.; Crommie, M. F., Reversible Photomechanical Switching of Individual Engineered Molecules at a Metallic Surface. *Phys. Rev. Lett.* **2007,** *99* (3), 038301.

125. Dryza, V.; Bieske, E. J., Electron injection and energy-transfer properties of spiropyran–cyclodextrin complexes coated onto metal oxide nanoparticles: toward photochromic light harvesting. *J. Phys. Chem. C* **2015,** *119* (25), 14076-14084.

126. Ito, M.; Wei, T. X.; Chen, P.-L.; Akiyama, H.; Matsumoto, M.; Tamada, K.; Yamamoto, Y., A novel method for creation of free volume in a one-component self-assembled monolayer. Dramatic size effect of para-carborane. *J. Mater. Chem.* **2005,** *15* (4), 478-483.

127. Kumar, A. S.; Ye, T.; Takami, T.; Yu, B.-C.; Flatt, A. K.; Tour, J. M.; Weiss, P. S., Reversible Photo-Switching of Single Azobenzene Molecules in Controlled Nanoscale Environments. *Nano Lett.* **2008,** *8* (6), 1644-1648.

128. Yasuda, S.; Nakamura, T.; Matsumoto, M.; Shigekawa, H., Phase Switching of a Single Isomeric Molecule and Associated Characteristic Rectification. *J. Am. Chem. Soc.* **2003,** *125* (52), 16430-16433.

129. Kilså, K.; Mayo, E. I.; Brunschwig, B. S.; Gray, H. B.; Lewis, N. S.; Winkler, J. R., Anchoring Group and Auxiliary Ligand Effects on the Binding of Ruthenium Complexes to Nanocrystalline TiO2 Photoelectrodes. *J. Phys. Chem. B* **2004,** *108* (40), 15640-15651.

130. Dilbeck, T.; Hill, S. P.; Hanson, K., Harnessing molecular photon upconversion at sub-solar irradiance using dual sensitized self-assembled trilayers. *J. Mater. Chem. A* **2017,** *5* (23), 11652-11660.

131. Durrant, J. R.; Haque, S. A.; Palomares, E., Towards optimisation of electron transfer processes in dye sensitised solar cells. *Coord. Chem. Rev.* **2004,** *248* (13-14), 1247-1257.

132. Tachibana, Y.; Moser, J. E.; Grätzel, M.; Klug, D. R.; Durrant, J. R., Subpicosecond interfacial charge separation in dye-sensitized nanocrystalline titanium dioxide films. *J. Phys. Chem.* **1996,** *100* (51), 20056-20062.

133. Sundin, E.; Johansson, F.; Saavedra Becerril, V.; Hedberg Wallenstein, J.; Gasslander, A.; Mårtensson, J.; Abrahamsson, M., Two-Colour Photoswitching in Photoresponsive Inorganic Thin Films. *Materials Advances* **2021**.

134. Cordones, A. A.; Lee, J. H.; Hong, K.; Cho, H.; Garg, K.; Boggio-Pasqua, M.; Rack, J. J.; Huse, N.; Schoenlein, R. W.; Kim, T. K., Transient metal-centered states mediate isomerization of a photochromic ruthenium-sulfoxide complex. *Nat. Commun.* **2018,** *9* (1), 1989.

135. Garg, K.; Engle, J. T.; Ziegler, C. J.; Rack, J. J., Tuning Excited State Isomerization Dynamics through Ground State Structural Changes in Analogous Ruthenium and Osmium Sulfoxide Complexes. *Chem. Eur. J.* **2013,** *19* (35), 11686-11695.

136. Göttle, A. J.; Dixon, I. M.; Alary, F.; Heully, J.-L.; Boggio-Pasqua, M., Adiabatic Versus Nonadiabatic Photoisomerization in Photochromic Ruthenium Sulfoxide Complexes: A Mechanistic Picture from Density Functional Theory Calculations. *J. Am. Chem. Soc.* **2011,** *133* (24), 9172-9174.

137. McClure, B. A.; Mockus, N. V.; Butcher Jr, D. P.; Lutterman, D. A.; Turro, C.; Petersen, J. L.; Rack, J. J., Photochromic ruthenium sulfoxide complexes: evidence for isomerization through a conical intersection. *Inorg. Chem.* **2009,** *48* (17), 8084-8091.

138. McClure, B. A.; Rack, J. J., Two-Color Reversible Switching in a Photochromic Ruthenium Sulfoxide Complex. *Angew. Chem. Int. Ed.* **2009,** *48* (45), 8556-8558.

139. Yeh, A.; Scott, N.; Taube, H., S to O and O to S linkage isomerization in sulfoxide complexes of pentaammineruthenium. *Inorg. Chem.* **1982,** *21* (7), 2542-2545.

140. King, A. W.; McClure, B. A.; Jin, Y.; Rack, J. J., Investigating the Effects of Solvent on the Ultrafast Dynamics of a Photoreversible Ruthenium Sulfoxide Complex. *J. Phys. Chem. A* **2014,** *118* (45), 10425-10432.

141. Brennaman, M. K.; Dillon, R. J.; Alibabaei, L.; Gish, M. K.; Dares, C. J.; Ashford, D. L.; House, R. L.; Meyer, G. J.; Papanikolas, J. M.; Meyer, T. J., Finding the Way to Solar Fuels with Dye-Sensitized Photoelectrosynthesis Cells. *J. Am. Chem. Soc.* **2016,** *138* (40), 13085-13102.

142. Song, W.; Chen, Z.; Glasson, C. R. K.; Hanson, K.; Luo, H.; Norris, M. R.; Ashford, D. L.; Concepcion, J. J.; Brennaman, M. K.; Meyer, T. J., Interfacial Dynamics and Solar Fuel Formation in Dye-Sensitized Photoelectrosynthesis Cells. *ChemPhysChem* **2012,** *13* (12), 2882-2890.

143. Alibabaei, L.; Sherman, B. D.; Norris, M. R.; Brennaman, M. K.; Meyer, T. J., Visible photoelectrochemical water splitting into H2 and O2 in a dye-sensitized photoelectrosynthesis cell. *Proc. Natl. Acad. Sci. U.S.A.* **2015,** *112* (19), 5899-5902.

144. Li, F. S.; Fan, K.; Xu, B.; Gabrielsson, E.; Daniel, Q.; Li, L.; Sun, L. C., Organic Dye-Sensitized Tandem Photoelectrochemical Cell for Light Driven Total Water Splitting. *J. Am. Chem. Soc.* **2015,** *137* (28), 9153-9159.

145. Wang, D.; Wang, L.; Brady, M. D.; Dares, C. J.; Meyer, G. J.; Meyer, T. J.; Concepcion, J. J., Self-Assembled Chromophore–Catalyst Bilayer for Water Oxidation in a Dye-Sensitized Photoelectrosynthesis Cell. *J. Phys. Chem. C* **2019,** *123* (50), 30039-30045.

146. Song, W.; Brennaman, M. K.; Concepcion, J. J.; Jurss, J. W.; Hoertz, P. G.; Luo, H.; Chen, C.; Hanson, K.; Meyer, T. J., Interfacial Electron Transfer Dynamics for [Ru(bpy)2((4,4′-PO3H2)2bpy)]2+ Sensitized TiO2 in a Dye-Sensitized Photoelectrosynthesis Cell: Factors Influencing Efficiency and Dynamics. *J. Phys. Chem. C* **2011,** *115* (14), 7081-7091.

147. Reisner, E.; Powell, D. J.; Cavazza, C.; Fontecilla-Camps, J. C.; Armstrong, F. A., Visible light-driven H2 production by hydrogenases attached to dye-sensitized TiO2 nanoparticles. *J. Am. Chem. Soc.* **2009,** *131* (51), 18457-18466.

148. Warnan, J.; Willkomm, J.; Ng, J. N.; Godin, R.; Prantl, S.; Durrant, J. R.; Reisner, E., Solar H 2 evolution in water with modified diketopyrrolopyrrole dyes immobilised on molecular Co and Ni catalyst–TiO 2 hybrids. *Chem. Sci.* **2017,** *8* (4), 3070-3079.

149. Willkomm, J.; Orchard, K. L.; Reynal, A.; Pastor, E.; Durrant, J. R.; Reisner, E., Dye-sensitised semiconductors modified with molecular catalysts for light-driven H 2 production. *Chem. Soc. Rev.* **2016,** *45* (1), 9-23.

150. Reginato, G.; Zani, L.; Calamante, M.; Mordini, A.; Dessì, A., Dye-Sensitized Heterogeneous Photocatalysts for Green Redox Reactions. *Eur. J. Inorg. Chem.* **2020,** *2020* (11-12), 899-917.

151. Mohamed, H. H.; Dillert, R.; Bahnemann, D. W., Reaction dynamics of the transfer of stored electrons on TiO 2 nanoparticles: a stopped flow study. *J. Photochem. Photobiol. A* **2011,** *217* (1), 271-274.

152. Mohamed, H. H.; Mendive, C. B.; Dillert, R.; Bahnemann, D. W., Kinetic and mechanistic investigations of multielectron transfer reactions induced by stored electrons in TiO2 nanoparticles: a stopped flow study. *J. Phys. Chem. A* **2011,** *115* (11), 2139-2147.

153. Lakadamyali, F.; Reisner, E., Photocatalytic H 2 evolution from neutral water with a molecular cobalt catalyst on a dye-sensitised TiO 2 nanoparticle. *ChemComm* **2011,** *47* (6), 1695-1697.

154. Lakadamyali, F.; Reynal, A.; Kato, M.; Durrant, J. R.; Reisner, E., Electron Transfer in Dye-Sensitised Semiconductors Modified with Molecular Cobalt Catalysts: Photoreduction of Aqueous Protons. *Chem. Eur. J.* **2012,** *18* (48), 15464-15475.

155. Won, D. I.; Lee, J. S.; Cheong, H. Y.; Cho, M.; Jung, W. J.; Son, H. J.; Pac, C.; Kang, S. O., Organic-inorganic hybrid photocatalyst for carbon dioxide reduction. *Faraday Discuss.* **2017,** *198*, 337-351.

156. Bozal-Ginesta, C.; Mesa, C. A.; Eisenschmidt, A.; Francàs, L.; Shankar, R. B.; Antón-García, D.; Warnan, J.; Willkomm, J.; Reynal, A.; Reisner, E.; Durrant, J. R., Charge accumulation kinetics in multi-redox molecular catalysts immobilised on TiO2. *Chem. Sci.* **2021**.

157. Le-Quang, L.; Stanbury, M.; Chardon-Noblat, S.; Mouesca, J.-M.; Maurel, V.; Chauvin, J., Immobilization of Mn(i) and Ru(ii) polypyridyl complexes on TiO2 nanoparticles for selective photoreduction of CO2 to formic acid. *ChemComm* **2019,** *55* (90), 13598-13601.

158. Swierk, J. R.; McCool, N. S.; Mallouk, T. E., Dynamics of electron recombination and transport in water-splitting dye-sensitized photoanodes. *J. Phys. Chem. C* **2015,** *119* (24), 13858-13867.

159. Gregg, B. A.; Pichot, F.; Ferrere, S.; Fields, C. L., Interfacial recombination processes in dye-sensitized solar cells and methods to passivate the interfaces. *J. Phys. Chem. B* **2001,** *105* (7), 1422-1429.

160. Gish, M. K.; Lapides, A. M.; Brennaman, M. K.; Templeton, J. L.; Meyer, T. J.; Papanikolas, J. M., Ultrafast recombination dynamics in dye-sensitized SnO2/TiO2 core/shell films. *J. Phys. Chem. Lett.* **2016,** *7* (24), 5297-5301.

161. McCool, N. S.; Swierk, J. R.; Nemes, C. T.; Schmuttenmaer, C. A.; Mallouk, T. E., Dynamics of Electron Injection in SnO2/TiO2 Core/Shell Electrodes for Water-Splitting Dye-Sensitized Photoelectrochemical Cells. *J. Phys. Chem. Lett.* **2016,** *7* (15), 2930-2934.

162. Sherman, B. D.; Ashford, D. L.; Lapides, A. M.; Sheridan, M. V.; Wee, K.-R.; Meyer, T. J., Light-driven water splitting with a molecular electroassembly-based core/shell photoanode. *J. Phys. Chem. Lett.* **2015,** *6* (16), 3213-3217.

163. Knauf, R. R.; Kalanyan, B.; Parsons, G. N.; Dempsey, J. L., Charge recombination dynamics in sensitized SnO2/TiO2 core/shell photoanodes. *J. Phys. Chem. C* **2015,** *119* (51), 28353-28360.

164. Becerril, V. S.; Sundin, E.; Mapar, M.; Abrahamsson, M., Extending charge separation lifetime and distance in patterned dye-sensitized SnO 2–TiO 2 μm-thin films. *Phys. Chem. Chem. Phys.* **2017,** *19* (34), 22684-22690.

165. Gust, D.; Moore, T. A.; Moore, A. L., Molecular mimicry of photosynthetic energy and electron transfer. *Acc. Chem. Res.* **1993,** *26* (4), 198-205.

166. Hayashi, H.; Lightcap, I. V.; Tsujimoto, M.; Takano, M.; Umeyama, T.; Kamat, P. V.; Imahori, H., Electron transfer cascade by organic/inorganic ternary composites of porphyrin, zinc oxide nanoparticles, and reduced graphene oxide on a tin oxide electrode that exhibits efficient photocurrent generation. *J. Am. Chem. Soc.* **2011,** *133* (20), 7684-7687.

167. Swierk, J. R.; McCool, N. S.; Nemes, C. T.; Mallouk, T. E.; Schmuttenmaer, C. A., Ultrafast Electron Injection Dynamics of Photoanodes for Water-Splitting Dye-Sensitized Photoelectrochemical Cells. *J. Phys. Chem. C* **2016,** *120* (11), 5940-5948.

168. Ai, X.; Anderson, N. A.; Guo, J.; Lian, T., Electron Injection Dynamics of Ru Polypyridyl Complexes on SnO2 Nanocrystalline Thin Films. *J. Phys. Chem. B* **2005,** *109* (15), 7088-7094.

169. Benkö, G.; Myllyperkiö, P.; Pan, J.; Yartsev, A. P.; Sundström, V., Photoinduced Electron Injection from Ru(dcbpy)2(NCS)2 to SnO2 and TiO2 Nanocrystalline Films. *J. Am. Chem. Soc.* **2003,** *125* (5), 1118-1119.

170. Snaith, H. J.; Ducati, C., SnO2-Based Dye-Sensitized Hybrid Solar Cells Exhibiting Near Unity Absorbed Photon-to-Electron Conversion Efficiency. *Nano Lett.* **2010,** *10* (4), 1259-1265.

171. Ellis, H.; Schmidt, I.; Hagfeldt, A.; Wittstock, G.; Boschloo, G., Influence of dye architecture of triphenylamine based organic dyes on the kinetics in dye-sensitized solar cells. *J. Phys. Chem. C* **2015,** *119* (38), 21775-21783.

172. Reynal, A.; Lakadamyali, F.; Gross, M. A.; Reisner, E.; Durrant, J. R., Parameters affecting electron transfer dynamics from semiconductors to molecular catalysts for the photochemical reduction of protons. *Energy Environ. Sci.* **2013,** *6* (11), 3291-3300.

173. Becerril, V. S.; Sundin, E.; Abrahamsson, M., Evidence for Conduction Band Mediated Two-Electron Reduction of a TiO2-bound Catalyst Triggered by Visible Light Excitation of Co-adsorbed Organic Dyes. *J. Phys. Chem. C* **2018**, *122 (45), 25822-25828.*

174. Dron, P. I.; Michl, J.; Johnson, J. C., Singlet Fission and Excimer Formation in Disordered Solids of Alkyl-Substituted 1, 3-Diphenylisobenzofurans. *J. Phys. Chem. A* **2017,** *121* (45), 8596-8603.

175. Küçüköz, B.; Adinarayana, B.; Osuka, A.; Albinsson, B., Electron transfer reactions in sub-porphyrin–naphthyldiimide dyads. *Phys. Chem. Chem. Phys.* **2019,** *21* (30), 16477-16485.

176. Rehm, D.; Weller, A., Kinetics of fluorescence quenching by electron and H-atom transfer. *Isr. J. Chem.* **1970,** *8* (2), 259-271.

177. Mockus, N. V.; Rabinovich, D.; Petersen, J. L.; Rack, J. J., Femtosecond isomerization in a photochromic molecular switch. *Angew. Chem. Int. Ed.* **2008,** *120* (8), 1480-1483.

178. Garg, K.; King, A. W.; Rack, J. J., One Photon Yields Two Isomerizations: Large Atomic Displacements during Electronic Excited-State Dynamics in Ruthenium Sulfoxide Complexes. *J. Am. Chem. Soc.* **2014,** *136* (5), 1856-1863.

179. Livshits, M. Y.; Wang, L.; Vittardi, S. B.; Ruetzel, S.; King, A.; Brixner, T.; Rack, J. J., An excited state dynamics driven reaction: wavelength-dependent

photoisomerization quantum yields in [Ru(bpy)2(dmso)2]2+. *Chem. Sci.* **2020,** *11* (22), 5797-5807.

180. King, A. W.; Jin, Y.; Engle, J. T.; Ziegler, C. J.; Rack, J. J., Sequential Picosecond Isomerizations in a Photochromic Ruthenium Sulfoxide Complex Triggered by Pump-Repump-Probe Spectroscopy. *Inorg. Chem.* **2013,** *52* (4), 2086-2093.

181. Benkö, G.; Kallioinen, J.; Korppi-Tommola, J. E. I.; Yartsev, A. P.; Sundström, V., Photoinduced Ultrafast Dye-to-Semiconductor Electron Injection from Nonthermalized and Thermalized Donor States. *J. Am. Chem. Soc.* **2002,** *124* (3), 489-493.

182. Hagfeldt, A.; Grätzel, M., Molecular Photovoltaics. *Acc. Chem. Res.* **2000,** *33* (5), 269-277.

183. Williams, G.; Watts, D. C., Non-symmetrical dielectric relaxation behaviour arising from a simple empirical decay function. *Transactions of the Faraday society* **1970,** *66*, 80-85.

184. Abrahamsson, M.; Johansson, P. G.; Ardo, S.; Kopecky, A.; Galoppini, E.; Meyer, G. J., Decreased interfacial charge recombination rate constants with N3-type sensitizers. *J. Phys. Chem. Lett.* **2010,** *1* (11), 1725-1728.

185. Dryza, V.; Bieske, E. J., Does the triphenylamine-based D35 dye sensitizer form aggregates on metal-oxide surfaces? *J. Photochem. Photobiol. A* **2015,** *302*, 35-41.

186. Green, A. N.; Palomares, E.; Haque, S. A.; Kroon, J. M.; Durrant, J. R., Charge transport versus recombination in dye-sensitized solar cells employing nanocrystalline TiO2 and SnO2 films. *J. Phys. Chem. B* **2005,** *109* (25), 12525-12533.

187. Kamat, P. V.; Bedja, I.; Hotchandani, S.; Patterson, L. K., Photosensitization of Nanocrystalline Semiconductor Films. Modulation of Electron Transfer between Excited Ruthenium Complex and SnO2 Nanocrystallites with an Externally Applied Bias. *J. Phys. Chem.* **1996,** *100* (12), 4900-4908.

188. Roose, B.; Pathak, S.; Steiner, U., Doping of TiO 2 for sensitized solar cells. *Chem. Soc. Rev.* **2015,** *44* (22), 8326-8349.

189. Listorti, A.; O'Regan, B.; Durrant, J. R., Electron Transfer Dynamics in Dye-Sensitized Solar Cells. *Chem. Mater.* **2011,** *23* (15), 3381-3399.

190. Kuang, D.; Ito, S.; Wenger, B.; Klein, C.; Moser, J.-E.; Humphry-Baker, R.; Zakeeruddin, S. M.; Grätzel, M., High molar extinction coefficient heteroleptic ruthenium complexes for thin film dye-sensitized solar cells. *J. Am. Chem. Soc.* **2006,** *128* (12), 4146-4154.

191. Martinson, A. B.; Hamann, T. W.; Pellin, M. J.; Hupp, J. T., New Architectures for Dye-Sensitized Solar Cells. *Chem. Eur. J.* **2008,** *14* (15), 4458-4467.